Recent progress on polymer materials for additive manufacturing

Lisa Jiaying Tan [a,†], *Wei Zhu* [a,†], *Kun Zhou* [a,b,*]

L. J. Tan, Dr. W. Zhu, Prof. K. Zhou

[a] Singapore Centre for 3D Printing, School of Mechanical and Aerospace Engineering, Nanyang Technological University, 50 Nanyang Avenue, Singapore 639798, Singapore
[b] Environmental Process Modelling Centre, Nanyang Environment and Water Research Institute, Nanyang Technological University, 1 Cleantech Loop, Singapore 637141, Singapore
[†] These authors should be considered as co-first authors

E-mail: kzhou@ntu.edu.sg

Keywords: 3D printing; additive manufacturing; polymer materials; composites

Abstract

Additive manufacturing (AM) is the process of printing three-dimensional (3D) objects in a layer-by-layer manner. Polymers and their composites are some of the most widely used materials in modern industries and are of great interest in the field of AM due to their vast potential for various applications, especially in the medical, aerospace and automotive industries. Many studies have been conducted to develop new polymer materials for AM techniques, which include vat photopolymerization, material jetting, powder bed fusion, material extrusion, binder jetting and sheet lamination. Although several reviews on the development of polymer materials for AM have been published, most of them only focus on a specific application, process, or type of material. Therefore, this article serves to provide a comprehensive review on the progress in polymer material development for AM techniques. It begins with an introduction to different AM techniques, followed by highlighting the progress of their development. Material requirements, notable advances in newly developed materials and their potential applications are discussed in detail and summarized. This review concludes by identifying the major challenges currently encountered in using AM for polymer materials and providing insights into the valuable opportunities it presents, in hopes of spurring further development in this field.

Contents

1. Introduction

Additive manufacturing (AM), commonly known as three-dimensional (3D) printing, has emerged as a disruptive technology that fabricates products of complex geometries through accumulating materials in a layer-by-layer manner according to computer-aided design (CAD) model data. AM enables low-volume, customized production and great design freedom, and products that comprise multiple components can now be redesigned and produced without assembly, thereby resulting in enhanced product performance and efficiency. [1] AM is also viewed as an environmentally sustainable manufacturing technology, and can potentially reduce up to 525.5 Mt of total carbon dioxide emissions by 2025. [2] In product development, the use of AM can reduce development costs by up to 70% and time to market by up to 90%. [1b] With such remarkable benefits, the global market for AM is projected to reach nearly $23 billion by 2023, with a rapid compound annual growth rate of 22%. [3]

Polymers are macromolecules composed of covalently bonded repeating units and can be classified into thermoplastics and thermosets according to their thermomechanical behaviors. Polymers and their composites are widely used in AM due to their intrinsic lightweight and corrosion-resistant properties and the achievable mechanical, thermal, electrical, fire-resistance and biocompatible properties of their printed parts. Some polymer materials are responsive to external stimuli such as temperature, light, electric or magnetic fields, moisture, or pH, and can be used to print structures that can undergo shape or property changes over time under an environmental stimulus. The additive manufacturing of such structures that have an additional fourth dimension of time is termed four-dimensional (4D) printing.

Photosensitive resins, thermoplastic powders and filaments, and viscous polymer inks are the most extensively used polymer materials for various AM techniques, which have a multitude of applications in different domains including biomedical engineering, aerospace, automotive, electronics, soft robotics, energy, environment, and social-culture **(Figure 1)**.

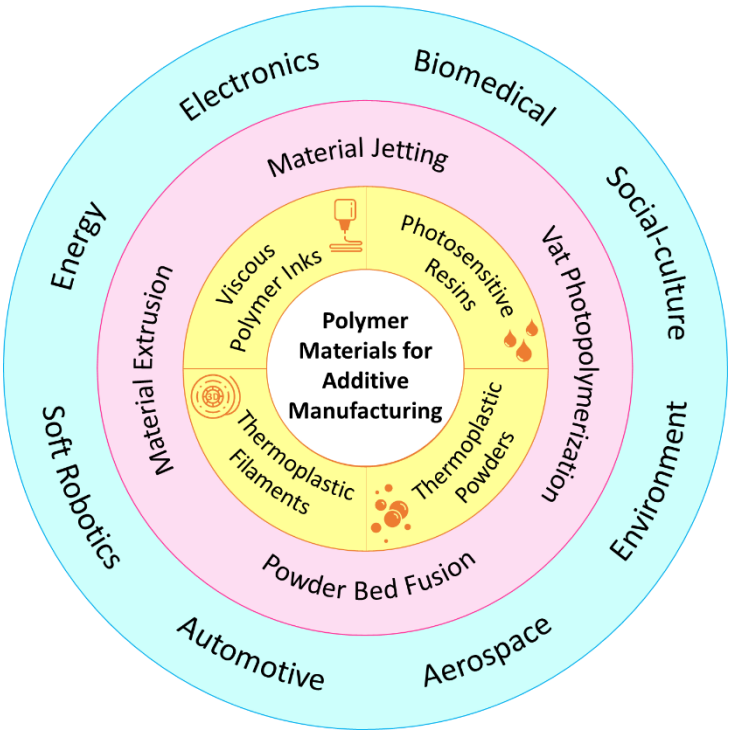

Figure 1. Overview of polymer materials that are widely used for typical polymer AM techniques, and applications.

As AM was originally developed as a rapid prototyping technique, the used materials only had to have sufficient mechanical and surface properties for demonstration purposes. The reproducibility and consistency of the mechanical and functional properties and the reliability of printed parts were not considered. Naturally, the need for different materials was not evident then. Now that AM is increasingly used to manufacture end-use parts, it is apparent that one of the major constraints is the limited range of materials that can be processed. Many commercial AM materials are often insufficient for real part replacement as they lack high mechanical strength, good temperature resistance, and functionalities such as thermal and electrical conductivity, biocompatibility, and shape memory behavior that are required. [4] Therefore, extensive research has been done over the past decade on developing new materials for the AM of polymers. On the other end of the spectrum, improvements are constantly being made to AM systems so that parts can be printed with a wider selection of materials and at a better resolution, higher accuracy, and much faster rates.

This article provides a comprehensive review on the recent progress in polymer material development for the mainstream polymer AM techniques. The disruptive innovations in polymer AM methodologies and systems are first discussed. The guidelines critical for material development are then summarized. Afterwards, the recent developments on polymers for each AM technique are evaluated, and the notable advances in material development and their potential applications are highlighted. This review concludes by identifying the major challenges currently faced in using AM as a manufacturing tool, and its prospects and research directions in the future.

2. AM techniques for polymers

Based on the ASTM (American Society of Testing and Materials) standard, the techniques for the AM of polymers can be classified into the following categories: vat photopolymerization (VP), material jetting (MJ), powder bed fusion (PBF), material extrusion (ME), binder jetting (BJ) and sheet lamination. Each technique has its unique fundamentals and materials used for manufacture, and the suitability of a process would depend on the polymer materials used and the desired part properties.

2.1. Vat photopolymerization

VP is a category of AM techniques that utilize radiation (e.g., ultraviolet (UV) and visible light) to selectively polymerize liquid photosensitive resins in a vat to form solid 3D structures. The VP processes are known for their high part accuracy and high resolution achievable as compared to the other AM processes. [5]

Since the invention of stereolithography (SLA), VP systems that support higher volume throughput and higher resolution, and that are more capable of large-scale manufacturing have been developed. Such VP systems include the now-common digital light processing (DLP) and

continuous liquid interphase printing (CLIP) **(Figure 2a)**. [6] It is worth mentioning that CLIP can achieve up to 100 times higher printing speed than SLA.

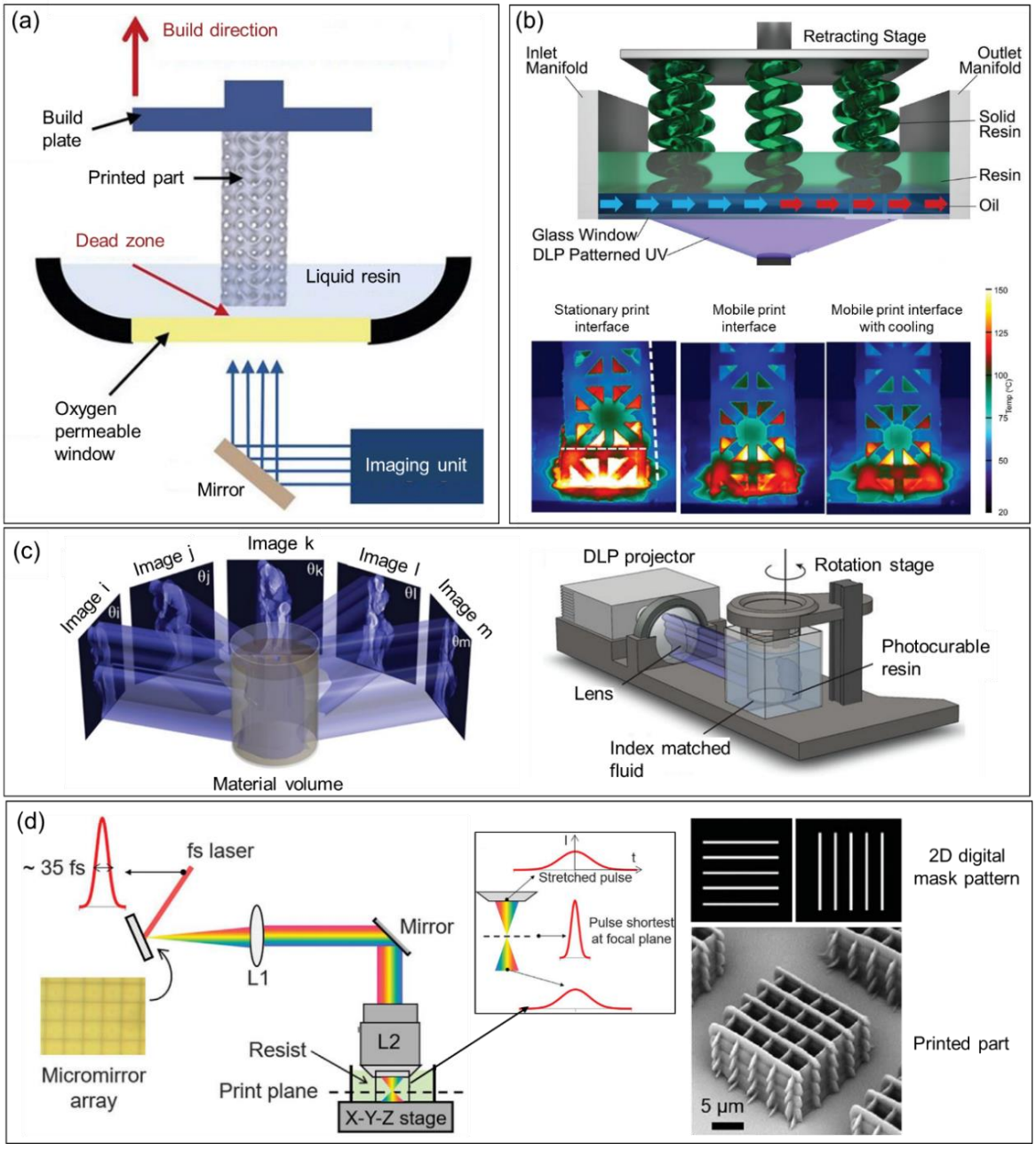

Figure 2. Schematics of various VP processes. (a) CLIP. Reproduced with permission. [6] Copyright 2015, AAAS. (b) HARP. Reproduced with permission. [7] Copyright 2019, AAAS. (c) CAL. Reproduced with permission. [8] Copyright 2019, AAAS. (d) Femtosecond projection two-photon lithography. Reproduced with permission. [9] Copyright 2019, AAAS.

Unlike CLIP that uses an oxygen-permeable window to reduce the adhesive forces between the printed object and vat surface, the high-area rapid printing (HARP) process

developed by Walker et al. utilizes flowing fluorinated oil as the mobile liquid interface **(Figure 2b)**. [7] In addition to being compatible with both oxygen-sensitive and oxygen-insensitive resins, the oil can further be recirculated through a heat exchanger to maintain thermostatic control across the entire print bed. Moreover, the oil can be filtered to remove the microparticles generated during the print, which lower the part resolution due to light scattering. As a result of the active heat dissipation and filtration, parts of high fidelity can be fabricated at a high throughput of 100 L/h.

Different from the layer-wise VP processes, a volumetric AM process, computed axial lithography (CAL), was developed by Kelly et al. recently. [8] Light energy is delivered as dynamically evolving two-dimensional (2D) images to a rotating vat containing the photosensitive resin **(Figure 2c)**. Each image projection propagates through the resin from a different angle, and the 3D energy dose generated from the superposition of those exposures cures selective regions of the photosensitive resin. The CAL process fabricates parts by rotating the print stage, circumventing the need for the resin recoating process and thus enabling the printing of highly viscous photosensitive resins that are otherwise difficult or slow to process using layer-wise VP processes. The use of highly viscous or gel-like precursor materials is also important for minimizing the displacement of the cured regions, and molecular diffusion-induced blurring. The CAL process is fast and scalable to large print volumes and can be used for the fabrication of custom geometries onto existing objects, allowing for multi-material fabrication.

Two-photon photopolymerization (2PP) offers a much higher resolution than typical SLA systems, and in fact, the best resolution (< 100 nm) among all AM processes. It is a direct laser writing process based on the two-photon absorption (TPA) principle, where the electronic transitions involved are not driven by the absorption of a single photon as that in typical UV- or visible light-based VP, but rather by two photons in combination. [10] To achieve TPA, a

laser beam with sufficiently high photon density, typically pulsed femtosecond laser, must be used. The resolution of 2PP is restricted not by the diffraction limit of the laser wavelength but only by the focal volume of the laser, which is on the scale of a few attoliters. [11] As the focus of the laser can be shifted in any direction, layer fabrication can occur in any 3D space within the resin; therefore, 2PP does not require the recoating process.

Owing to the point-wise lithography technique, 2PP processes are generally slow. Attempts to improve the fabrication speed typically involve parallelizing with, for example, digital masks at the cost of resolution, or holographic methods that are more suited for periodic structures. However, by pairing the temporal focusing technique with a digital micromirror device, a femtosecond projection two-photon lithography process was developed. [9] In this process, the entire 2D layer is projected at once and the resolution is unaffected by the number of voxels per layer **(Figure 2d)**. This process can achieve an improved printing rate of at least 1,000 times that of 2PP, and demonstrates high potential for the large-scale production of sub-micron structures.

2.2. Material jetting

MJ is a printing process analogous to traditional 2D inkjet printing, during which liquid materials are deposited from inkjet print-heads onto a build platform using either a drop-on-demand or continuous approach, and subsequently solidify through photopolymerization, cooling, etc. MJ is one of the most popular AM processes today, capable of producing multi-material parts owing to the use of multiple print-heads. MJ can be used for photosensitive resins, thermoplastics, wax, and reactive materials, but this review focuses on the use of photosensitive resins that solidify through photopolymerization.

Stratasys and 3D Systems have developed their own MJ systems, PolyJet and MultiJet printing (MJP), respectively. The working principles of PolyJet and MJP are largely similar, and their main difference lies in the type of support material used. PolyJet uses gel-like water

soluble support materials that can be removed by using high-pressure water jet systems and chemical dissolution, while MJP uses a paraffin wax support material that can mostly be removed by heat. The multi-material capability of MJ systems makes it a versatile technique for fabricating functionally graded materials with low surface roughness and high dimensional accuracy, through precise control of material deposition at the voxel scale. [12]

Unlike PolyJet and MJP where photopolymer inks are dropped on demand, an electrohydrodynamic (EHD) jetting process was developed by Liashenko et al., where the ink is electrostatically drawn to the substrate in the form of a thin, continuous jet from the nozzle. [13] By tuning the electrostatic field between the nozzle and substrate, the trajectory of the ink jet can be deflected and controlled onto desired substrate positions **(Figure 3a, b)**. Since EHD does not involve droplet deposition, the challenges associated with the droplet formation deposition control can be avoided. Furthermore, the thickness of the jet is unaffected by the nozzle size and can go below 100 nm, allowing the fabrication of thin-walled structures with high height-to-thickness ratios, for example, cylindrical structures that are 100 nm in width and 100 μm in height **(Figure 3c)**. The high jetting speed of EHD makes it possible to achieve printing speeds on the scale of 10^3–10^6 layers per second (0.5 m/s in-plane), making it the fastest AM process so far for submicron-scale fabrication.

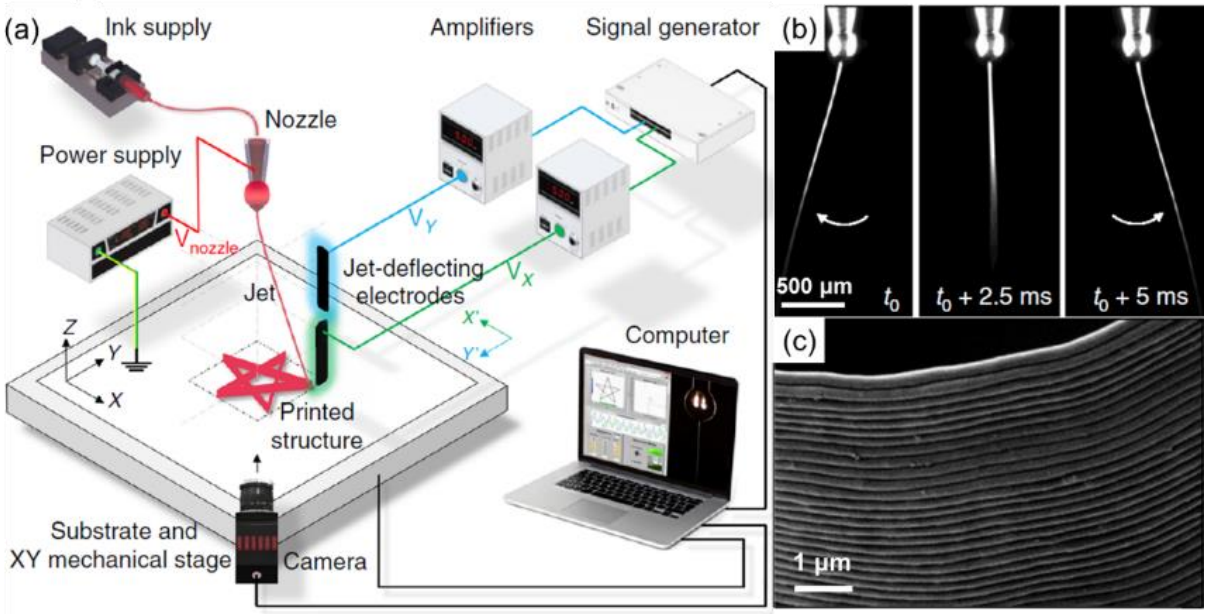

Figure 3. EHD jetting process: (a) the schematic of an EHD printer, (b) jet deflection at 100 Hz using two electrodes positioned on both sides of the video capture, and (c) SEM image of a fabricated cylindrical wall structure. Reproduced with permission. [13] Copyright 2020, Springer Nature.

2.3. Powder bed fusion

In PBF, a heat source (e.g., laser and infrared (IR) radiation) is used to coalesce powder particles in a powder bed to build 3D objects. PBF is versatile as it can theoretically process any material available in powder form, as long as the powder particles can be softened or melted upon heating. Furthermore, for polymers, no support structures are required as printed parts are embedded within the powder bed.

Selective laser sintering (SLS) is such a process that uses a laser (typically CO_2 laser) to selectively sinter thermoplastic polymer powder particles in successive layers. SLS is one of the most established and widely used AM processes due to its high potential for the manufacturing of functional parts, and is versatile as it can theoretically process any polymer available in powder form, as long as the powder particles are sinterable. [4, 14] Furthermore, no support structures are required. However, SLS has limited part resolution, compared to VP and MJ, because of the over-sintering phenomenon and the finite laser beam diameter. The SLS

process is also relatively slow because of the point-wise laser scanning track. Endeavors by equipment manufacturers to address these challenges have brought about the development of the High Speed Sintering (Voxeljet), LaserProFusion (EOS), Fine Detail Resolution (EOS) and Flight (Farsoon) processes that boast a higher fabrication speed and resolution by using laser arrays and different laser types.

Combining PBF with its specialization in inkjet printing, Hewlett-Packard (HP) developed a new process, Multi Jet Fusion (MJF), that promises a higher resolution and faster print speeds, and has opened a new dimension for the production of industrial-grade functional parts and prototypes **(Figure 4)**. [15] MJF is largely similar to SLS, with the main difference being the way that polymer powder particles are fused. In MJF, fusing and detailing agents are selectively deposited onto the powder particles in the form of droplets, and the IR lamps subsequently scan across the powder bed to fuse the powder layers in a line-wise manner**.** The fusing agent is used to facilitate the heat absorption of the areas that need to be sintered, while the detailing agent is jetted around the contours to impede heat absorption, thus improving the part resolution. The line-wise fusion of powders in MJF speeds up the printing process by up to 10 times that of SLS. [16] Additionally, MJF is able to overcome the challenge of reduced tensile strength along the Z-axis that is commonly found in other AM processes. The MJF system is also able to produce fully colored functional parts owing to its multi-agent jetting capability. The overwhelming advantages in terms of lead time and cost efficiency offer MJF an edge for industrial applications.

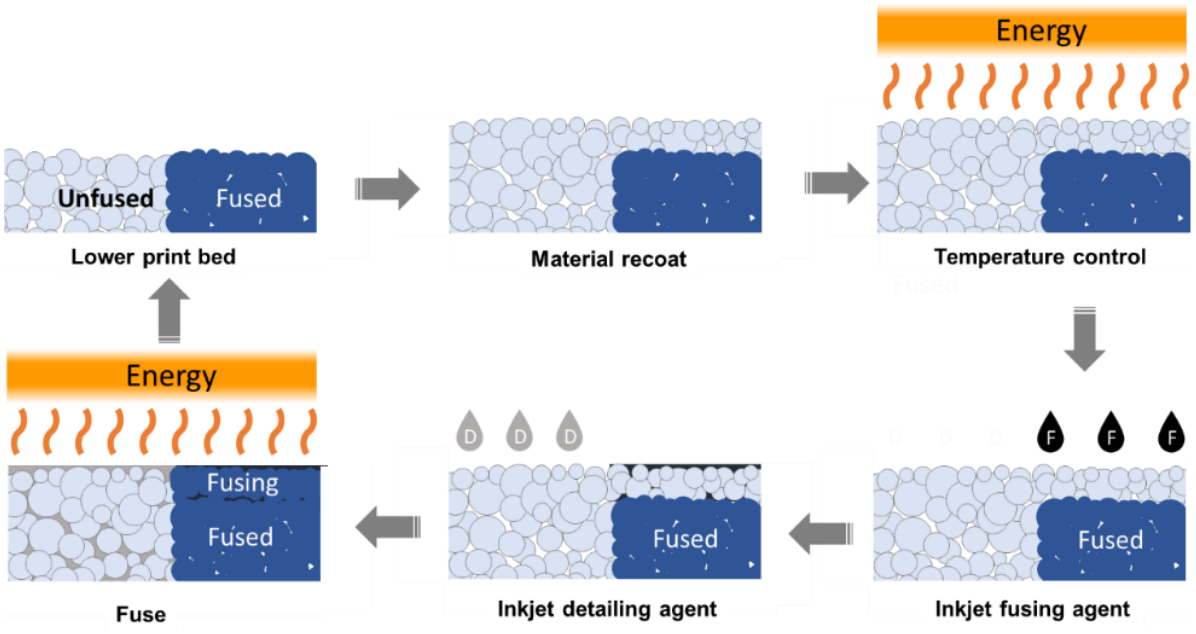

Figure 4. Schematic of the cross-sectional view of the MJF process. Reproduced with permission. [15] Copyright 2018, HP.

2.4. Material extrusion

The ME technique involves a continuous extrusion of polymer filaments, viscous inks or even polymer pellets, through a nozzle or orifice onto a build platform, where they subsequently solidify. ME systems are affordable compared to those of other AM techniques, and they are compatible with a wide variety of materials.

Fused deposition modeling (FDM) is one of the ME processes where a thermoplastic material is softened or melted and extruded through a nozzle and solidifies upon cooling. FDM is one of the most affordable AM processes and is currently the most commonly used one that is being adopted even in households. [5b, 17] A typical FDM process uses thermoplastic filaments as feedstock, but in recent years, screw extrusion-based systems that allow the use of pellets as feedstock show promise in processing a more diverse range of thermoplastics.

Different from FDM that extrudes thermoplastics at elevated temperatures, direct ink writing (DIW), also known as 3D dispensing, 3D extrusion or 3D plotting, is an ME process capable of printing viscous inks such as pastes and concentrated polymer solutions that solidify

through cooling, drying, chemical reactions, etc. The advantages of DIW lie in its ambient temperature operation and flexible material requirements, and it offers the broadest spectrum of printable materials at present. [18] Because of the diverse ink materials that can be processed, the nozzle size used for DIW varies from several micrometers to centimeters.

A multi-material multi-nozzle 3D printing system based on DIW was recently developed by Skylar-Scott et al., which brings multi-material printing to the next level. [19] The system allows the design and fabrication of soft matter at the voxel level with high material complexity and high build rates. The nozzle arrays were specially designed and fabricated with SLA, with each print-head connected to multiple syringes containing different materials **(Figure 5a, b)**. The syringes were then actuated by fast-cycling pneumatic solenoids to enable high-frequency switching **(Figure 5c)**. The backflow of ink from one channel to the other was avoided with careful control of the back-pressure, thus enabling the printing of voxelated multi-materials **(Figure 5d)**. This advanced DIW system capable of printing multiple viscous inks can complement MJ processes that use low-viscosity photopolymer inks. With this multi-material multi-nozzle 3D printing system, the design and voxel-level printing of intricate motifs can be achieved with a much wider variety of materials.

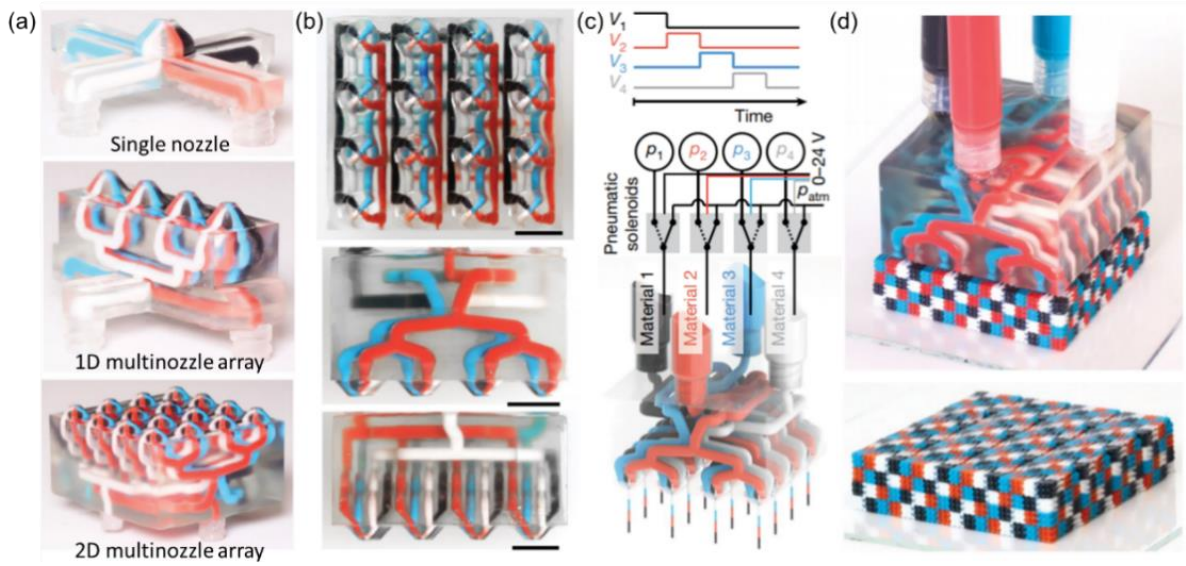

Figure 5. Multi-material multi-nozzle 3D printing: (a) the 0D, 1D and 2D print-heads, (b) the top and side views of a 4×4 nozzle array, (c) the schematic of the nozzle array operation where V_1–V_4 represent the voltage waveforms controlling the extrusion pressures p_1–p_4 for materials 1–4, and the p_{atm} denotes atmospheric pressure, and (d) a voxelated structure produced using the 4×4 nozzle array. Reproduced with permission. [19] Copyright 2019, Springer Nature.

2.5. Binder jetting

BJ is a powder-based AM technique that utilizes an inkjet print-head to deposit the droplets of a liquid binder onto the powder particles in a powder bed and selectively glue them together to build 3D objects. BJ possesses some advantages of PBF, such as being free of support structures and capable of fabricating large parts.

Owing to the relative simplicity of the setup and elimination of an expensive heat source such as a laser, BJ systems are significantly cheaper and able to build much larger objects than typical PBF systems. However, because of the absence of sintering or melting processes, green parts produced by BJ are porous and relatively fragile. Hence, post-treatments such as high-temperature sintering and liquid infiltration are needed.

Powder materials used in BJ are mostly metals and ceramics, and polymers are often used as binders and hardly as base materials. [20] Therefore, polymers for BJ are not discussed in this review.

2.6. Sheet lamination

Sheet lamination is a technique of printing a 3D object by stacking and laminating thin sheets of material together. Sheet lamination processes are relatively cheap and can be used to rapidly fabricate large parts.

Laminated object manufacturing (LOM) is the earliest sheet lamination process that uses both additive and subtractive methods to bond sheets of materials to form a 3D object. Based on this construction principle, several other processes have been developed. They involve different cutting (e.g., computer numerical control [CNC] milling, laser cutting and water jet cutting) and bonding (e.g., adhesive bonding, thermal bonding and ultrasonic welding) strategies. There are also variations on the sequence of the shaping and bonding of sheet materials, and they can be categorized into the shape-then-bond and bond-then-shape processes.

Printing materials for LOM can be papers, metal sheets, ceramic tapes, woven fiber composite sheets, and thermoplastic foils. However, because the cutting process renders the fabrication of internal cavities difficult and produces significant material waste, LOM is not widely used. Therefore, polymers for LOM is not further discussed.

2.7. Summary

Each AM technique has its unique advantages and specific feedstock requirements **(Table 1)**. Photosensitive resins are used for VP and MJ, and parts fabricated by these techniques typically exhibit a higher resolution and dimensional accuracy than those of the other techniques. Meanwhile, PBF uses thermoplastic powders to fabricate parts with a moderate resolution but with better mechanical and functional properties. ME uses thermoplastic filaments or viscous inks, and is one of the most popular AM techniques due to its low cost, simple equipment set-up and fast fabrication. By utilizing multi-nozzles or multi-print-heads,

MJ and ME can realize multi-material printing with ease, which popularizes their use for fabricating full-color, multi-functional and smart structures.

Since specific types of materials are required for the VP, MJ, PBF and ME techniques, the subsequent discussion on the recent progress in polymer material development for AM is classified according to the type of material, into photosensitive resins, thermoplastic powders, thermoplastic filaments and viscous polymer inks.

Table 1. Comparison of the different AM techniques. Most data are obtained from the manufacturers' websites.

AM technique		Typical *xy*-resolution (µm)	Typical layer thickness (*z*-resolution) (µm)	Typical accuracy	Maximum build rate	Typical and maximum build size (mm^3)	Support material	Multi-material	Manufacturer
Vat photopolymerization	SLA	6.5–25	25–300	± 0.15% (with a lower limit on ± 50 µm)	-	145×145×175 1500×750×550 (ProX® 950)	Yes	No	Stratasys 3D Systems Formlabs
	DLP	35–100	25–150	-	-	140×79×100 800×330×400 (ProMaker L7000)	Yes	No	EnvisionTEC Prodway
	[a] PμSL	2–25	5–50	-	-	48×27×50	Yes	No	Boston Micro Fabrication
	CLIP	75	0.4–100 [21]	-	100 cm/h [6]	150×80×300	Yes	No	Carbon
	2PP	0.16–0.2	0.3–5		3 mm^2/h	100×100×3	Yes	No	Nanoscribe
Material jetting	PolyJet	42–85	16–28	± 0.06% (with a lower limit on ± 100 µm)	-	294×192×148.6 1000×800×500 (Objet 1000 Plus)	Yes	Yes	Stratasys
	MJP	16–42	13–32	± 0.15% (with a lower limit on ± 100 µm)	-	294×211×144 518×381×300 (Projet MJP 5600)	Yes	Yes	3D Systems
Powder bed fusion	SLS	30–100	60–180	± 0.3% (with a lower limit on ± 300 µm)	15 L/h	340×340×600 1400×1400×500 (HKS1400)	No	No	EOS 3D Systems Farsoon Huake 3D
	MJF	21.2	80	± 0.3% (with a lower limit on ± 200 µm)	5058 cm^3/h	380×285×380	No	No	HP
Material extrusion	FDM	100–150	100–200	± 0.15% (with a lower limit on ± 200 µm)	50 mm^3/s	223×223×305 1005×1005×1005 (BigRep ONE)	Yes	No	Stratasys Makerbot Ultimaker BigRep
	DIW	100–1200 (Needle tip diameter)	100-400	-	150 mm/s	260×220×70 200×220×140 (3D-Bioplotter)	Yes	Yes	EnvisionTEC
Binder jetting	3DP	100	260–380	± 2% (with a lower limit on ± 500 µm)	135 L/h	1800×1000×700 4000×2000×1000 (VX4000)	No	No	Voxeljet ExOne
Sheet lamination	LOM	200–300	100–190	± 3% (with a lower limit on ±100 µm)	-	160×210×135 180×280×150 (Katana PLT-20)	No	Yes	EnvisionTEC Katana

[a] Projection micro-SLA

3. Photosensitive resins

Photosensitive resins, mostly used by the VP and MJ techniques, are liquid prepolymers that are activated upon irradiation to form cross-linked chemical networks, thereby undergoing irreversible hardening. They consist mainly of photoinitiators, monomers, oligomers and additives.

Single-photon photopolymerization (SLA, DLP, etc.) can occur via the free radical or ionic (mostly cationic) pathway; the main difference between the two pathways lies in the type of active center on the propagating species, which is determined by the initiating reactive species generated by photoinitiators upon irradiation. Photoinitiators for free radical polymerization are single molecules that undergo homolytic bond cleavage to form two radical fragments (Norrish Type-I), or a photoinitiator radical and a co-initiator radical (Norrish Type-II), upon irradiation. Acetophenones and acyl phosphine oxides are typical Norrish Type-I photoinitiators, while benzophenones and thioxanthones are typical Norrish Type-II photoinitiators. Cationic photoinitiators are typically iodonium and sulfonium salts that produce strong acid species usually in the form of MX_nH upon irradiation, where M and X are metal and halide, respectively. [22] Owing to the positive charge on the active sites, the anions should be minimally nucleophilic to prevent undesired termination reactions; in this aspect, many complex metal halides and fluorinated anions appear promising. [23]

Photoinitiators for 2PP undergo a TPA mechanism, and an important criterion for a 2PP photoinitiator is the presence of a π-conjugated core in its molecular structure. Upon TPA, an intramolecular charge transfer first occurs from the terminal donor group of the photoinitiator to its π-conjugated core with a state of [D - π-core$^{\bullet -}$ - D$^{\bullet +}$]*, followed by an intermolecular charge transfer from the π-conjugated core to a monomer ([D - π-core - D$^{\bullet +}$]---[monomer$^{\bullet -}$]). [24] Suitable 2PP photoinitiators include molecules with π-conjugated cores based on

benzylidene ketones, stilbene and bis(styryl)benzene, etc. that are bonded to both electron-donating and electron-accepting moieties. [25]

Monomers are small molecules that can have one or multiple functional groups (e.g., mono-, di-, tri- and tetra-functional) that influence the curing speed, cross-link density, and final part properties. Monomers for free radical photopolymerization typically have the vinyl functional group and are commonly based on acrylates due to their high reactivity and wide availability. [8, 26] Examples of vinyl monomers that undergo free radical polymerization are urethane acrylate, bisphenol A (BPA) acrylate and poly(ethylene glycol) (PEG) acrylate. The downsides of using acrylates include high shrinkage and oxygen sensitivity, which can be alleviated by using thiol-ene systems instead. In the case of cationic photopolymerization, monomers with epoxides and vinyl ether functional groups are most common; cycloaliphatic epoxides that have the fastest polymerization rate among epoxides, are widely used in today's industries. [27] Epoxides are known for their good mechanical properties, low shrinkage, and reduced warpage during post-gelation polymerization. [1b] Popular epoxide monomers include BPA diglycidyl ether and trimethylolpropane triglycidyl ether. Vinyl ethers are usually used in tandem with epoxides to increase their reactivities and curing rates. To incorporate the benefits of both radical and cationic photopolymerization pathways, dual-cure photosensitive resins (e.g., acrylate/epoxide) that photopolymerize via both free radical and cationic pathways have been developed. [28] Such resins benefit from high reactivity, high green strength, and low polymerization shrinkage. [25a, 29]

Oligomers, also known as prepolymers, form the backbone of polymer chains. They are larger molecules with a higher degree of functionality and more voluminous groups than monomers and are thus much more viscous. The degree of functionality of oligomers influences their cross-link density and curing rate. Oligomers also greatly affect the final part properties such as toughness, strength, adhesion, and surface finish. Since different oligomers

can impart different properties, it is common to use a combination of different oligomers to achieve the desired properties.

Additives are added to improve the performance of resins. Inhibitors or retarders are necessary for controlling the penetration depth and gel time, and for limiting the negative effects of reflected light. Typical inhibitors and retarders are quinones, sterically hindered phenols and oxygen. [30] Sensitizers are chemicals that absorb well at the radiation wavelength, and they are used to promote the formation of active species from photoinitiators. Solvents function as diluents to alter the resin viscosity and aid the transfer of heat of polymerization.

3.1. Material requirements

In the development of photosensitive resins suitable for VP processes, their chemical, optical and rheological properties should be carefully considered. Of utmost importance is that monomers and oligomers contain functional groups that can react with the radicals or cationic radicals generated from photoinitiators. Functional groups such as acrylates and epoxides are the most common, and other functional groups include thiol-enes and fumarates. [25a] The curing kinetics is another critical consideration; a moderate curing rate is desired as it facilitates rapid part fabrication while ensuring sufficient time for interlayer adhesion. The curing kinetics is influenced by the degree of functionality, steric effects, and the stability of the radical or cationic active centers in addition to the polymerization pathway. A higher curing rate is achieved with a higher degree of functionality, and active centers with less steric hindrance and lower stability; for instance, acrylate radicals that are less sterically hindered and have lower stability than methacrylate radicals undergo faster curing under identical conditions. [31]

The cure depth C_d (m) is another important consideration for the VP processes. It should be sufficiently large to avoid excessive fabrication time, yet low enough to allow accurate control of the polymerization and reduce over-cure to ensure part resolution. The cure depth is

related to the penetration depth D_p (m) of radiation into the resin, the light exposure E (J/m^2), and the critical exposure E_c (J/m^2) at which gelation starts to occur, by a semi-empirical equation based on the Beer-Lambert Law [32]

$$C_d = D_p \ln \frac{E}{E_c} \ . \quad (1)$$

In equation 1, D_p is defined as the depth where a reduction of 1/e in irradiation is reached, and is influenced by the optical properties of the resin, including transmission, absorption, reflection, and scattering; E_c is a constant intrinsic to each resin formulation. A plot of C_d against E produces a working curve that is used to determine the viable processing parameters for VP. [25a]

The viscosity of the resins should be low enough, preferably between 0.1 Pa·s and 10 Pa·s, to ensure their smooth spreading on the build platform. [26, 31] The molecular weight, molecular architecture and chain entanglement of the monomers and oligomers have a predominant effect on the viscosity of the resins, which affects the processing conditions and the part properties. [33] Resins containing low-molecular-weight oligomers usually have low viscosity due to fewer inter-chain entanglements, which allows them to be used directly for VP processes. However, this can result in cross-linked structures with low glass transition temperatures T_g and poor mechanical properties. Oligomers of higher molecular weight and degree of functionality are desired for highly cross-linked parts, but they tend to be too viscous; thus, a diluent, usually in the form of monomers, is required. [31, 34] An alternative solution to lower the viscosity is to process the resins at higher temperatures, but this is limited to formulations that are insensitive to heat. [25a] The spreading of a resin is also influenced by its surface tension. A high surface tension can cause difficulties in achieving a smooth spreading of the resin on the printed layers, which can result in poor printability and therefore low-quality printed parts.

Photosensitive resins used for MJ have formulations that are similar to those used in VP. [35] Because typical material-jetting frequencies are within 1–20 kHz, [1b] the resins have to remain stable up to 20 kHz, and their photopolymerization rates need to be fast enough to ensure the prompt solidification of the parts. One of the most critical challenges faced in ink design for MJ is the droplet formation behavior, which affects the jettability of the ink. The droplet formation behavior can be characterized by several physical constants including the Reynolds *Re*, Weber *We*, and Ohnesorge *Oh* numbers that are largely associated with the ink rheology as described by [36]

$$Oh = \frac{\sqrt{We}}{Re} = \frac{\eta}{\sqrt{\gamma \rho r}} \ , \tag{2}$$

where γ, ρ and η are the surface tension (N/m), density (kg/m^3) and dynamic viscosity (Pa·s) of the ink, respectively, and r the radius (m) of the inkjet nozzles.

The stability of droplet generation can be evaluated by the parameter *Z*, the inverse of *Oh*, which should range between 1 and 10; [37] this corresponds to a maximum fluid viscosity of 20–40 mPa·s. [1b] Resins with low *Z* will resist flow through the nozzle because of the high viscosity, whereas those with high *Z* will either splash or form satellite droplets. [38] As an additional requirement, the droplets must possess sufficient energy to overcome the surface tension at the nozzle, which implies that *We* needs to be greater than 4. Lastly, to ensure that the droplets do not splash upon impact, the product of $We^{1/2}$ and $Re^{1/4}$ has to be greater than the function of surface roughness *f(R)*. By combining the above conditions, Derby constructed a map that can be used as a guide to illustrate the allowable fluid properties for successful droplet formation **(Figure 6)**. [36]

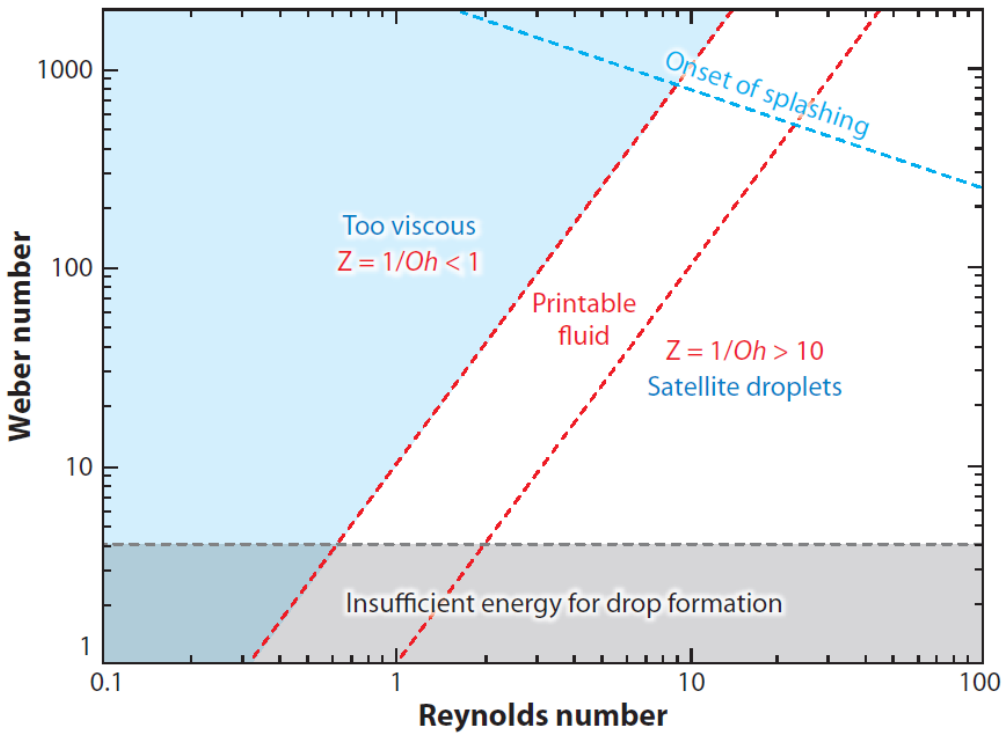

Figure 6. Regimes of the *Re*, *We* and *Oh* numbers to generate stable droplets in MJ, assuming a linear Newtonian behavior of the fluid. Reproduced with permission. [36] Copyright 2010, Annual Reviews.

The critical material requirements for VP and MJ are summarized in **Figure 7**. They can be classified into chemical, optical and rheological properties that influence the curing kinetics, cure depth and resin spreading or droplet formation behavior, respectively. These properties can be tuned by varying the type and amount of photoinitiators, monomers, oligomers and additives used.

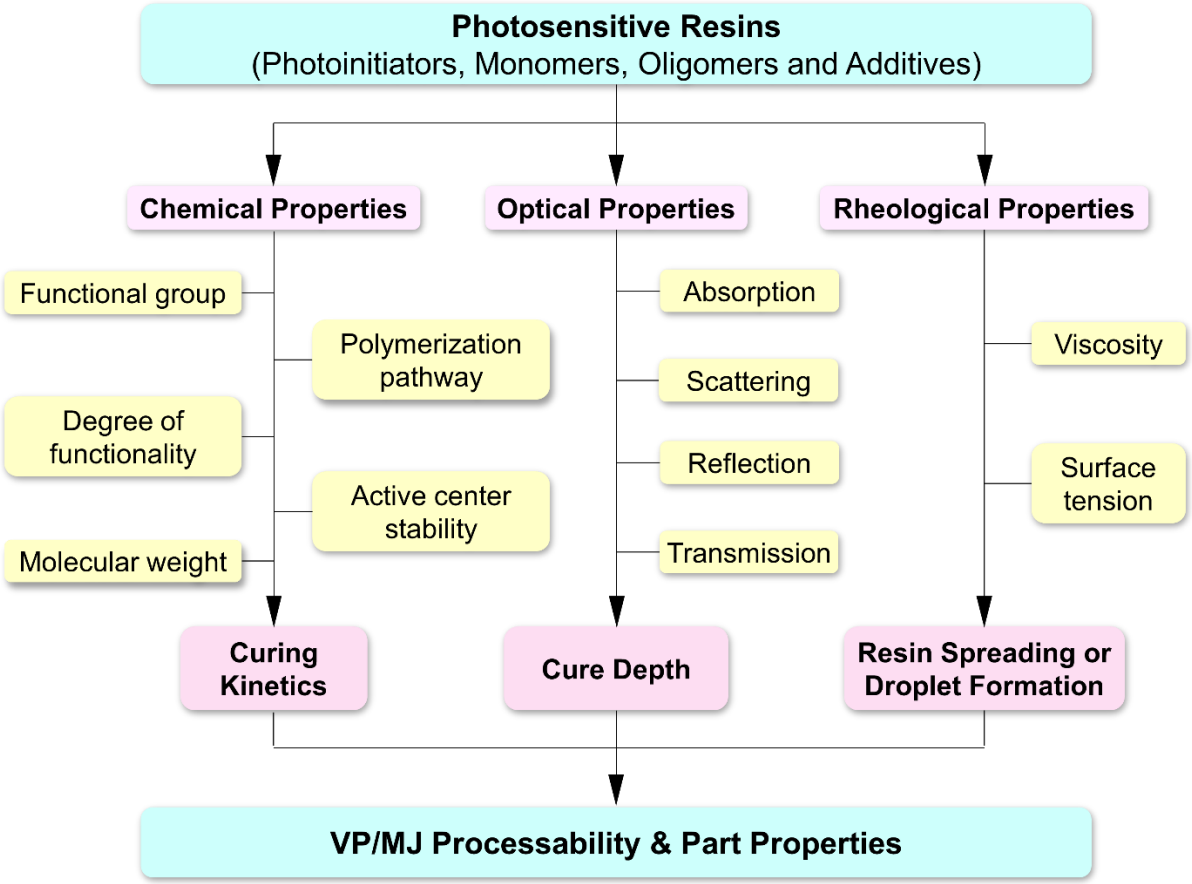

Figure 7. Key properties of a photosensitive resin material and their influences on VP or MJ processability and part properties.

3.2. Pure photosensitive resins

Even with the long-standing history of photopolymerization, research on the development of new VP resins remains highly active; most recent studies on material development for VP have focused on biocompatible and shape memory polymers, and digital multi-materials.

3.2.1. *Biocompatible polymers*

VP has great potential for biomedical applications due to its high resolution, controlled pore size and architecture achievable **(Figure 8a-d)**, and the wide availability of biocompatible resins. The applications of biocompatible polymers vary from soft or hard tissue engineering scaffolds **(Figure 8e-h)** to prosthetic devices and implants **(Table 2)**. In developing resins for

biomedical applications, the suitability of all the components must be considered, including their effects on the biocompatibility, biodegradability, and mechanical properties of the final parts.

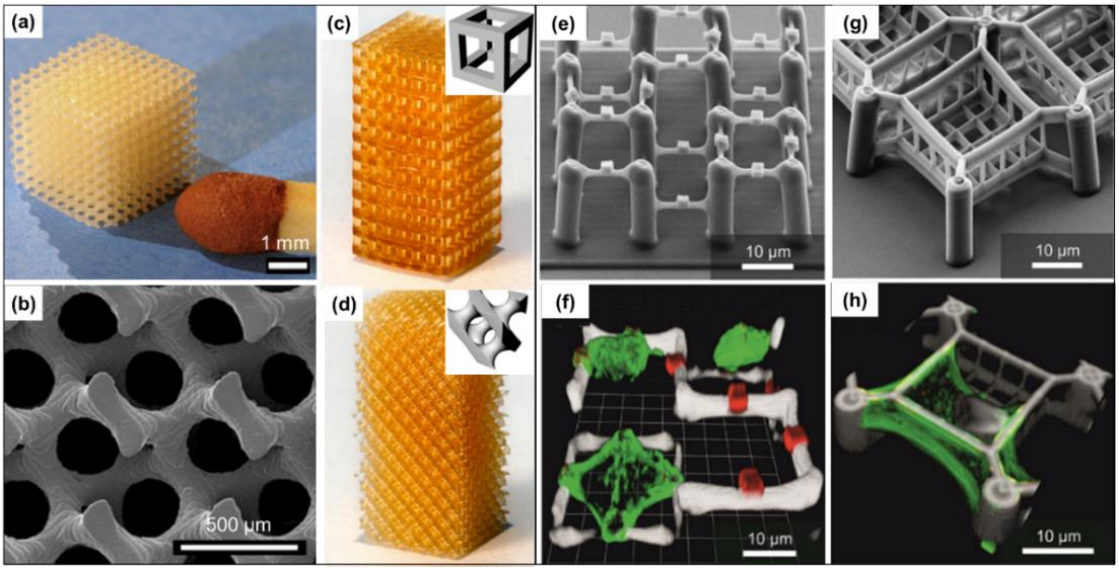

Figure 8. Biocompatible scaffolds with different pore architectures printed by DLP: (a, b) gyroid; [34] (c) cube and (d) diamond. [39] Reproduced with permission. Copyright 2009 and 2010 Elsevier. 2PP-printed scaffolds for the single-cell studies of: (e, f) fibroblasts and (g, h) cardiomyocyte. Reproduced with permission. [40] Copyright 2012, Wiley.

Any resin meant for implant fabrication must be biocompatible, meaning that it must not be cytotoxic or mutagenic, and the cells must be able to adhere to, function normally, and proliferate on the implants. [41] Cytotoxicity is an issue especially with photoinitiators, and it generally increases with the concentration of photoinitiators. Nonetheless, a balanced photoinitiator concentration should be considered since small quantities of photoinitiators would result in a slow curing rate. [31] The photoinitiator system consisting of N,N-dimethylaminobenzoic acid ethyl ester and camphorquinone is known for its biocompatibility and is commonly used for dental applications. [42] Apart from using biocompatible reagents, another solution to minimize the abovementioned issues is to develop photosensitive resins made up of fewer components, such as an inhibitor- and solvent-free resin based on PEG diacrylate. [43]

Table 2. Biocompatible resins used for VP and their corresponding part properties.

Polymer		Biodegradability	Pore size [a] (μm)	Modulus (MPa)		Shrinkage (%)	Application	Reference
				Tensile	Compressive			
Polyester	PPF	Yes	249–260	-	-	-	Cell culture	[47]
			200–800	-	16–47	-	Osteogenesis	[48]
			250	-	-	25	Osteogenesis	[49]
	PLA	Yes	390–540	-	63	14–16	Osteogenesis	[50]
			170–240	3300	-	-	Osteogenesis	[34]
			378–537	-	169–324	22	Tissue engineering	[39]
	PCL	Yes	350–550	6.7–15.4	-	0	Cell culture	[33]
	P(LA-*co*-EG-*co*-LA)	Yes	387–558	-	7.35	-	Cell culture	[51]
	P(LA-*co*-CL) [b]	Yes	352–462	-	0.12	22	Tissue engineering	[39]
	PCL/PEG/Chitosan		300	0.29–0.81	-	-	Cell culture	[52]
	PLA/NVP [c]	Yes	240–350	1500–2100	-	16	Osteogenesis	[53]
Polycarbonate	PTMC	Yes	300–415	-	0.12	18	Chondrogenesis	[54]
			309–407	-	3.1–4.2	21–31	Tissue engineering	[55]
			-	7.9	-	8	Angiogenesis	[56]
	PTMC/Gelatin	Yes	-	0.1–0.9	-	-	Cell culture	[57]
	Trimethylolpropane carbonate	-	-	10–100	-	-	Cell culture	[58]
	Polycarbonate-based polyurethane silicone	No	-	6.9	-	-	Angiogenesis	[59]
Polyether	PEG	No	-	137.9–153.5	-	6	Cell culture	[43]
	P(EG-*co*-depsipeptide)	Yes	-	0.03–0.38	-	-	Angiogenesis	[60]
	PEG/Chitosan	Yes	25–100	-	0.1–1.0	-	Chondrogenesis	[61]
	PEO/PEG	No	-	-	0.001	0.5	Chondrogenesis	[62]
	Polytetrahydrofuranether	No	-	5.7–27.5	-	-	Angiogenesis	[63]
Polyacrylate	Poly(BPA-*co*-IBA-*co*-IL) [d]	No	100–200	18–25	-	-	Angiogenesis	[64]
Polypeptide	Gelatin	Yes	250–500	-	0.5–0.9	-	Tissue engineering	[65]
		Yes	90–120	0.0096	-	-	Angiogenesis	[66]

[a] Diameter of pores in the fabricated porous scaffolds; [b] poly(D,L-lactide-co-ε-caprolactone); [c] *N*-Vinyl-2-pyrrolidone; [d] Poly(BPA ethoxylate diacrylate-lauryl acrylate-isobornyl acrylate).

Polyacrylates are biocompatible and are one of the most prolific and versatile polymers used for biomedical applications. The commonly used acrylate and methacrylate monomers are cytotoxic, and thus post-curing is required to maximize the conversion of unreacted groups, and the built parts should be extracted with supercritical CO_2 before implantation. [44] Acrylates are generally more toxic than their corresponding methacrylates. [45] In addition to cytotoxicity, cell viability, which is influenced by the functional groups in the monomers, is an important consideration. Resins that use acrylates with urethane units and trimethylolpropane triacrylates exhibit outstanding biocompatibility for the fabrication of cellular bone replacement materials. [46] Such biocompatible resins can be used to manufacture medical implants with tailored geometries and physical properties, such as bone fracture fixation devices, parts for artificial hips or knees, nerve guidance channels and prostheses. [5a]

Biodegradability is essential for drug delivery systems and especially for scaffolds serving as temporary supports for tissue regeneration. [67] Biodegradable polymers usually contain hydrolyzable ester-, amide- or carbonate-linkages along their polymer backbone chains. [68] Such resins proposed for SLA have largely been based on poly(propylene fumarate) (PPF), poly(trimethylene carbonate) (PTMC), poly(ε-caprolactone) (PCL), and poly(lactic acid) (PLA). [5a, 69] More recently, hydrogel structures based on natural or synthetic biodegradable polymers have also been printed by VP. [33-34, 60, 70]

The by-products of biodegraded polymers should be non-toxic and have little or no effect on the human body, but some biodegradable polymers (e.g., PCL) degrade into free acids that can cause inflammation or tissue necrosis when present in large amounts. Fortunately, oligomers that are functionalized with fumarates can be degraded *in vivo* into a non-toxic fumaric acid that is also present in the human body. As a result, fumarates are more suitable for clinical applications. [71] PPF is commonly used for bone graft applications, and PPF of lower molecular weight facilitates scaffold resorption by neobone formation. [72] PPF can also

be used to print precise scaffolds capable of supporting cell culture such as for angiogenesis. [47-48, 73] Since fumarates have relatively low reactivity, reactive diluents such as diethyl fumarate are often added to adjust the resin viscosity and increase the cross-linking density of the printed parts. [34, 74] An additional point of consideration for the design of biodegradable implants is the biodegradation rate of the polymer that should be well controlled; otherwise the degradation may occur too quickly due to autocatalytic hydrolysis, leading to a rapid loss of the structural integrity of the implant. Enzymatically degradable materials such as gelatin are favoured in this aspect because of their controllable degradation and the neutral products formed. [31]

The mechanical properties of natural tissues vary depending on the anatomical site; for example, the compressive modulus of human articular cartilage ranges between 0.25 MPa and 1 MPa, [75] while those of human trabecular bone varies from 3.5 MPa to 3000 MPa. [76] Therefore, the mechanical properties of tissue engineering scaffolds have to be tailored specifically for each application. [41] Two of the most critical factors affecting the mechanical properties of scaffolds is the type of oligomer used, and the ratio between the different oligomers if more than one oligomer is used. For instance, PLA copolymers formed with PEG (PLA-PEG-PLA) and PCL (poly(D,L-lactide-co-ε-caprolactone)) are suitable for soft and hard tissue engineering, respectively, because of the low modulus of PEG compared to that of PCL. [39, 50-51]

The mechanical properties of scaffolds vary with their cross-link density as well; a higher cross-link density generally leads to a higher modulus and lower toughness. The cross-link density can be increased by, for example, using larger amounts of reactive diluent, [48, 73] or using oligomers with a higher degree of functionality. The mechanical properties of scaffolds are also dependent on the scaffold structure (e.g., pore architecture, pore size and porosity), [39, 77] which can be readily designed and fabricated with AM. It is worthwhile to mention that the

architecture of a scaffold is also essential for cell migration, nutrient transport and waste removal, which are important for promoting cell expression. [48] As an example, scaffold pore size greater than 300 μm is generally required for osteogenesis to occur.

3.2.2. *Shape memory polymers*

Shape memory polymers (SMPs) are materials that undergo large, reversible shape change when triggered by an external stimulus such as temperature, electric field, moisture, or pH change. SMPs can be considered as copolymers consisting of two different molecular regions, with the hard and soft segments acting as netpoints and switches, respectively. The netpoints are what memorize the permanent shape and can be formed by physical or chemical cross-links, while switches allow temporary shape deformation and shape recovery. Shape recovery occurs upon exposure to stimuli as the strain energy stored in the temporary shape is released. [78]

Acrylate resins are one of the most widely studied materials for the development of SMPs. Mono-functional acrylate monomers that act as switches can be *tert*-butyl acrylate, 2-ethoxyethyl methacrylate, benzyl acrylate, and ethylene glycol phenyl ether methacrylate, etc. with *tert*-butyl acrylate being the most popular. [79] Netpoints are formed by multifunctional oligomers, also known as cross-linkers, which can be ethylene glycol acrylates, BPA ethoxylate acrylates, 1, 6-hexanediol diacrylate, etc. [80] As an example, Choong et al. used *tert*-butyl acrylate and di(ethylene glycol)-diacrylate as monomers and cross-linkers, respectively, to fabricate a buckminsterfullerene structure **(Figure 9a)**. [80b] The printed structure exhibited exceptional shape memory cycle life, with a 100% recovery and stability of the shape memory properties over 14 thermomechanical cycles.

The thermomechanical properties (i.e., T_g, storage modulus, loss modulus and strain at break) of SMPs are critical for the performance of active materials as they determine the shape

recovery temperature and rate, capability of shape change and actuation. The shape memory properties can be tailored by varying the type of monomers and cross-linkers used, [79] and by the ratio of the netpoints to switches, i.e., cross-link density. [83] A higher cross-link density enhances the shape fixity ability of the polymers, but reduces the shape recovery properties because of the increased stiffness. [83a]

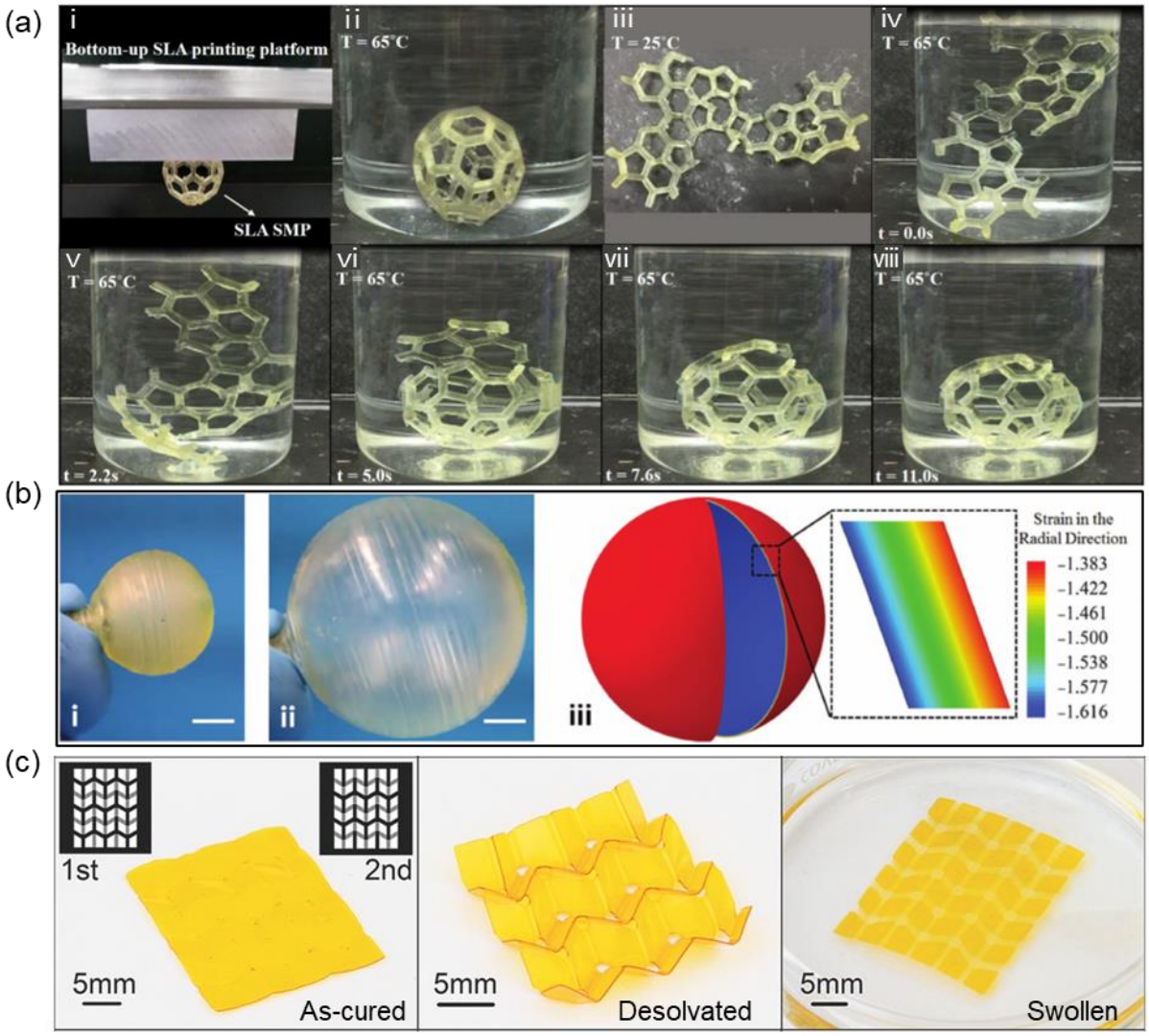

Figure 9. (a) Shape memory behavior of a thermo-responsive buckminsterfullerene structure fabricated via the SLA of *tert*-butyl acrylate-co-di(ethylene glycol)-diacrylate. Reproduced with permission. [80b] Copyright 2017, Elsevier. (b) A DLP-printed highly elastic balloon based on aliphatic urethane diacrylate and epoxy aliphatic acrylate, which can be inflated into three times the original size. Reproduced with permission. [81] Copyright 2017, Wiley. (c) A PEG diacrylate Miura pattern fabricated by DLP, exhibiting desolvation-induced folding. Reproduced with permission. [82] Copyright 2017, Wiley.

Polyurethane-based SMPs are more suitable for applications that involve much higher strains. [80c] Polyurethanes contain both hard and soft segments that serve as netpoints and switches. Thermoset polyurethanes are particularly popular because of their versatile polymer chemistry; the ratio of the soft to hard segments can be varied with ease to program the strain at break and the shape memory properties of the final part. However, thermoset elastomeric resins that are currently available on the market have values of strain at break below ~250%. [81] The strain at break can be increased by reducing the cross-link density, which, however, inevitably reduces the modulus. By introducing a secondary cross-link network where one of the polymer networks is based on reversible, non-covalent cross-links for shape recovery properties, the modulus and the strain at break can increase concurrently. This was exemplified by Patel et al. with a resin containing mono-functional epoxy aliphatic acrylate monomers and aliphatic urethane diacrylate oligomers, where the modulus and the strain at break (1100%) of the printed specimens increased concurrently with an increasing cross-link density **(Figure 9b)**. [81] Such elastomer systems can significantly enhance the capability of the VP process in fabricating deformable structures with sufficient strength for devices such as actuators, flexible electronics and acoustic metamaterials.

Hydrogels are also capable of exhibiting shape memory behavior. Several aqueous photosensitive resins have been developed for VP to construct shape memory hydrogel (SMH) structures that are thermo- (e.g., poly(N,N-dimethyl acrylamide-*co*-stearyl acrylate), moisture- (e.g., poly(ethylene glycol-*co*-2-hydroxyethyl methacrylate)), or chemical-responsive (e.g., alginate/polyacrylamide). [84] Moisture-responsive SMHs, for example, the PEG diacrylate-based SMH developed by Zhao et al., depend on the absorption/desorption (swelling/de-swelling) of solvents for shape memory effect **(Figure 9c)**, [82] whereas chemical-responsive SMHs rely on changes to the electrostatic interactions between polymer chains (e.g., pH or ion concentration change) for shape change. Owing to their soft nature, high hydrophilicity and

possible biocompatibility, SMH structures are desirable for stents, self-healing structures, and soft actuators. [85]

3.2.3. *Digital multi-materials*

Digital multi-materials refer to variable, automated mixtures of at least two resins that can be tuned to achieve desirable properties such as high stiffness, hardness and flexibility. [86] This is achieved by MJ processes owing to their capability in dispensing multiple materials in an accurate and controlled manner. With MJ, hybrid materials that are required for the fabrication of multi-functional structures or devices can be created. The advances in multi-material printing with MJ has boosted the recent developments in fabricating 4D structures, [80e, 87] microfluidic devices, [88] sensors, [89] and biomimetic composite structures.

4D structures can be fabricated with single materials that serve as both soft and hard segments as described in Section 3.2.2, or with multi-materials where each component act as either soft or hard segments. Unlike single-material 4D structures that only allow global shape change, multi-material 4D structures can realise localized shape changes. Digital multi-materials with varying glass transition temperatures T_g can be deposited at different structural sections, which allows the structures to demonstrate local and global, or spontaneous and sequential, shape changes upon heating. [90] A major challenge of 4D printing using digital multi-materials is the proper structural design and appropriate material choice that will allow the structures to transform into their pre-determined shapes. This involves complex material programming for a variety of joint designs for different purposes, and precise multi-material deposition.

Ge et al. developed printed active composite (PAC) structures that functioned similarly to SMP structures, but had significantly greater material complexity and architecture **(Figure 10a)**. [91] The PACs were layered composite structures consisting of hard and soft segments,

for example, an elastomeric polymer matrix (soft) that was embedded with glassy polymer fibres (hard) of predetermined orientation. The fibre loading and orientation affected the relaxed modulus and the shape memory behavior of the composite layers, and the strain mismatch between the printed composite layers was utilized to engineer the overall structure deformation. PACs can be used to develop thin-layer active hinges or smart objects with non-uniform curvature. The active hinges can be incorporated into the design of 2D sheets that self-assemble upon heating into 3D structures, and they are useful for tackling engineering issues related to storage and transportation such as the packing of large structures into small volumes. [91-92] Load-bearing, rapid self-morphing and reversible structures were also exemplified alongside origami and actuators of varying designs. [86]

In most cases, the permanent shapes of the structures are as-printed, and the temporary shapes are achieved after a programming step (e.g., heat-assisted mechanical deformation). The structures are reinstated to their permanent form upon shape recovery. Direct 4D printing through MJ simplifies this process by integrating the printing and programming steps into one: the printed shapes are temporary, while the actuated shapes are permanent. Ding et al. achieved this by printing laminated strips comprised of an SMP and a pre-strained elastomer; the pre-strain is built-in the elastomer by controlling the printing parameters such as the temperature and the irradiation intensity **(Figure 10b)**. [93] Upon heating, the printed strip then relaxes and recovers into its permanent shape.

Most SMPs have high moduli and fast response rates, but they only undergo one-way actuation; each shape change must be manually re-programmed. In contrast, SMHs can undergo reversible shape change (swelling or de-swelling) via solvent absorption and desorption, but their low moduli and slow response rates limit their applications. By combining typical SMPs and SMHs, their properties can complement each other to produce stiffer structures with two-way actuation capability and a controllable rate of deformation. This was

demonstrated by Mao et al. with a two-way reversible actuator that had a hydrogel layer sandwiched between the SMP and the elastomer layers **(Figure 10c)**. [86] The swelling of the hydrogel layer was used as the driving force for shape change, while the temperature-dependent modulus of the SMP layers was used to regulate the rate of the shape change. Bending occurred due to the difference between the moduli of the SMP and the elastomer. By cooling the bent actuator, the shape was retained even after the removal of water. The linear shape of the actuator was then re-obtained by heating the dried structure above its T_g, and this reversible actuation cycle could be repeated.

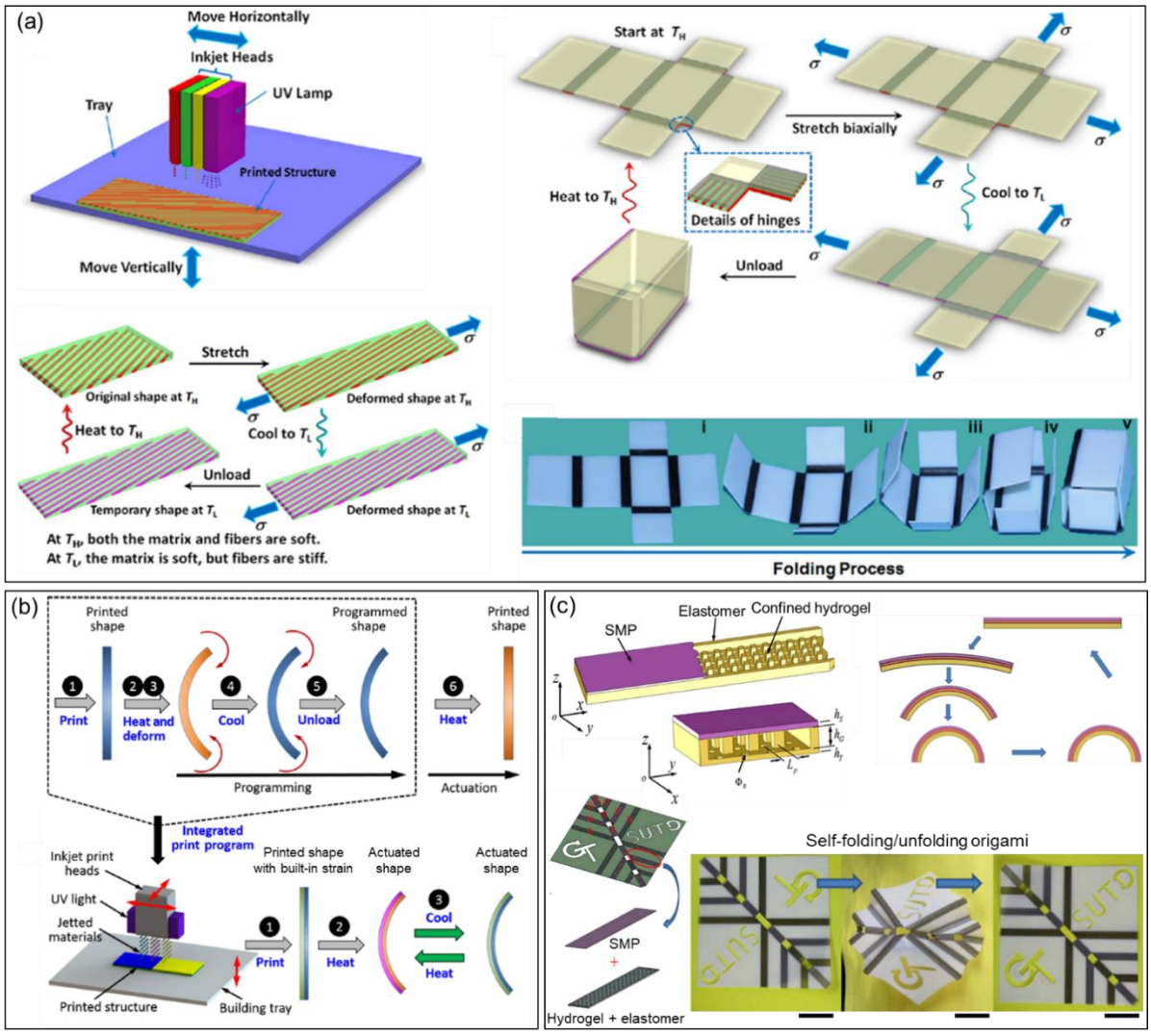

Figure 10. (a) Schematic of the PolyJet printing of a PAC with the coloured inkjet heads representing the printing of different materials, and illustrations of the shape memory cycle of

a self-folding box. Reproduced with permission. [91] Copyright 2013, AIP Publishing. (b) Schematic of the steps required to print shape memory structures using a typical 4D printing (top) and direct 4D printing (bottom) of SMPs. Reproduced with permission. [93] Copyright 2017, AAAS. (c) A self-folding origami where the hinges were made from a combination of SMP and hydrogel structures that were fabricated using PolyJet. The origami can undergo two-way reversible actuation (scale bars represent 45 mm). Reproduced with permission. [86] Copyright 2016, Springer Nature.

Multi-material printing is also excellent for fabricating composite structures, where one material serves as the matrix and the other as the reinforcement. [94] This is particularly useful for composites with biomimetic topologies that are difficult to fabricate even by typical AM processes due to the precise and complex composite architecture involved. When further combined with modeling, MJ can be used to fabricate composite materials with tailored mechanical properties such as fracture strength. [95]

3.3. Photosensitive composite resins

The continuous expansion of the photosensitive resin market for VP processes has prompted extensive research on the development of new types of resins. Composite resins with microfillers or nanofillers have been developed not only for enhanced mechanical properties and functionalities (e.g., biocompatibility, piezoelectricity and magnetism) of printed parts, but also for reduced part shrinkage upon polymerization. [96] Photopolymerizable suspensions of ceramic powders have also been popularized for an indirect fabrication of ceramics.

A critical consideration for composite resins is the effect of filler addition on their optical properties. [97] The filler chosen should contribute minimally to scattering and be sufficiently transparent to incident radiation to ensure an acceptable cure depth of the resin. Scattering-induced turbidity limits the penetration depth and cure depth of the resin; although in some cases, scattering increases the interaction path length, thus increasing the probability of a photon initiating the polymerization. [98] The scattering effects of a filler depend on its size and concentration, and the difference in refractive index between the filler and the resin. [99] When

metal particles are dealt with, their high reflectivity in the UV-visible range deprives the photosensitive resin of incident energy, making the resin more difficult to process. [100]

Filler loadings have to be carefully controlled to minimize the increase in viscosity, which impedes the recoating process during printing and reduces the molecular mobility, thus slowing down the diffusion of active centers and reducing the polymerization rate. The challenge of processing viscous resins can be addressed by increasing the processing temperature. [101] Another solution to overcome the large increase in resin viscosity upon filler addition is to use nanofillers. Owing to their high surface-area-to-volume ratio, nanofillers offer significant property enhancements at low loadings, and can be used in much smaller quantities than microfillers. The small size of nanofillers also ensures that the minimum layer height achievable is unaffected. To avoid the challenge of an increased resin viscosity in fabricating composite parts, the in situ generation of nanoparticles is a novel solution. [102] The precursor to the nanofillers (e.g., silver nitrate) is added into the resin formulation, and a part containing the precursor is printed by VP; the part is subsequently post-processed to generate the nanoparticles, forming the final composite part.

The filler requirement for MJ is more stringent as the use of nozzles (typically 60 μm) restricts the filler size to ~5 μm. Moreover, the addition of fillers can dramatically change the droplet-forming behavior of the resin, leading to the formation of irregularly shaped droplets that negatively affect build accuracy. [38, 103] Since the agglomeration and sedimentation of fillers may occur, their sedimentation rate should be sufficiently slow to ensure their homogeneous distribution from resin storage to the entire print process. [104]

Photosensitive composite resins for VP and MJ will be discussed according to the type of fillers and their applications, with a focus on bioactive fillers, functional fillers with thermal and electrical conductivity, dielectricity, and magnetism, etc. and photopolymerizable ceramic suspensions.

3.3.1. *Bioactive fillers*

VP has been widely used for biomedical applications due to its capability in fabricating accurate and intricate structures that are required of scaffold implants **(Figure 11)**. Biocompatible and/or biodegradable polymers are available and have been widely studied for

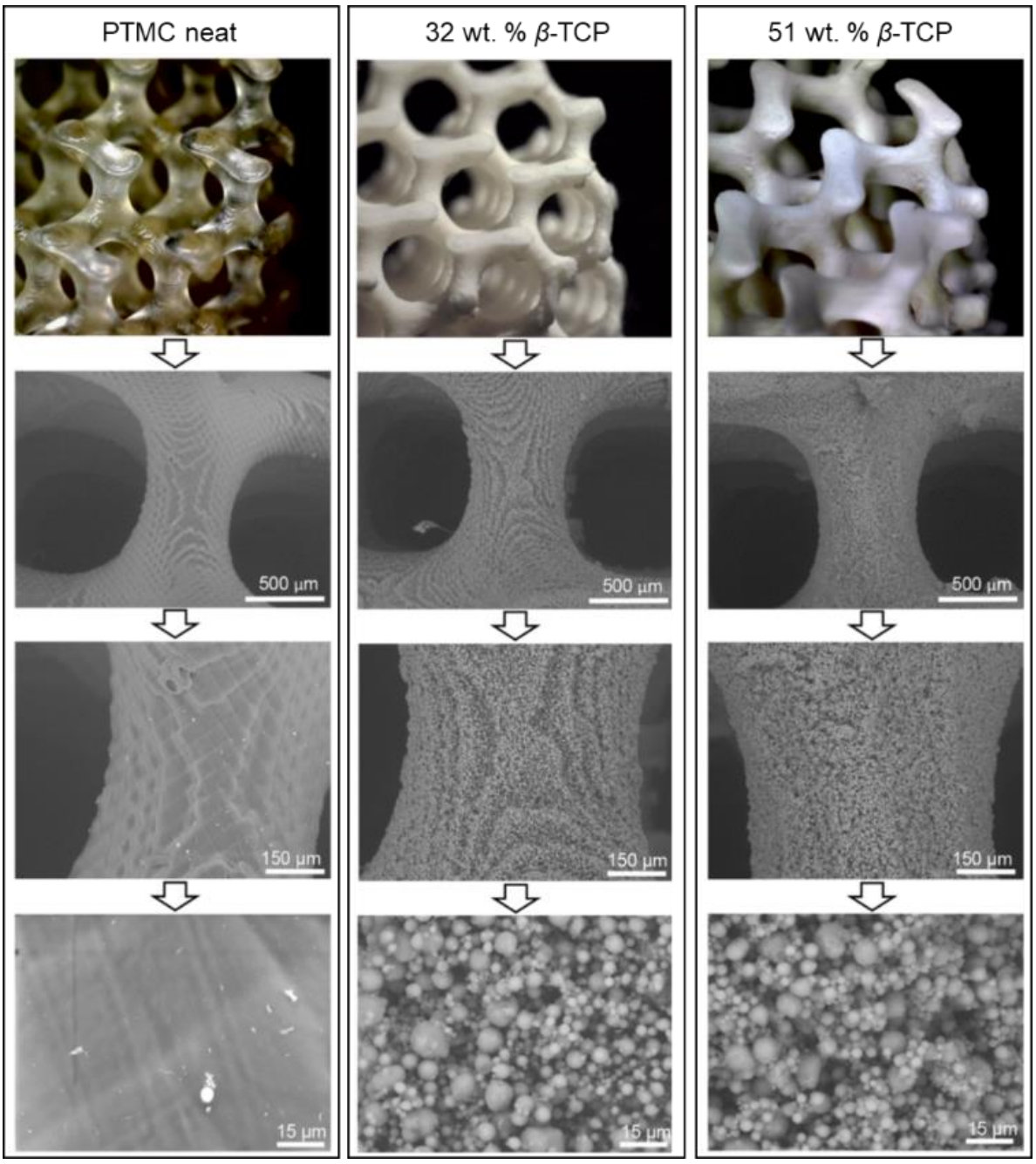

Figure 11. PTMC scaffolds with 0, 32 and 51 wt% *β*-TCP, fabricated by DLP. The topographical roughness is formed by the *β*-TCP particles. Reproduced with permission. [106] Copyright 2019, ACS.

tissue engineering and cell culture applications, and their biological performance (e.g., hydrophilicity, cell attachment and cell proliferation) can be further enhanced by adding bioactive fillers. [52] Ceramic fillers, in particular calcium phosphates (e.g., hydroxyapatite (HA), tricalcium phosphate (TCP) and bioactive glass (BAG)), [105] are the most popular because they are known osteoconductive materials and have been widely used for bone grafting procedures. [5b, 17] Materials such as growth factors and other biomaterials can also be incorporated. [49]

In conventional methods such as salt leaching, fillers in scaffolds are covered by a layer of polymer material, limiting their exposure to biological fluids. However, with VP, it is possible to fabricate scaffolds that have fillers that are homogeneously distributed on their surfaces. This allows for greater interaction between bioactive fillers and biological fluids, thus enhancing the bioactivity, cell attachment and proliferation of composite scaffolds. [107]

3.3.2. *Other functional fillers*

Functional fillers that can impart thermal and electrical conductivity, dielectricity, and magnetism properties have also been widely studied for photosensitive resins. [108] Carbon nanofillers such as carbon nanotubes (CNTs) are attractive fillers and have been incorporated into different photosensitive resins due to their high tensile moduli and strength; [109] it was reported that with an addition of 0.25 wt% CNT, the tensile stress and strain at break of the fabricated specimens increased by 70% and 46%, respectively. [109c] Improved electrical and thermal properties are also attainable using carbon nanofillers such as multi-walled CNTs (MWCNTs) and graphene. [110]

Dielectric materials are popular for strain sensors, actuators, and flexible electronics. Photosensitive resins incorporating dielectric nanoparticles can be used to fabricate piezoelectric polymer architectures, which are ideal for applications in flexible devices and

small active elements. As with many other composite resins, the interfacial interactions between the fillers and the polymer matrix is critical in determining the functional properties of fabricated parts. Kim et al. demonstrated that nanoscale interfacial tuning shows great promise. [111] They developed a barium titanate/polyethylene glycol diacrylate (barium titanate/PEGDA) resin for a microscale DLP process using barium titanate particles that were modified with photosensitive surface groups (m-$BaTiO_3$), and the printed parts showed significantly enhanced piezoelectric output. The modified nanoparticles were grafted onto the polymer backbone chains directly upon photopolymerization, thus enhancing the mechanical-to-electrical conversion efficiency of the composites by 10 times more than that of those fabricated with unmodified barium titanate. This nanoscale interfacial tuning method can be extended to other composite materials for the fabrication of functional components with significantly enhanced functionalities.

To realise engineered structures with unique properties, control over the spatial arrangement of fillers within a polymer matrix is desired. External field- (e.g., electric, magnetic and ultrasound) directed particle orientation is a viable solution as it enables the quasi-instantaneous organization of large quantities of fillers into pre-defined patterns within low-viscosity resins. [112] Martin et al. established 3D magnetic printing, an SLA-based process that utilizes magnetic fields to orient anisotropic magnetic particles during part fabrication, which allows highly-customized particle orientation **(Figure 12a)**. [113] The process was used to align alumina particles magnetized with iron oxide nanoparticles to fabricate biomimetic composite structures that showed exceptional mechanical behavior **(Figure 12b)**. Similarly, Yang et al. fabricated nanocomposite structures with biomimetic anisotropic reinforcement architectures by controlling the alignment of MWCNTs using an electric field **(Figure 12c)**. [114] An engineered composite structure that mimicked the structure of the human meniscus

demonstrated a significant increase in tensile strength from 8.7 MPa (pure polymer) to 176 MPa (circumferential modulus) and 143 MPa (radial modulus).

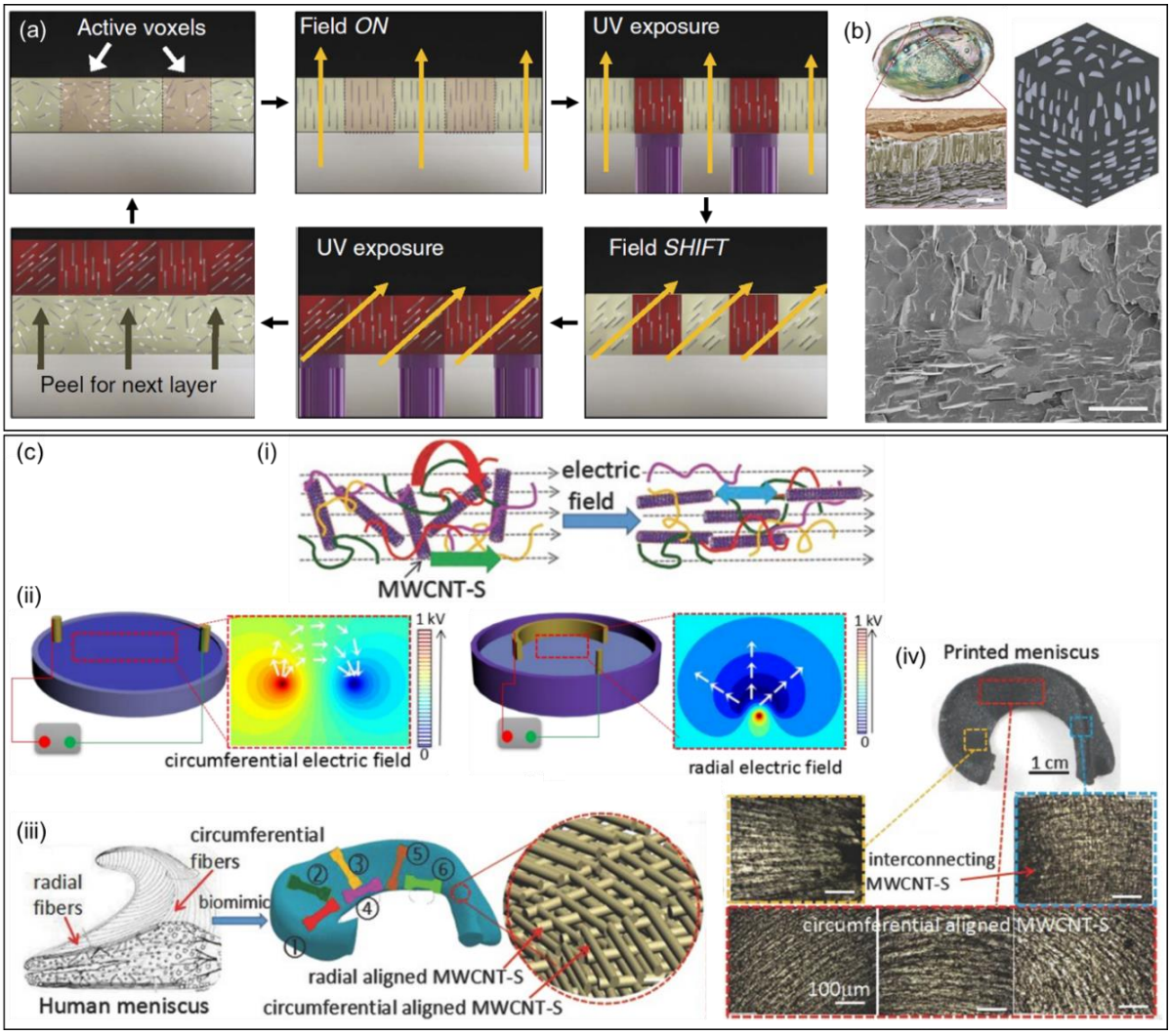

Figure 12. Magnetic field-assisted DLP: (a) the schematic of the 3D magnetic printing process and the programmed alignment of magnetic fillers, and (b) reinforcement architecture inspired by abalone shells and the SEM image of the fabricated composite structure. Reproduced with permission. [113] Copyright 2015, Springer Nature. (c) Electrical field-assisted DLP: (i) the schematic of the programmed alignment of MWCNTs using an electric field; (ii) the electric potential lines for the circumferential and radial alignment of MWCNTs; (iii) the schematic of fiber alignment in a human meniscus and (iv) a DLP-printed meniscus with the circumferential and radial alignment of MWCNTs. Reproduced with permission. [114] Copyright 2017, Wiley.

3.3.3. *Photopolymerizable ceramic suspensions*

The use of a VP process to fabricate ceramic components is often termed as ceramic stereolithography. A highly concentrated ceramic suspension typically containing 40–55 vol%

ceramic powders is first used to print a green AM part via a VP process. The green part is then post-processed to remove the polymer component, leaving only the ceramic component in the final part **(Figure 13a, b)**. [115] This method is extensively applied for ceramic part fabrication because of the advantages of a high dimensional resolution and precision. [116]

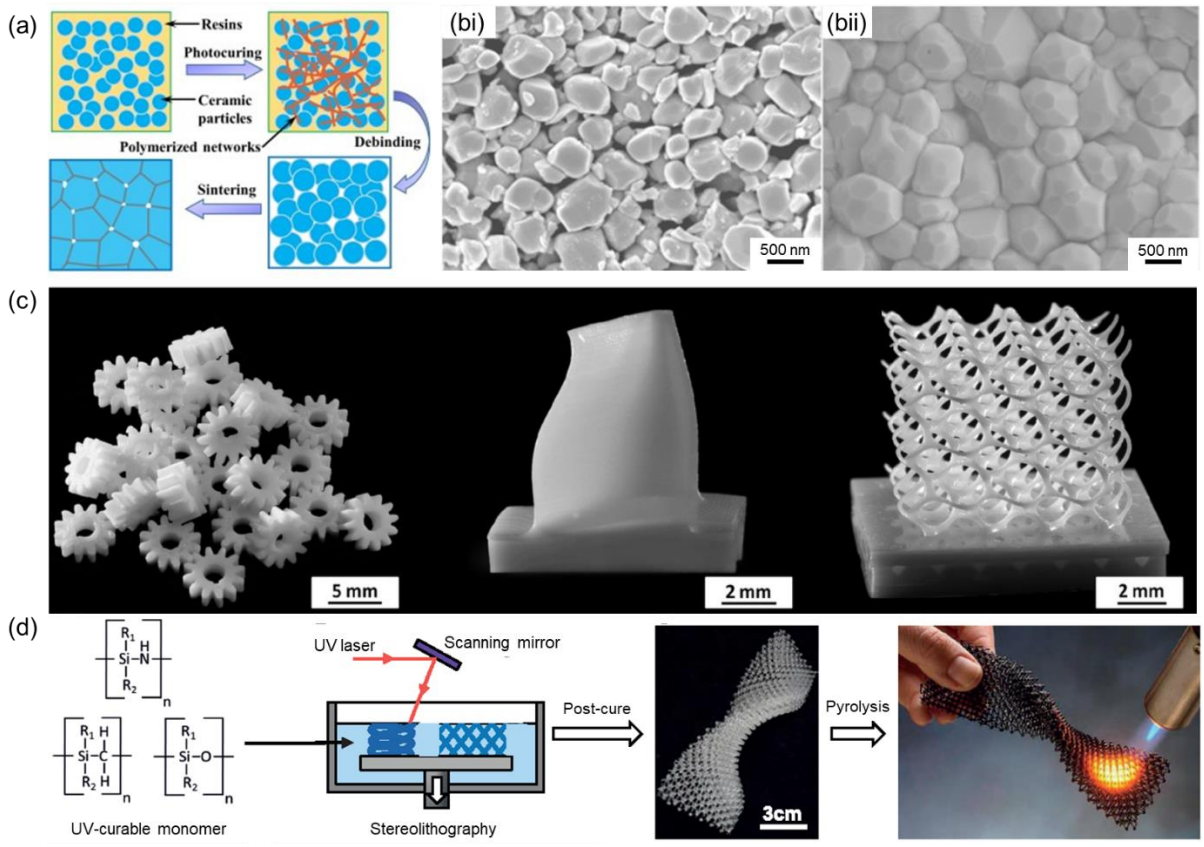

Figure 13. Ceramic stereolithography process: (a) the schematic of the process mechanism, and (b) the SEM images of a green barium titanate ceramic part after (i) debinding and (ii) sintering. Reproduced with permission. [115] Copyright 2020, Elsevier. (c) Sintered alumina parts, from left to right: gear wheels, turbine blade, cellular cube. Reproduced with permission. [116] Copyright 2014, The American Ceramic Society. (d) Schematic of the ceramic stereolithography process using a preceramic polymer precursor. Reproduced with permission. [117] Copyright 2016, AAAS.

The resin suspension needs to be carefully developed since a high loading of ceramic particles aggravates light scattering and affects the cure depth of the composite resin. Nevertheless, this indirect fabrication method has been successfully applied to produce biomedical implants, prototypes, cellular ceramics, and complex investment casting cores

(Figure 13c). Ceramics that have been used include alumina, zirconia, refractory silica and HA among many others. [118] The recent development of preceramic polymer precursors that can yield ceramic parts upon pyrolysis may serve as a good alternative for fabricating silicon- and carbon-rich ceramic structures, since the use of highly loaded suspensions can be avoided **(Figure 13d)**. [119]

Polymer composite resins compatible with VP processes have been developed to utilize the unique properties of fillers such as bioactivity, thermal stability piezoelectricity and mechanical strength. Nanofillers have proved to be a huge advantage because of their low loading required, which has a small impact on the resin viscosity. The composite reins that have been studied for VP in recent years and their applications are summarized in **Table 3**.

Table 3. Composite resins that have been studied for VP in recent years and their applications.

Filler		Monomer/Oligomer	Filler size (μm)	Filler loading	Viscosity (Pa·s)	Purpose	Reference
Bioactive filler	HA	PPF	0.55	7% (w/w)	-	Osteogenesis	[105a]
		PLA methacrylate	< 0.2	5–20 wt%	4.69–14.61	Osteogenesis	[105b]
		Oligocarbonate methacrylate	1	30 wt%	-	Osteogenesis	[120]
		PTMC methacrylate	0.2–0.4 (length)	10–40 wt%	57.5–71.9	Osteogenesis	[105c]
	BAG	PCL methacrylate	< 45	5–20 wt%	-	Osteogenesis	[107]
Functional filler	MWCNT	DSM Somos® WaterShed™	5–20 (length)	0.05% (w/v)	0.26	Mechanical reinforcement	[109b]
		DSM Somos® WaterClear™	5–20 (length)	0.5% (w/v)	0.13	Mechanical reinforcement	[109b]
	GO	EnvisionTEC Pic 100	0.3–10 (diameter)	0.2–0.5 wt%	-	Mechanical reinforcement	[109a]
	$Al_{59}Cu_{25.5}Fe_{12.5}B_3$	Accura Si40®	< 25	20–40 vol%	12	Mechanical reinforcement	[100]
	Cellulose nanocrystal	Cycloaliphatic epoxide	220 (length)	0.5–10% (w/w)	0.1–0.9	Mechanical reinforcement	[121]
	TiO_2	Epoxy diacrylate	0.03	0.1–2%	0.31–0.46	Mechanical, thermal reinforcement	[97]
	Surface-modified SiO_2	HSL1	-	1–5 wt%	0.4–0.75	Mechanical, thermal reinforcement	[122]
	$BaTiO_3$	PEG acrylate	-	1–10 wt%	-	Piezoelectric device	[111]
	Polyvinylidene fluoride	1,6-hexanediol acrylate	-	15–35 wt%	< 200	Piezoelectric device	[108a]
	Fe_3O_4	EnvisionTEC R11	0.05	25 wt%	-	Flow sensor	[96a]
	CNT	Acrylic ester	-	0.5–1.5 wt%	-	Radar absorbing material	[108b]
	$AgNO_3$	PEG acrylate	-	15 phr	-	Electrically conductive structure	[102]
	Diamond	BV-001	2–4	10–30% (w/v)	-	Thermally conductive heat sink	[123]
	Magnetized Al_2O_3	Urethane/isobornyl acrylate	7.5 (diameter)	15 vol%	-	Biomimetic architecture	[113]
	Montmorillonite	CYRACURE UV-6105	-	0.3–1 wt%	-	Functional prototype	[28a]
	Boehmite	CYRACURE UV-6105	-	5 wt%	-	Functional prototype	[28b]
Photopoly-merizable ceramic suspension	$BaTiO_3$	EnvisionTEC SI500	1	30–80 wt%	-	Piezoelectric device	[124]
	Al_2O_3	Acrylamide	0.05–9	65 wt%	-	Ceramic stereolithography	[125]
		Formlabs FLGPCL01	0.7–2.5	3–40 vol%	-	Ceramic overhanging structure	[126]
	ZrO_2	Acrylamide/methylenebisacrylamide	0.2	40 vol%	0.127	Ceramic dental bridge	[118b]
	Y_2O_3-stabilized ZrO_2	1,6-hexanediol diacrylate	0.81–1.09	19–27 vol%	2.5	Ceramic stereolithography	[118a]

4. Thermoplastic powders

Thermoplastics soften or melt upon heating, and solidify upon cooling. This characteristic allows thermoplastics to be remolded and recycled. Thermoplastics are further classified into amorphous and semi-crystalline thermoplastics. Amorphous thermoplastics such as polystyrene (PS) and polycarbonate (PC) have randomly ordered molecular structures that impart flexibility to the material. They have glass transition temperatures T_g above which they slowly soften and transform into a glassy state. Amorphous polymers do not have a defined melting temperature T_m. In contrast, semi-crystalline thermoplastics such as polyamides (PAs) have both T_m and T_g that correspond to the crystalline and amorphous regions, respectively. The viscosity of a semi-crystalline thermoplastic rapidly decreases as it changes from the solid to the viscous liquid phase when heated above its T_m value. Thermoplastics and their composites in powder form can be processed by the PBF technique, of which SLS and MJF are two major processes. As both processes are largely similar in terms of their sintering mechanism and material requirements, discussions in the following sections only use SLS as an example for clarity purposes.

In SLS, the consolidation of amorphous and semi-crystalline thermoplastic powders occur by heating them above their T_g and T_m values, respectively. [4, 14d] Upon the initial softening of a material, two adjacent polymer particles form a neck at the contact surface. Subsequently, the neck grows while the intermediate liquid-air interface disappears under the action of surface tension. The particle doublet then gradually transforms into a single sphere. The particle coalescence process can be described by the modified Frenkel-Eshelby model, which assumes the isothermal condition and that two ideal spherical particles can flow and coalesce as a function of time: [127]

$$\frac{x(t)}{a(t)} = \sqrt{\frac{\gamma t}{a_0 \eta}}\,. \tag{3}$$

In equation 3, $x(t)$ and $a(t)$ are the radii (m) of the neck and the powder particle as a function of sintering time t (s), respectively; a_0 the initial radius (m) of the particle; γ and η the surface tension (N/m) and viscosity (Pa·s) of the polymer, respectively. This model applies only to the initial sintering stages when the particle radius remains relatively constant. In this analytical model, the sintering process is driven by surface tension and counteracted by viscous dissipation. [128] The sintering kinetics of a polymer material is also likely affected by its viscoelastic effects, whereby a decreased relaxation time can slow down the sintering process. [128] Investigations on the sintering mechanism and kinetics of polymer powder particles are still ongoing.

4.1. Material requirements

Polymer powders used for the SLS process must be able to absorb energy at the laser wavelength efficiently. During the laser scanning process, only a fraction of the laser energy is absorbed by powder particles on the powder bed surface, because of laser reflection and refraction at the particle interfaces and laser transmission through the particles. CO_2 lasers are the most used in commercial SLS systems because most polymers contain C-H bonds that absorb well at the laser wavelength of 10.6 μm. When lasers of other wavelengths or different irradiation sources are used, appropriate light absorbers may be required to ensure sufficient absorbance. For the MJF process where IR lamps are used to scan across a powder bed in a line-wise manner, the selective sintering of powder particles is enabled by the selective deposition of a fusing agent that improves the absorptivity of powder particles to IR irradiation. An implicit requirement of powders for MJF is that in the absence of a fusing agent, they should have low absorption throughout the IR range to avoid unwanted sintering.

The thermal properties of a polymer are crucial for its successful application in SLS. During the SLS process, polymer powders are preheated to a bed temperature T_b as close to the

melting temperature T_m of semi-crystalline polymers or the glass transition temperature T_g of amorphous polymers as possible, to lower the laser energy required to melt or sinter them Nevertheless, for a semi-crystalline polymer, its T_b value should not be larger than its onset melting temperature $T_{m,\ onset}$ to avoid the premature melting of its powder particles that would lead to powder caking **(Figure 14)**. The preheating of the powder bed also serves to reduce the temperature gradient between its sintered and unsintered regions, thus mitigating the non-uniform shrinkage of sintered parts, especially at the part contours.

For a semi-crystalline polymer, the control of its powder bed temperature T_b between its onset crystallization temperature $T_{c,\ onset}$ and onset melting temperature $T_{m,\ onset}$ is especially important for suppressing the crystallization of its melt for as long as possible during the part fabrication process, as the premature crystallization of sintered layers would lead to part warpage and curling. This metastable thermodynamic region of a polymer melt, $T_{m,\ onset} - T_{c,\ onset}$, is termed the 'sintering window', [129] and is a critical thermal parameter to be considered when the sinterability of semi-crystalline polymers is evaluated **(Figure 14)**.

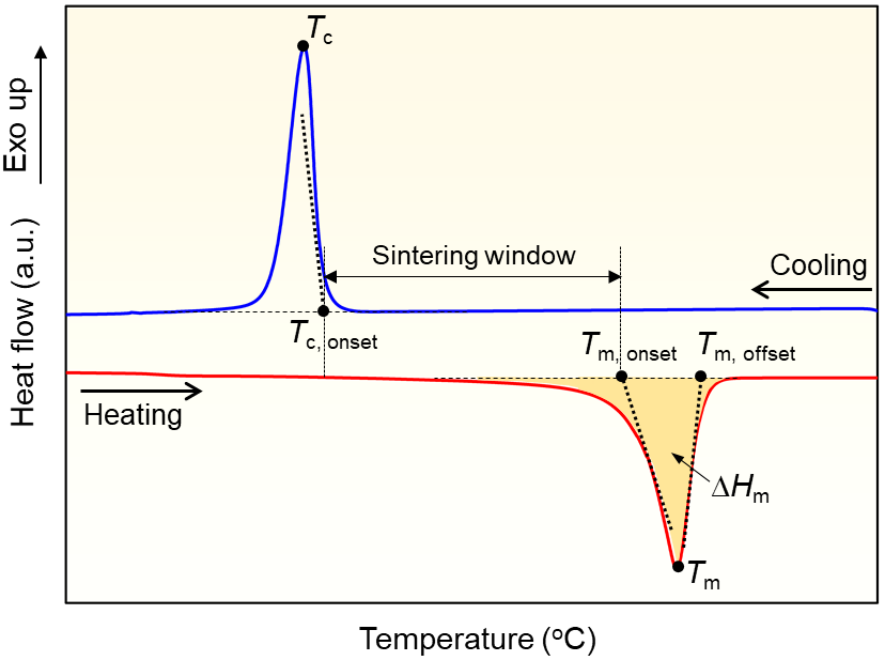

Figure 14. Dynamic DSC curve of a polymer and the parameters for evaluating its sinterability.

The sintering window is normally characterized by dynamic differential scanning calorimetry (DSC) at heating and cooling rates of 10 ºC/min, although the real rate of temperature change during SLS is determined by complex factors and is hardly controllable. As crystallization is a kinetic process, the measured $T_{c,\ onset}$ value depends on the cooling rate used, where a slower cooling rate induces a higher $T_{c,\ onset}$ value, which implies that during the timescale of the SLS process, crystallization may occur even if the T_b value is slightly above the $T_{c,\ onset}$ value obtained through the standard DSC procedure. Thus, a large difference between the T_b and $T_{c,\ onset}$ values is desirable to minimize such crystallization. The large difference also allows great temperature fluctuations that inevitably occur in the printing chamber, without any local temperature going below its $T_{c,\ onset}$ value. Isothermal DSC can be applied to mimic the quasi-isothermal crystallization conditions at a given temperature near the T_b value, and provide additional information on the actual $T_{c,\ onset}$ value in the SLS process.

Polymers that have wider sintering windows are favored over those that have narrower sintering windows. As a reference for the development of new materials, the most popular commercial SLS powder, polyamide 12 (PA12), has a sintering window width in the range of 20–30 ℃.

The crystallization kinetics of a polymer, which characterizes its time- and temperature-dependent crystallization behavior, has a great influence on the part warpage and curling during SLS processing. Drummer et al. introduced the use of crystallization activation energy as an indicator to evaluate the sensitivity of the crystallization behavior of a polymer toward temperature changes. [130] Polymers with higher crystallization activation energy, such as polyoxymethylene (POM), are more sensitive to small temperature change, i.e., more prone to fast crystallization even at a temperature slightly below their crystallization temperature, and thus are extremely susceptible to warping and more difficult to process. [130]

The melting range from the onset melting temperature $T_{m,\ onset}$ to the offset melting temperature $T_{m,\ offset}$ is also crucial for the sintering process. A polymer with a narrow melting range and a sharp melting peak is preferable because an ideal powder bed temperature T_b should be close to T_m but lower than $T_{m,\ onset}$, as previously discussed. Furthermore, a polymer with a wide melting range contains crystals with lamellae that vary significantly in thicknesses, and some lamellae are so thin that their melting temperatures are lower than the T_b value used. Such lamellae would soften or even melt prematurely to cause powder caking.

Specific heat capacity, defined as the energy required to induce a unit change in temperature for a unit mass of material, is a fundamental property to be considered for an SLS material as it is related to the amount of energy needed for sintering. The melting enthalpy ΔH_m of a semi-crystalline polymer, which is related to the specific heat capacity and can be calculated from the area under the endothermic peak in the DSC curve **(Figure 14)**, is a parameter that is more commonly used for powder evaluation. A high ΔH_m value is desired during the sintering process mainly because of the increased thermal threshold of powder particles adjacent to the sintered region against undesirable melting, since more energy would be required. As a result, the unintended melting of nearby powder particles can be minimized, and the dimensional accuracy of the printed parts can be increased.

The shrinkage of a polymer upon cooling from its softened or melt state is another factor that determines the warping tendency of printed layers during SLS. For amorphous polymers, shrinkage is mainly due to thermal contraction, which is influenced by their temperature-dependent coefficients of thermal expansion. In contrast, the shrinkage of semi-crystalline polymers is not only due to thermal contraction, but also crystallization shrinkage. Semi-crystalline polymers usually undergo large shrinkage upon crystallization, which aggravates the warpage issues during sintering. In contrast, amorphous polymers that have much lower shrinkage tend to curl less during sintering. [131] Polymer shrinkage can be measured by

volumetric dilatometry and is related to the degree of crystallinity of the polymer and its coefficient of thermal expansion; the higher the degree of crystallinity, the larger the shrinkage expected. For instance, PAs have relatively low shrinkage (3–5%) compared to highly crystalline polymers such as high-density polyethylene (HDPE), which shrinkage can go up to 13%. [131-132]

The rheological behavior of polymers is another essential consideration for SLS. Since the particle coalescence and flow of polymer melts in the SLS process proceed without external forces, according to the Frenkel-Eshelby model, the surface tension γ and zero-shear viscosity η_0 of a polymer are the most important parameters. Because the γ values of various commercial SLS polymer powders at operating temperatures vary only within an order of magnitude, it is currently assumed that differences in their particle coalescence behavior is dominated by η_0. [133]

Polymers with lower zero-shear viscosity η_0 have higher coalescence rates and can thus be printed into parts of higher density and strength within a given time frame. [127] In contrast, if η_0 is high, voids and air traps can remain in the printed part, reducing the achievable tensile strength. [14b] Therefore, polymers with low η_0 at the processing temperatures are desired. The η_0 value of a polymer is usually measured with cone-plate or parallel-plate rheometers, although the melt flow index is occasionally used as a rough reference. The viscosity of polymers generally follow the Arrhenius relationship and change rapidly with temperature. [132-133] As temperature increases, the viscosity of amorphous polymers such as acrylonitrile butadiene styrene (ABS) gradually decreases when $T > T_g$; in contrast, semi-crystalline polymers such as PA12 exhibit a rapid decrease in viscosity when $T > T_m$. For reference, the η_0 value of PA12 estimated by extrapolation is 1,400 Pa·s at 210 °C. The coalescence of polymer powder

particles is frequently studied by hot stage microscopy where a visual representation of the sintering process can be obtained. [127]

The physical state of polymer particles at the microscopic level, i.e., particle shape, size and size distribution, has a decisive effect on the powder flow behavior and powder packing density at the macroscopic level, which influences the deposition of a thin, dense, and smooth layer of powder that is required for SLS.

For a good powder flow and high powder packing density, spherical or potato-shaped powder particles with a narrow Gaussian distribution are desired. The ideal particle size range is 20–80 μm. [4, 134] Powder flow is enhanced with low inter-particle adhesion and friction, which is facilitated with spherical or near-spherical particles as they ensure minimal contact between particles. [135] With a Gaussian powder particle size distribution, voids between larger particles can be filled by those that are smaller, which allows a high powder packing density to be achieved. Smaller particles have a faster particle coalescence rate according to equation 3, and thus have a faster sintering rate despite having the same melting temperature as larger particles, which favors a higher part density achievable. Smaller particles also allow lower layer thickness to be used, thus reducing the stair-stepping effect, particularly in the printing of inclined or curved surfaces, and improving the surface quality achieved. [4, 14c] However, there lies a lower limit for the particle size as particles that are too small are difficult to spread due to static forces and particle coagulation. [134a] Furthermore, such too small particles are more likely to soften or even melt prematurely to induce powder caking when a high powder bed temperature is used, especially for a polymer with a wide melting range, because they have a faster sintering rate. [4]

A standardized method for characterizing powder flow behavior during the SLS process has not yet been developed. [136] Powder flowability can be evaluated under static and dynamic conditions, but the parameters used are valid only for the particular flow field applied during

the measurement. [131] The Hausner ratio (HR), the angle of repose, and the flow rate through an orifice are common indices used to assess powder flowability. Owing to the ease of measurement, many studies have used HR, defined as the ratio between the tapped and bulk density values, to gauge powder flowability; powders with HR $\leq$ 1.25 are considered free-flowing. Powders with good flowability would also exhibit low angles of repose and high flow rate through the orifice. The revolution powder analyzer, which analyzes the avalanche behavior of powders as they rotate in a sample drum, is considered a more suitable powder flowability measurement method since the temperature, dynamic and stress conditions similar to those in SLS can be imposed. [131, 137] Since the mechanical movement of film applicators are similar to that of recoaters, they can be used to simulate powder deposition. Using a film applicator that is modified with a weighing balance and a measurement plate, the mass of the powder spread over a known layer volume can be measured. [131] The layer density, which provides a quantitative measure for powder flowability, can then be calculated.

The key material requirements for SLS are summarized in **Figure 15**. They can be classified into intrinsic and extrinsic properties. The intrinsic properties include the optical, thermal, and rheological properties, while the extrinsic properties include the size, shape and size distribution of the powder particles. The intrinsic properties are determined by the chemistry and molecular structure of the polymer and are not easily influenced by external factors, whereas the extrinsic properties are largely controlled by powder production processes.

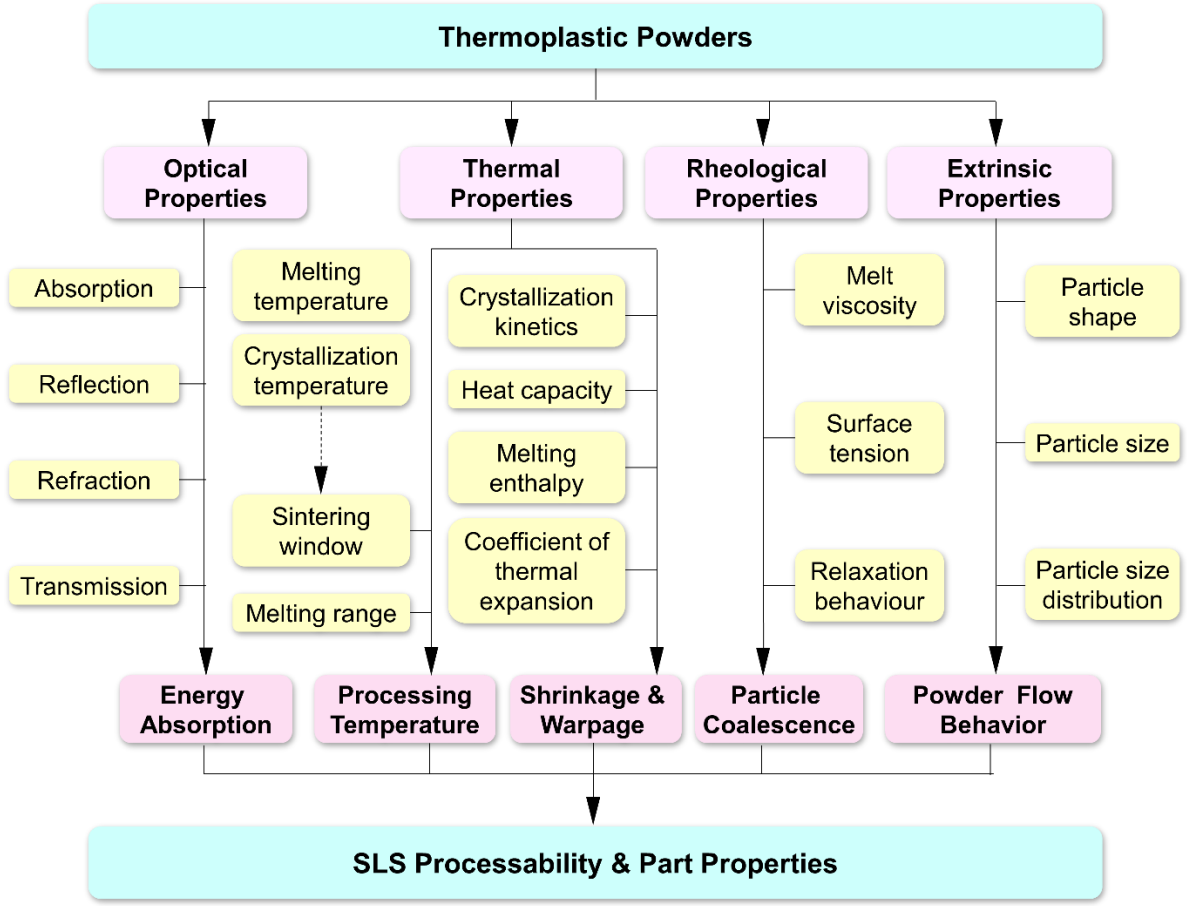

Figure 15. Key properties of a powder material and their influences on SLS processability and part properties.

4.2. Pure polymer powders

As a result of the stringent requirements that polymer powders must fulfill to be suitable for SLS, the variety of SLS materials available currently is incomparable to those for conventional manufacturing methods. The SLS polymer market (1,500 tons per year) is only 1/200,000th that of the entire polymer market today, with the cost of SLS polymer powders being as high as 30 times that of their conventional counterparts. [133]

Amorphous and semi-crystalline polymers have been studied for SLS, with the latter being more popular. Semi-crystalline polymers that have been investigated vary from commodity polymers to engineering polymers and high-performance polymers **(Figure 16)**. Although several polymer powders have been commercialized, most of them are limited to laboratory

investigation and reported in scientific literature. The most widely used SLS materials are engineering polymers based on PAs, with PA12 making up ~90% of the SLS material market despite taking up only 8% of the global polymer market share. [4, 14d, 134a] Other engineering polymers include polyesters (e.g., poly(butylene terephthalate) (PBT) and poly(ethylene terephthalate) (PET)), polyethers (e.g., POM) and thermoplastic elastomers (TPEs). Commodity polymers, such as polypropylene (PP), polyethylene (PE) (e.g., low-density PE (LDPE), HDPE and ultra-high-molecular-weight PE (UHMWPE)), and high-performance polymers, such as polyether ether ketone (PEEK), polyether ketone (PEK), polyether ketone ketone (PEKK) and poly(phenylene sulfide) (PPS), are gaining increasing attention for SLS.

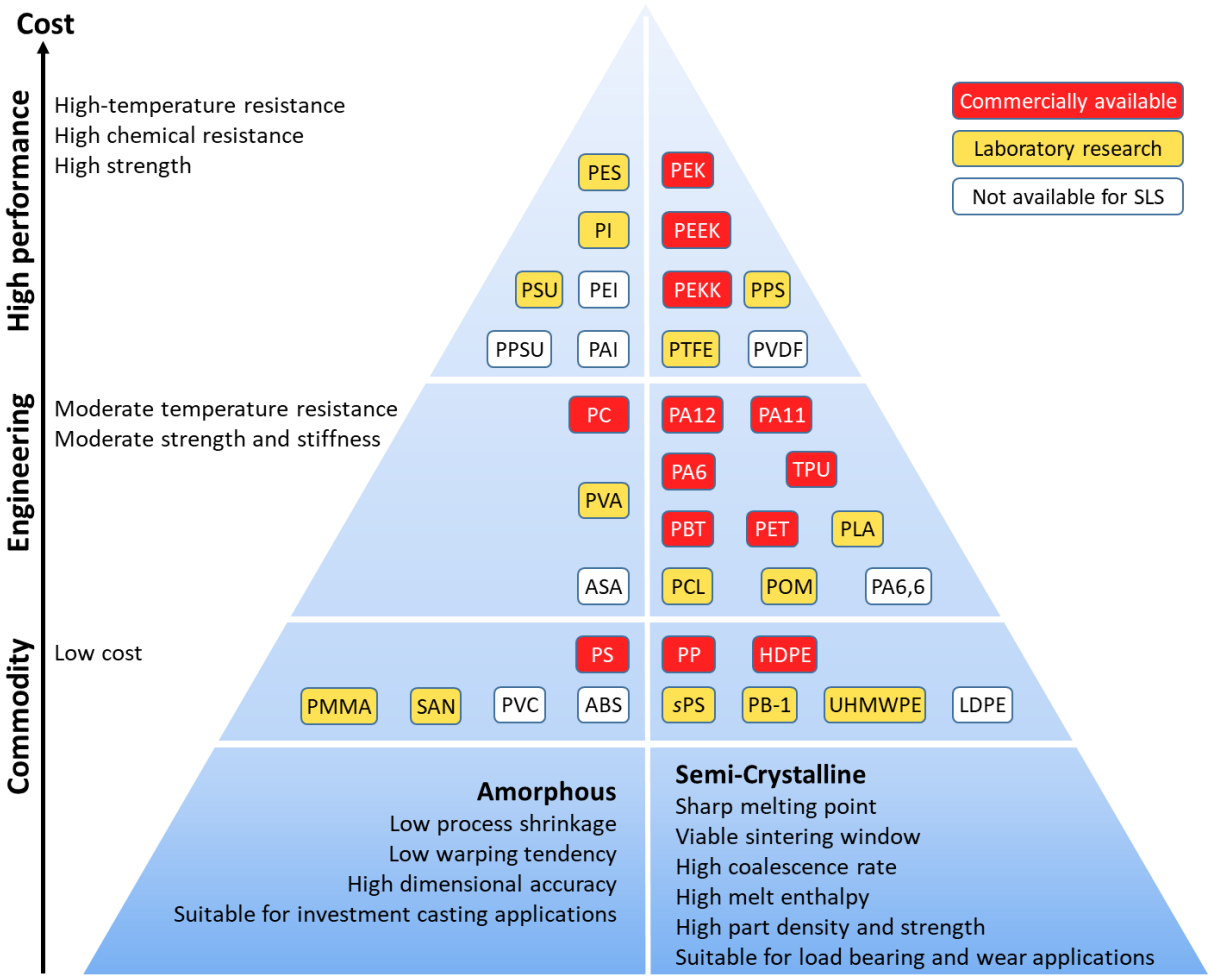

Figure 16. An overview of polymer powders for SLS that are commercially available or have been reported in scientific literature. The abbreviations listed in this figure that are not used in

the main text are as follows: polyamideimide (PAI), polybutylene (PB-1), polyethersulfone (PES), polyimide (PI), poly(phenyl sulfone) (PPSU), polysulfone (PSU), polytetrafluoroethylene (PTFE), poly(vinyl alcohol) (PVA), poly(vinyl chloride) (PVC), polyvinylidene fluoride (PVDF), styrene-acrylonitrile (SAN) and syndiotactic polystyrene (*s*PS).

The powder preparation process is of great importance for a polymer to be used for SLS. Polymer powders are often produced from the form of pellets, and they are also occasionally obtained from monomers through direct polymerization. The methods for producing polymer powders can be broadly classified into three categories: mechanical, solution-based, and melt-based methods **(Table 4).**

The mechanical method mainly refers to the mechanical grinding process, where a mill is used to break millimeter-sized polymer pellets into micro-sized powders. To embrittle viscoelastic polymers and reduce heat generated during the mechanical grinding process, a cryogenic refrigerant (e.g., liquid nitrogen) should be used to cool them below their embrittlement temperatures, and thus this process is often termed cryogenic grinding. Due to the high energy consumption brought about by using a continuous stream of liquid nitrogen, an alternative grinding process, wet grinding, that uses organic solvents (e.g., ethanol and hexane) as coolant was developed. [145] The mechanical grinding processes are versatile and suitable for most polymers; however, their biggest disadvantage is the irregular shape of powder particles that are produced.

To address the problem of irregular particle shape, a post-processing method involving particle rounding can be employed to produce spherical polymer powders with good flow. [154] The ground powder particles are fed into a downer reactor where the dispersed particles are melted and rounded due to the effect of surface tension, and subsequently solidify to produce spherical powder particles. [155] This post-processing method is versatile and scalable; more importantly, it can be applied to any polymer that may be ground and melted without

degradation, i.e., most thermoplastics and thermoplastic blends such as PS and PBT/PC. [143-144]

Table 4. The advantages and disadvantages of different powder preparation methods and their applications.

Powder preparation method		Material	Pro and con
Mechanical	Cryogenic grinding	PA11 [138] TPU [139] PP [140] PE [141] PS [142] PBT/PC [143]	• Simple process, widely used • Suitable for most polymers ▪ Irregular particle shape ▪ Poor powder flowability ▪ Particle rounding or other post-processing treatment required
	Wet grinding	PBT [144] POM [144] PS [144] PEEK [145]	• Lower energy consumption than cryogenic grinding ▪ Irregular particle shape ▪ Poor powder flowability ▪ Particle rounding or other post-processing treatment required
Solution-based	Dissolution-precipitation/ Thermally induced phase separation	PA12 [129, 133, 146] PA11 [138] PA6 [147] PP [148] POM [149] PC [150]	• Potato-shaped particles • Good powder flowability ▪ Complex and time-consuming procedure ▪ Specific process know-how required ▪ Solvent intensive
	Direct polymerization	PA12 [133, 151]	• Spherical particle shape • Good powder flowability • Narrow unimodal particle size distribution ▪ Complex and time-consuming procedure ▪ Specific process know-how required
Melt-based	Melt emulsification/ Coextrusion	PP [133] PE [152] PBT [152] PA12 [153]	• Spherical particle shape • Good powder flowability • Extrusion equipment readily available • Continuous production possible ▪ Complex and time-consuming procedure ▪ Post-processing required

A widely used solution-based method for producing polymer powders is the dissolution-precipitation process, also known as thermally induced phase separation. In this process, a polymer is first dissolved in a solvent at high temperatures, and often under high pressure. Subsequently, the solution is cooled at a controlled rate to allow polymer powder particles to precipitate. The dissolution-precipitation process is known for being able to produce spherical

micro-sized powder particles with a good control over the particle size and size distribution. The dissolution-precipitation process is used to produce commercial PA12 powders; it can also be used for other polymers such as PP, PC and POM. [148-150]

Another solution-based method to produce polymer powders is the direct polymerization of monomers into polymer powder particles, which is termed the direct polymerization method in this paper. In the direct polymerization process, the monomers are initially dispersed or dissolved in a solvent, and subsequently stabilized into spherical droplets or micelles upon the addition of suitable surfactants. [133] The polymerization reaction then starts upon the addition of an initiator, ultimately forming polymer powder particles. This method allows good control of the average molecular weight of the polymer chains and the size of the powder particles.

The melt-based powder preparation method involves melt emulsification, which is also known as coextrusion. The polymer of interest is first melt-blended with an incompatible or immiscible polymer (matrix phase) at a temperature above both their T_m values. Spherical droplets of the polymer of interest are then created within the matrix phase upon shear and elongational stress, which can be achieved with, for example, extrusion, forming a melt emulsion. The melt emulsion is then cooled and the matrix phase is subsequently dissolved in a suitable solvent such as water, leaving behind insoluble spherical powder particles that can be retrieved by filtration and sieving. [156] Polyolefins such as PP that are highly hydrophobic and resistant to chemical degradation are well suited for this process by using a water soluble matrix phase. Other polymers, for example, PBT and PA12 powders, have also been produced through this melt-based method by employing different matrix phases and solvents. [152-153]

4.2.1. *Amorphous polymers*

Amorphous polymers were the first type of polymers to be used for SLS. Since the mobility of molecular chains increase more significantly as the temperature approaches the T_g

value of amorphous polymers, the T_b value should be lower than the T_g value. Although amorphous polymers gradually soften and ultimately become a viscous liquid with increasing temperature, their viscosity values remain very high in general, even when the temperature is above their T_g values. Consequently, for these amorphous polymers, proper powder particle coalescence does not typically take place within the short sintering timescale. In theory, the consolidation of amorphous polymer powders can be improved with higher energy input, which, however, tends to cause over-sintering, part curling and even polymer degradation. [157] Therefore, in actual practice, most laser-sintered amorphous polymer parts are only partially consolidated with a high concentration of voids, and they exhibit lower strength than their conventionally manufactured counterparts.

Despite their high viscosity, amorphous polymers, especially PS and PC, are valued for a high dimensional accuracy and low residual ash content of printed parts, which render these polymers very ideal for investment casting applications. In addition, the common problem of shell expansion and cracking due to the formation of decomposition gases during the pattern removal process of investment casting can be mitigated, since the high porosity of printed parts allows the gases to escape. The high accuracy of laser-sintered parts of amorphous polymers is a result of their low process shrinkage (0.5–1.5%); [132] as there is no volume change associated with their glass transition, their process shrinkage is mainly attributed to thermal contraction, with sintering densification also contributing to this phenomenon. Because of its low coefficient of thermal expansion and hence higher dimensional accuracy, PS is preferred over PC, and remains available in the SLS material market today. [142a] A solution for producing tougher patterns is to use high-impact PS that has comparable sinterability to PS but with better mechanical properties. In other cases, the mechanical properties of printed parts can be improved via post-infiltration with thermosets such as acrylic or epoxy to reduce porosity. [142]

4.2.2. *Semi-crystalline polymers*

As semi-crystalline thermoplastics can undergo a higher degree of consolidation than amorphous thermoplastics, the mechanical properties of their printed parts can approach and possibly exceed those of their injection-molded counterparts, although the printed parts may still depict some porosity. As a result, semi-crystalline thermoplastics are preferred over amorphous thermoplastics for applying SLS to print functional parts and are more widely studied.

Engineering polymers

Engineering polymers promise better mechanical and/or thermal properties than amorphous polymers and have been used to replace traditional materials in the automotive, textile, food, and electronics industries. Engineering polymers that have been used for SLS include PAs, polyesters and polyethers.

Polyamide (PA) is a generic designation for the family of polymers that contain amide linkages along the polymer backbones. A unique characteristic of PAs is their ability to form hydrogen bonds between amide groups, which gives them intrinsically high melting points and good mechanical properties. PA12, the most popular SLS material, is usually synthesized by the ring-opening polyaddition of laurolactam. The good processability of PA12 powders is a result of the high congruence of their material properties with the intrinsic and extrinsic properties that are required for SLS. The weight-average molecular mass of virgin PA12 powder is 20–50 kDa. [158] PA12 powders have wide sintering windows with the values of 20–30 °C that makes them more tolerant to temperature deviations and thus easier to process. Their relatively high melting points of ~180 °C also render them suitable for applications requiring thermal resistance.

Commercial PA12 powders are most commonly supplied by Evonik and distributed through EOS and 3D-Systems as PA 2200 and Duraform® PA, respectively **(Figure 17a)**. The

PA12 powder from Evonik is prepared by the dissolution-precipitation method, which exhibits higher crystallinity than the pellet feedstock due to the high mobility of the polymer chains during the process. High polymer chain mobility provides more possibilities to improve the crystalline structure, as well as the high pressure involved that promotes the growth of larger lamellae with higher melting points. [129] Owing to the above reasons, the PA12 powder from Evonik has a much wider sintering window than the conventional polymer feedstock, making them more suitable for SLS **(Figure 17d)**. The high chain mobility involved during the dissolution-precipitation process can additionally be used to convert an amorphous feed material, for example, PC, into a semi-crystalline material, which would otherwise be impossible with conventional grinding processes. [150] This is especially advantageous for widening the type of semi-crystalline powders that can be used for SLS.

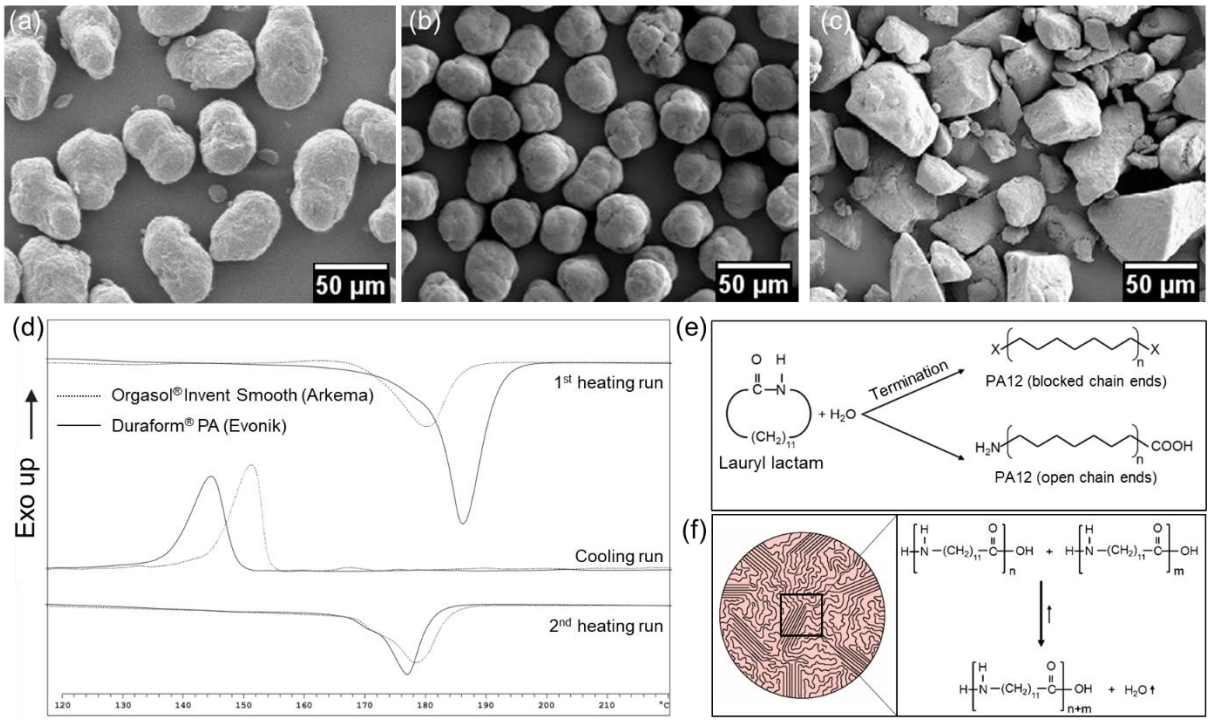

Figure 17. SEM images of the powders produced by different methods: (a) dissolution-precipitation (PA12), (b) direct polymerization (PA12), and (c) milling (PA11); (d) DSC curves of the PA12 powders from Arkema and Evonik, showing the difference between their sintering windows. Reproduced with permission. [133] Copyright 2018, Hanser. (e, f) Schematic of

polymer chain end-capping and its effects on the molecular weight change. Reproduced with permission. [14a] Copyright 2014, Springer Nature.

PA12 powders for SLS can alternatively be produced by direct polymerization, and this method has been employed by Arkema to produce spherical PA12 powders that are commercialized as Orgasol® Invent Smooth. PA12 powder prepared via this method exhibits a sintering window similar to that of the polymer feedstock (10–15 °C), but has better sphericity and a narrower particle size distribution. **(Figure 17b, d)**. The polymer chains of Arkema's PA12 powder are also end-capped so that post-condensation does not occur, whereas those of Evonik's PA12 powder are not **(Figure 17e, f)**. Consequently, the melt viscosity of Arkema's PA12 powder is fixed, while that of Evonik's PA12 powder increases with successive process loops. [129]

Another commercial PA12 powder, HP 3D HR PA12, is used by HP for the MJF process that it has developed. Sillani et al. revealed that the HP PA12 powder was different from the Duraform® PA powder that is used for SLS. [159] In particular, the HP PA12 powder was less prone to aging, i.e., post-condensation, as evidenced by the 18% increase in the weight-average molecular mass of the HP PA12 powder after MJF, compared to the 170% increase observed with the Duraform® PA powder after SLS. It was speculated that the polymer chains in the HP PA12 were end-capped, and for this reason, its powder recyclability was visibly higher than the Duraform® PA. The commonly used powder refresh ratios (the ratio of new powder to recycled powder) for HP PA12 and Duraform® PA powders are 20:80 and 50:50, respectively. It is worth highlighting that the mechanical properties of PA12 specimens printed by MJF vary minimally with different print orientations. [160] Surprisingly, several studies reported that the specimens that are built in the *z*-direction exhibited higher tensile modulus and strength than those built in the *x*- or *y*-directions, contrary to what is typically observed with SLS. [159, 161] It is conjectured here that this phenomenon is attributed to the diffusion of the fusing agent along

the *z*-direction due to gravitational force, which creates a continuous transmission of thermal energy into the previous layer, thus promoting better melting and adhesion across the interlayers (*z*-direction) than within the layer planes (*x*- and *y*-directions). Nevertheless, investigations on the MJF process are limited and further studies on its underlying process mechanisms are required.

PA11 is another type of PA, produced by the polymerization of 11-aminoundecanoic acid. It has a melting peak at ~190 °C, and its main advantage over PA12 is the higher toughness and impact strength achievable. PA11 powders are normally prepared by mechanical grinding. As a result, the PA11 powders tend to exhibit poorer flow than spherical or potato-shaped powders **(Figure 17c)**. Coupled with their inherently narrower sintering window (~15 °C), PA11 powders are more difficult to process than PA12 powders. [162]

PA6, also a member of the PA family, has a good thermal resistance and is widely used for applications requiring creep and fatigue resistance, especially in the automotive industry. PA6 has higher tensile modulus and strength than PA12, and the price of PA6 pellets is only 20–30% that of PA12 due to the more extensive application and higher popularity of PA6. [147] In recent years, chemical companies such as BASF and Solvay have commercialized PA6 powders as Ultrasint® and Sinterline® Technyl®, respectively, for SLS. Nonetheless, the use of SLS for PA6 is still confronted with many challenges, the greatest being its high melting temperature (~220 °C) that most commercial SLS machines are unable to handle. Furthermore, it is necessary to pre-condition the highly hygroscopic PA6 powders before using them for SLS to ensure that the printed parts are not embrittled.

While PAs are the mainstay of SLS materials today, there has been an increase in studies on the use or development of new materials for SLS, with polyesters being one of them. Polyesters are another class of engineering polymers, and they contain ester linkages along the polymer backbone. They are formed from the esterification reaction between alcohols and

carboxylic acids or acid chlorides, or the transesterification reaction between alcohols and esters. PET and PBT are polyesters that are commonly used in the food, textile, and electronics industries, and they are produced from the polycondensation reaction between terephthalic acid and ethylene glycol or 1,4-butanediol, respectively. SABIC and DSM have recently commercialized PET and PBT powders, respectively, for SLS.

PET exhibits high strength and stiffness, good barrier properties, and good electrical insulating properties. Highly crystalline PET has a melting peak at ~250 °C, and a sintering window of ~50 °C that is much wider than that of PA12. [163] The intermediate melting point of PET helps to bridge the gap in SLS materials that mostly either have T_m below 200 °C (e.g., PA12) or above 300 °C (e.g., PEEK). [164] Due to the slow crystallization rate of PET, most injection molded PET parts are amorphous or have low crystallinity, but with the slow cooling conditions in SLS, it has been possible to fabricate semi-crystalline PET parts. [165] Unlike PA12, of which the powder reuse is only possible by blending with virgin PA12 powder, used PET powders exhibit only a small increase in molecular weight, and can be reused as they are. [163] Even with irregularly shaped PET powders formed from mechanical grinding, laser-sintered PET specimens can achieve superior dimensional accuracy, surface finish, and flexural modulus and strength over PA12 specimens. [164]

PBT is another type of polyester that exhibits good impact, chemical, and thermal resistance. Similar to PET, PBT powders for SLS are produced by mechanical grinding. [166] Most of the PBT materials that are used for conventional manufacturing, for example, injection molding, are homopolymers that have a melting temperature of ~230 °C. PBT homopolymer has been processed by SLS using a T_b value of 210 °C, but because of its fast crystallization rate, there was a high likelihood of warping during SLS processing. [154a] To reduce the warping tendency of PBT, a PBT copolymer containing 10 mol% isophthalic acid that demonstrated a reduced melting temperature and crystallization rate was successfully processed by SLS using

a T_b value of 190 °C. [166] The laser-sintered PBT specimens exhibited the tensile strength and elongation at break values of 54.9 MPa and 3.41%, respectively.

TPEs are another type of engineering polymer; unlike most elastomers that are thermosetting, TPEs are not chemically cross-linked and can undergo repeated melting and crystallization cycles, allowing them to be processed by SLS. TPEs are categorized into blends and block copolymers. A TPE blend is produced by a mechanical mixture of semi-crystalline and amorphous polymers, while a TPE block copolymer is produced by copolymerizing two or more monomers to form discrete blocks of crystalline and amorphous domains within the same molecular chain. Regardless of the type of TPE, the rigid, crystalline polymer domains function as the thermally stable component, while the soft, amorphous domains impart elastomeric character to the material.

TPU is the most common type of TPE block copolymer used for SLS, and different grades can be produced depending on the structure and ratio of the monomers used. TPUs are produced by reacting diisocyanates with long-chain diols and short-chain diols to form flexible and rigid segments, respectively. [167] The strain at break of laser-sintered TPU specimens generally exceed 200%, making them extremely suitable for applications involving large strains. [139a, 139c, 168] One of the greatest values of TPU is that its powders can be reused through several SLS processing cycles (~14 cycles), which generates significant material and cost savings. Even when recycled powders are used, the ultimate tensile modulus and strength of the specimens remain largely unchanged, even though the strain at break decreases. [139a]

By coupling the elastic and flexible nature of TPU with an appropriate structural design, TPU can be suitable for the fabrication of soft 3D mechanical metamaterials that can be used for wearable devices and energy absorption applications. [139b, 169] Yuan et al. exemplified this with laser-sintered TPU 3D auxetic lattice structures that were designed by using Bucklicrystal unit cells as building blocks. The laser-sintered TPU 3D auxetic lattice structures exhibited the

ability to sustain a wide range of compressive strains; they could also withstand repeated compression cycles over large deformations, showing a strong shape recovery capability **(Figure 18)**. [139c]

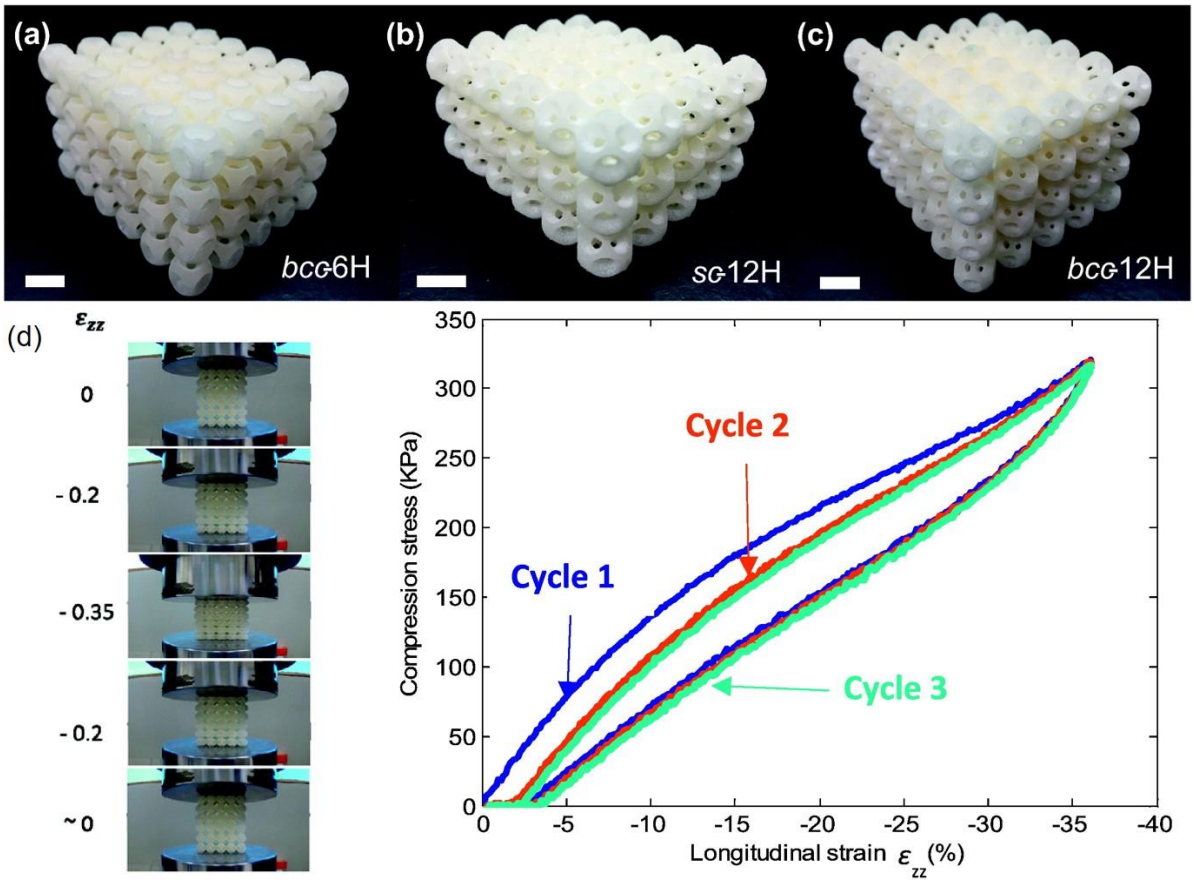

Figure 18. Laser-sintered TPU 3D auxetic lattice structures that were designed by assembling Bulklicrystal unit cells with 6 holes (6H) or 12 holes (12H) periodically, to form body center cubic (*bcc*) and simple cubic (*sc*) configurations: (a) *bcc*-6H, (b) *sc*-12H and (c) *bcc*-12H (scale bars represent 1 cm). (d) Stress-strain curves for the *sc*-12H lattice structure upon cyclic compressive loading at a strain rate of 1 mm/s. Reproduced with permission. [139c] Copyright 2017, Elsevier.

Apart from the abovementioned engineering polymers that are already available or on the verge of entering the SLS material market, some researchers also focus on the processability of other engineering-grade polymers, for example, semi-crystalline syndiotactic PS and POM. [141, 170]

High-performance polymers

High-performance polymers are characterized by their high mechanical performance and excellent thermal and chemical resistance. They are capable of retaining their desirable properties even when subjected to harsh conditions, and can serve as a lightweight alternative for applications that involve high operating temperatures. Polyaryletherketones (PAEKs), PPS, polyimides, [171] and fluoropolymers [172] belong to this class of polymers and have been studied for SLS. Due to their high melting temperatures, high-temperature SLS systems (e.g., EOSINT P800) are needed to process these polymers.

PAEK is a family of high-performance aromatic polymers that exhibit exceptional chemical resistance and thermal stability due to their aromatic backbones. These polymers can maintain their excellent mechanical properties even at high temperatures. The polymer backbone chains of PAEK contain alternating ketone and ether groups, and the ratio and sequence of the groups affect its T_g and T_m values. In general, the higher the ratio of the ketone groups, the higher the T_g and T_m values. In the PAEK family, PEEK, PEK and PEKK are promising and have been studied for SLS. PEEK has a high T_m value of ~340 °C, thereby requiring a high T_b value (> 300 °C). [173] Laser-sintered PEEK specimens can achieve a tensile modulus and strength of 3500–4500 MPa and 80–90 MPa, respectively, which are significantly higher than those of commonly used PA12. [130, 173-174] The high service temperature, excellent chemical resistance, and biocompatibility of PEEK parts make them very suitable for applications not only in the aerospace and automotive industries but also in the medical field, although most attempts to sinter PEEK have been focused on the production of medical devices **(Figure 19)**. [175]

PEK has a higher melting point than PEEK at ~370 °C, and sintered PEK specimens exhibit a higher service temperature, tensile modulus and strength than PEEK specimens. [176] PEK demonstrates a high load-bearing capacity and excellent chemical resistance and thermal

stability, which makes it very suitable for automotive, aerospace, and aeronautical applications. The mechanical properties of sintered PEK specimens could approach those of injection-molded specimens, and near-fully dense specimens with excellent thermal and mechanical properties that vary minimally with their build positions could be fabricated. [174a, 177]

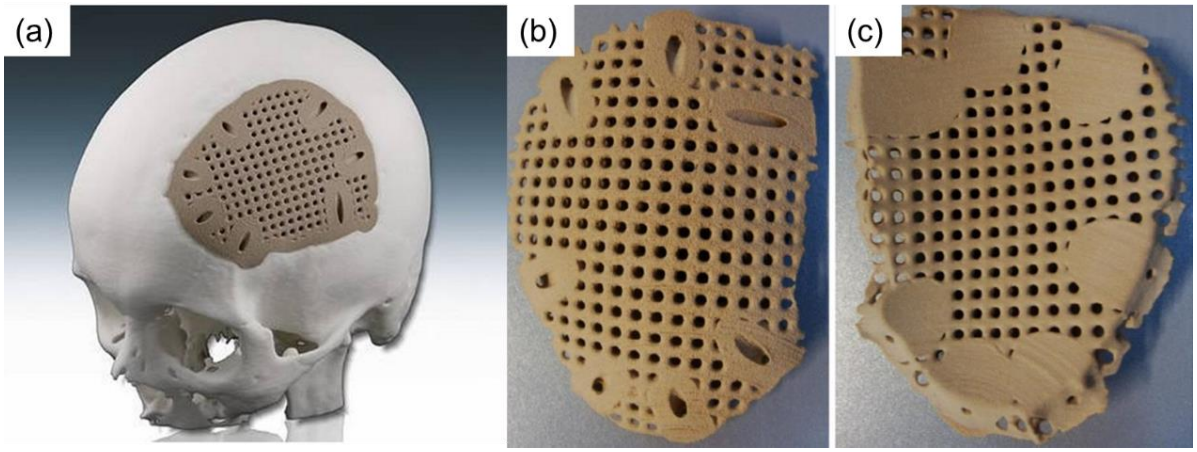

Figure 19. SLS of a cranial implant using PEEK powder: (a) location of the implant, and (b, c) the sintered implant. Reproduced with permission. [175] Copyright 2018, Elsevier.

PEKK has a significantly higher melting point (~390 °C) than PEEK and PEK. PEKK not only exhibits high tensile modulus, strength, and strain at break; it is also flame retardant and has a low hygroscopicity. Owing to its excellent properties, PEKK is extremely popular for aerospace applications. Although it is challenging to process PEKK due to its high melting point, its low shrinkage (30% lower than PA12) [171b] and potentially high powder reusability rate [176] make it a promising high-performance material for SLS.

PPS is a type of polyarylene, but with sulfide linkages. It has a melting temperature of ~285 °C. Like PAEKs, the aromatic backbone of PPS is responsible for its high chemical resistance and thermal stability. Although the achievable strain at break and tensile strength of PPS specimens are lower than those of PEEK and PEK specimens, a unique characteristic of PPS is its electrical conductivity, which makes it suitable for electronic applications. [176] The use of SLS for PPS powders is thus of interest, and related investigations are in the initial

stages. [178] Unfortunately, the limited availability of high-temperature SLS systems has greatly restricted the research opportunities involving high-performance polymers; therefore, researchers have been devising low-temperature methods to process such polymers. [172, 174b, 179] Recently, Chatham *et.al* reported the processing of PPS using a low T_b value of 230 °C by carefully choosing the process parameters to reduce part warping and curling. [178a] It is conjectured here that the successful printing might be due to the slow crystallization rate of PPS, which resulted in a low degree of crystallization and hence minimized shrinkage and warpage during the sintering process, even when a low T_b value was used. The laser-sintered PPS specimens exhibited average tensile strength and strain at break values of 61.8 MPa and 3.3%, respectively.

Commodity polymers

Commodity polymers are polymers that are used in high volumes for a diversity of applications. Polyolefins including PP, PE and polybutylene are such polymers that have been reported for SLS. [180] PP and PE take up the largest market share due to their well-balanced mechanical properties and excellent chemical resistance.

PP has been gaining attention as a new SLS material due to its low cost, good chemical resistance, hydrophobicity and widespread application in today's industries. PP homopolymer (homo-PP) is subdivided into atactic, syndiotactic and isotactic PP (*i*PP), where the methyl side groups are oriented randomly, alternatingly, and similarly along the polymer chain, respectively. Commercial homo-PP is mostly isotactic (*i*PP), due to the higher crystallinity, melting temperature (~160 °C) and modulus achievable; many studies investigating the use of SLS for PP have also focused on *i*PP. [130, 148, 152, 181] To address the brittle nature of *i*PP (strain at break of 1–7% for SLS specimens), ethylene has been incorporated into the polymer backbone to form PP copolymers that exhibit much higher toughness (strain at break of 75–400%). [141, 182] The melting temperature of PP varies with the tacticity and ethylene content in

the polymer chain, where lower tacticity and higher ethylene content generally leads to lower melting temperatures.

Most polyolefin powders available on the market are cryogenically ground and have irregular shapes, but studies have presented alternative powder production methods. For instance, PP microspheres can be prepared via the dissolution-precipitation process using xylene, [148] during which the PP concentration and quenching temperature can be adjusted to optimize the size and morphology of the spherical powder particles that are produced. When the dissolution-precipitation process is coupled with dry-coating, the powder flow can be further improved, and be comparable to that of a commercially available PA12 powder. [154c] Polyolefin powders can alternatively be produced by melt emulsification. [156] Melt emulsification is currently being used by ASPECT, an SLS material supplier, to produce spherical PP powders which are commercialized as Asphia PP. [133]

PE is a commodity polymer that has lower melting temperatures than PP, and is typically classified by its density and chain branching. UHMWPE, HDPE, and LDPE are the most popular PE materials. The use of PE in SLS has been largely restricted to research studies and thus far, HDPE [183] and UHMWPE with molecular weights ranging between 3500 kDa and 6000 kDa have been investigated because of their high potential for functional applications. [184] UHMWPE, in particular, has excellent corrosion and wear resistance, low coefficient of friction, and exceptionally high elongation, toughness, and impact strength. However, the high melt viscosity resulting from the ultrahigh molecular weight of UHMWPE leads to a slow sintering rate. [184c] The SLS process is complicated by the narrow sintering window (< 5 °C) and low part bed density of UHMWPE that contributes to a high degree of shrinkage. [184a, 184c] Therefore, despite the potentially excellent properties of UHMWPE, their printed specimens thus far unfortunately exhibit poor mechanical properties and require post-processing methods such as hot isotactic pressing to render them useful for functional applications.

4.2.3. *Polymer blends*

Polymer blending is attractive as an easy, cost-effective alternative to obtain parts with specific multiphase structures and properties. [185] It is versatile and has high potential for commercial applications since the properties of polymer blends can be controlled by a wise choice of polymers that form the blends. It has been demonstrated that a higher part accuracy and density can be achieved for SLS parts by blending amorphous polymers into a semi-crystalline matrix, e.g., the blending of PC into a PBT matrix to form a PBT/PC blend. [186] Nevertheless, polymer blends are much less studied than neat polymers and their composites due to the need for chemical compatibility between the blend materials, and the thermal constraints that render the sintering of the blends more difficult. [187] Furthermore, the temperature range between which the sintering process should take place tends to be narrower in polymer blends than their constituent neat polymers, implying that the polymer blend is more sensitive to changes in the part bed temperature, and thus fine temperature control is imperative. The use of SLS for polymer blends can only be achieved by a wise selection of the blend constituents. Nevertheless, several blends for SLS including PA12/HDPE, [185c] PA12/PA6 [185a, 185b] and PA12/PP [187a] have been reported.

Driven by the need for a wider range of materials for SLS so as to have more potential applications, researchers have been looking into the laser sintering of various polymers apart from PA12, whether on optimizing processing parameters to sinter the polymer powders successfully or on developing new polymer powders suitable for the process **(Table 5)**. TPEs such as TPU and high-performance and biocompatible polymers such as PEEK have been gaining increasing interest recently because these polymers exhibit unique properties that can enable entirely new applications, especially in the aerospace and medical fields.

Table 5. Polymer powders used for SLS and the mechanical and thermal properties of their printed parts.

Polymer			T_m (°C)	Modulus (MPa)	Ultimate strength (MPa)	Strain at break (%)	HDT [a] (°C)	Part density (kg/m^3)	Manufacturer/ Reference
Semi-crystalline	Engineering	PA12	176	1700	50	20	-	930	EOS
			182	1800	50	10	91	990	BASF
			183	1800	45	20	40	-	Arkema
			-	1586	43	14	95	1000	3D Systems
			183	1602	46	36	83.5	950	Prodways
		PA11	201	1600	48	45	46	990	EOS
			203	1750	52	28	76	1020	BASF
			201	1500	45	45	44	-	Arkema
			-	1590	51	64	56	1020	3D Systems
		PA6	220	3700	66	2	103	1150	BASF
		PET	251	2486 [F]	67.9 [F]	-	-	1339	[164]
			242	3000	66	4.9	-	-	[181d, 181e]
		POM	165	2900	42	3.5	-	-	[130]
		TPU	160	69	13	350	-	1170	BASF
			-	5.3	2	220	-	780	3D Systems
	High-performance	PEEK	-	3500	82	2	-	-	[130]
			340	3700	79	-	-	-	[174b]
		PEK	372	4250	90	2.8	165	1310	EOS
		PPS	285	2440	62	3	-	1190	[178a]
	Commodity	PP	140	1200	27	12	-	895	EOS
			140	1400	28	30	62	890	BASF
			125	599	19.9	122	-	-	[130]
		HDPE	128	1200	23	8.5	-	-	[130]
		UHMWPE	140	1500	0.2	-	-	-	[184a, 184c]
Amorphous		PS	105 (T_g)	1600	5.5	0.4	-	770	EOS
			-	1604	2.84	-	-	860	3D Systems
		PC	-	40	1	5	-	-	[142a]

[a] Heat deflection temperature under a 1.80 MPa load.
All modulus, ultimate strength and strain at break values were obtained under tensile conditions, except that those denoted by the superscript F were obtained under flexural conditions.

4.3. Polymer composite powders

Polymers and their blends tend to be insufficient for producing fully functional and load-bearing parts due to a lack of mechanical strength, thermal stability and/or functional properties. This restricts the application of SLS for the manufacture of end-use products, and thus composite powders for SLS have been developed to overcome this limitation. The addition of inorganic fillers usually serves to improve properties such as mechanical strength, thermal stability, electrical conductivity and bioactivity of composite parts. Being able to achieve properties that are unattainable by any of the constituents alone is a major reason that polymer composites are the most widely studied for SLS material development.

Polymer composite powders are prepared by two major routes, one of which uses pure polymer powder as the starting material, and the other uses pure polymer pellets, although pure polymer powders can also be used for the latter. There exist several composite powder preparation methods that can be used for SLS, including dry mixing, wet mixing, melt blending and mechanical grinding, and solution mixing. The dry mixing and wet mixing methods use pure polymer powders, while the melt blending and mechanical grinding, and solution mixing methods use pure polymer pellets. A less popular route for composite powder preparation is in situ polymerization, which uses monomers as starting materials **(Figure 20)**.

Dry mixing is the process of directly mixing polymer powders and fillers under dry conditions via mechanical agitation. At present, dry mixing is well established for the large-scale production of composite powders due to its simplicity and low cost. Unfortunately, due to the lack of chemical interaction between the fillers and the polymer powders, the filler dispersion is often poor; this is especially notable with nanofillers due to their high specific surface area and high surface energy, and hence a high tendency to aggregate. Therefore, dry mixing is more suitable for microfillers.

Wet mixing, often in the form of surface coating, is the process of mixing fillers and polymer powders in the presence of a solvent in which the polymer powders are insoluble. [188]

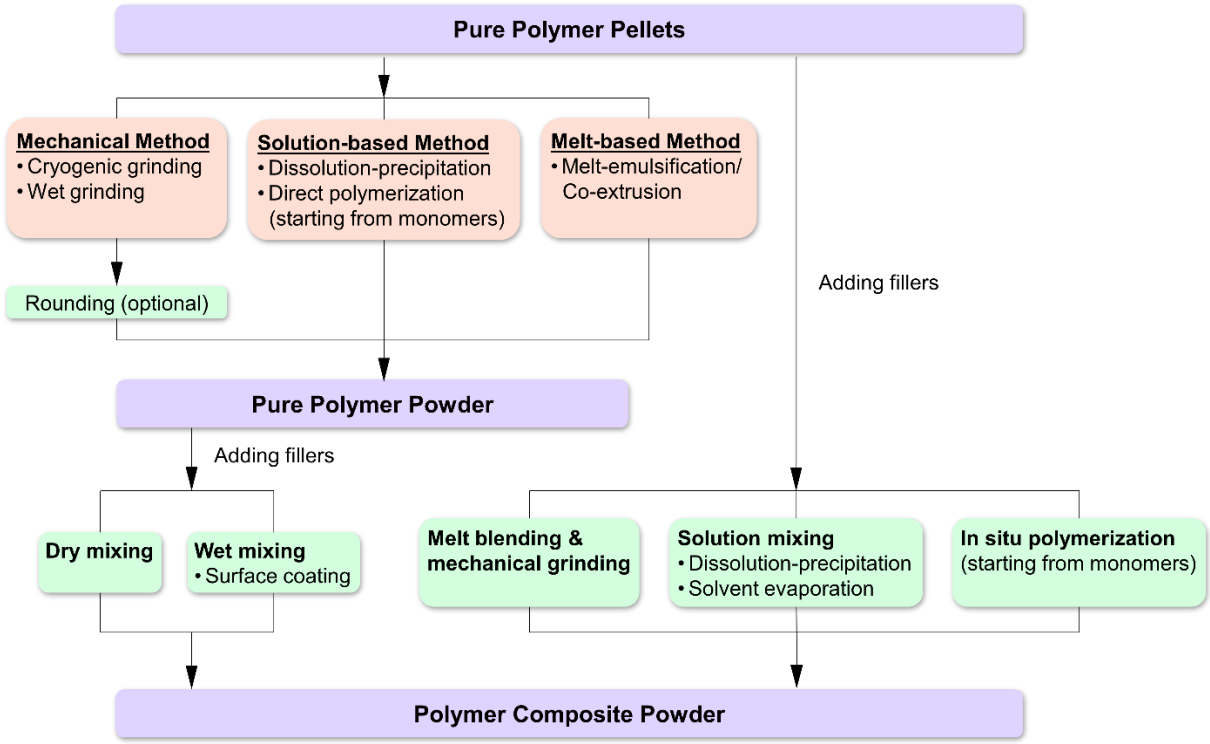

Figure 20. Summary of the composite powder preparation methods.

Fillers are coated onto the surfaces of polymer powder particles through van der Waals interaction, electrostatic attraction, etc. and the nature of the surface coating process allows the preservation of the initial powder particle morphology. Surface coating is well suited for nanofillers, since the use of solvent allows the dispersion of nanofillers to be improved using ultrasonication. The surface coating approach was first reported for preparing an MWCNT-coated PA12 powder, where PA12 powder and MWCNTs were dispersed in water to form a suspension, which was subsequently heated to soften the surface of the powder particles without melting them, to allow better adhesion of the MWCNTs on the powder particle surfaces. [189] This approach has been extended to other polymers such as TPU and PEEK, [190] and was further developed by the addition of appropriate surfactants that served to improve the

dispersion of fillers. [191] Surface coating can also be used with other nanofillers, including graphene and montmorillonite. [140, 190b, 192]

Melt blending is a common method to produce polymer composites by incorporating fillers into a molten polymer matrix under high temperature and shear force using an extruder. The combination of melt blending and subsequent mechanical grinding is a viable way to achieve composite powders with good filler dispersion. [140, 193] Goodridge et al. melt-blended 3 wt% carbon nanofiber (CNF) with PA12, and produced a CNF/PA12 composite powder by cryogenic grinding; the laser-sintered composite specimens exhibited a 22% increase in storage modulus. [194] However, the irregular powder morphology limited the enhancement in mechanical performance of the laser-sintered specimens. To further improve filler dispersion and filler-polymer interfacial interactions in composite powders, a pre-treatment process utilizing solid-state shear milling can be employed before the melt blending and mechanical grinding steps. This method was used to produce barium titanate/PA11 and boron nitride/PA12 composite powders. [162, 195]

Solution mixing is a method that utilizes a solvent in which a polymer is soluble and fillers can be dispersed. In this process, a polymer is first dissolved in a suitable solvent, followed by the dispersion of fillers, which is typically aided by ultrasonication or stirring to better mix the filler suspension with the polymer solution. Composite powder particles are subsequently produced from the solution either by precipitation or solvent removal. The dissolution-precipitation process that has been widely used to produce pure polymer powders can also be utilized to prepare composite powders for SLS. During the precipitation process, the polymer crystallizes from the solution by taking the fillers as heterogeneous nuclei, and thus the fillers are encapsulated within the powder particles formed. Nevertheless, because the addition of fillers complicates the crystallization and precipitation behavior of the polymer, careful process control is needed. Dissolution-precipitation has been used for preparing carbon fiber/PA12

(CF/PA12), [196] nanosilica/PA12, [197] and organically modified montmorillonite/PP (OMMT/PP) [140] composite powders. Another common solution mixing method is solvent evaporation, of which the spray drying process is popular. In spray drying, powder particles are produced by atomizing the composite solution through a nozzle to form a spray of fine droplets, which are subsequently subjected to contact with hot air or inert gases to vaporize the solvent rapidly. The solvent evaporation method has been used to produce, for example, HA/PLA and hectorite/PA6 composite powders for SLS. [198]

In situ polymerization involves the polymerization of monomers in the presence of fillers, typically nanofillers. It permits the grafting of polymer chains on filler surfaces and thus promotes the dispersion of fillers in a polymer matrix. However, the use of the in situ polymerization method for directly producing composite powders has been limited because of the involvement of numerous reactants and the fine process control required. This method has been used to prepare nano-alumina/PS core-shell and silica/PA12 powders for SLS. [151, 199]

The advantages and limitations of each preparation method, and some examples of the composite powders produced are summarized in **Table 6**.

Table 6. The advantages and disadvantages of different composite powder preparation methods and their applications.

Composite powder preparation method	Material	Pro and con
Dry mixing	Glass bead/PA12 [161a] Cu/PA12 [200] CF/PA12 [201] GF/PA12 [202] Carbon black/PA12 [203] OMMT/PP [140] GNP a)/PEEK [190b]	• Simple process • Low cost ▪ Poor filler dispersion ▪ Poor interfacial interaction
Wet mixing Surface coating	MWCNT/PA12 [189, 191, 204] MWCNT/TPU [190a, 204a] SWCNT b)/TPU [205] Carbon black/PA12 [206] Graphene/TPU [192] OMMT/PP [140]	• Low cost • Moderate filler dispersion on powder particle surfaces • Good interfacial interaction possible ▪ Solvent intensive

	GNP/PEEK [190b] GNP/PA12 [207]	
Melt blending and mechanical grinding	CNF/PA12 [194] OMMT/PP [140] $BaTiO_3$/PA11 [162]	• Good filler dispersion in powder particles • Good interfacial interaction possible ▪ Irregular particle shape ▪ Poor powder flowability ▪ Particle rounding or other post-processing treatment required
Solution mixing Dissolution-precipitation	CF/PA12 [196, 208] Nano-SiO_2/PA12 [197] OMMT/PA12 [197] OMMT/PP [140]	• Good filler dispersion in powder particles • Good interfacial interaction possible ▪ Complex and time-consuming procedure ▪ Difficult process control ▪ Solvent intensive
Solution mixing Solvent evaporation	HA/PLA [198b] Hectorite/PA6 [198a] Ca-P/PHBV [c] [198b, 209] CHAp [d]/PLA [198b, 209]	• Good filler dispersion in powder particles • Good interfacial interaction possible ▪ Solvent intensive
In situ polymerization	Nano-SiO_2/PA12 [151] Nano-Al_2O_3/PS [199]	• Good filler dispersion in powder particles • Good interfacial interaction possible ▪ Complex and time-consuming procedure ▪ Difficult process control

[a] Graphene nanoplatelet; [b] single-walled CNT; [c] calcium phosphate/poly(3-hydroxybutyrate-co-3-hydroxyvalerate); [d] carbonated hydroxyapatite nanoparticle.

4.3.1. *Microfillers*

Composite powders with micro-sized fillers are the most popular commercially, owing to a good balance between their ease of preparation, achievable part properties and material cost. Such composite powders are usually prepared by mechanical blending, and modification to the fillers is occasionally carried out to improve their interfacial interactions with the polymer matrix.

Glass beads are widely used in commercial SLS materials; in fact, many SLS material suppliers have glass bead/PA12 composite powders in their material database. Glass beads, being spherical, can be used to produce parts with isotropic enhancements. They are also able to provide high stiffness and dimensional accuracy, which are advantageous for SLS. Most importantly, glass beads can be obtained at low cost, making them well suited for commercialization. Metal fillers such as copper and aluminum are also used as reinforcements

to improve the modulus of printed parts as well as their thermal and electrical conductivity. [200] For instance, Alumide® from EOS is a commercial aluminum/PA12 composite powder that is used for the manufacture of stiff parts with metallic luster for automotive applications.

Fibers, especially glass fibers (GFs) and carbon fibers (CFs), are used for mechanical reinforcements due to their high tensile strength and lightweight nature. Depending on the fiber material, length and diameter, a range of property enhancements can be achieved. Generally, fibers with higher aspect ratios generate greater improvements to the tensile modulus of sintered parts. For instance, the PP copolymer composite specimens reinforced by GFs of 150 μm length exhibited higher tensile modulus than those with 50 μm long GFs of the same diameter. [182a] The mechanical properties can be further enhanced by increasing the fiber loading, as seen from the increase in tensile modulus (59%) when the loading of 50 μm GFs increased from 10 wt% to 30 wt%. [210] The addition of fibers reduces the flowability of the polymer powder, which can lower the powder processability and limit the achievable part properties. Therefore, the addition of flow agents such as silica may be required to ensure good powder flow, although in extreme cases, the poor powder flow from excessive quantities of fibers may be difficult to compensate for.

CFs normally have inert surfaces that often result in poor interfacial interactions with the polymer matrix, causing fiber pull-out of printed parts and reduction in their tensile strength. [210] Surface modification of CFs is necessary to introduce polar functional groups such as oxygen or hydroxyl groups onto them, which would improve the interfacial interactions between the CFs and polar polymers such as PA12. Yan et al. treated CFs with nitric acid, and prepared CF/PA12 composite powders via the dissolution-precipitation powder preparation method. [208] The CFs showed good interfacial adhesion and dispersion in the composite powder, and the laser-sintered composite specimens exhibited enhanced thermal stability, flexural modulus and flexural strength compared to the PA12 specimens. Using acid-treated

CFs, Wu et al. prepared CF/PA12 composite powders by dry mixing, and revealed that the functional groups on the CFs were thermally decomposed and released as a gas during the sintering process, which resulted in high porosity and poor mechanical properties of the printed specimens. [201] By subjecting the acid-treated CFs to further heat treatment at 400 ℃ under an inert atmosphere, the acid-modification effect was partly preserved, and the porosity of the sintered composite specimens could be reduced.

The increasing popularity of sustainability and green chemistry has prompted the development of composite powders using sustainable fillers. Environmentally friendly, biodegradable, and recyclable wood/plastic composites including eucalyptus/PA12 and eucalyptus/polyethersulfone have been developed for SLS. The printed parts show high dimensional accuracy because of the low thermal conductivity and sintering rate of the composite powder particles. [211] The low mechanical properties of printed parts can be further improved via the post-densification of their green parts by infiltration. [212]

4.3.2. *Nanofillers*

Known for delivering significant property enhancements at low loadings, nanofillers have huge advantages for load-bearing and functional applications. Unlike most microfiller-reinforced polymer composites where the increase in mechanical strength is typically accompanied by a notable reduction in strain at break, nanofiller-reinforced polymer composites can achieve a simultaneous increase in both strength and toughness when nanofillers are well dispersed.

Carbon nanofillers including CNTs, CNFs, graphene, graphene oxide (GO), and carbon black have been extensively studied as nanofillers for SLS composite powders. A critical condition to fulfill the maximization of the functionalities of these nanofillers is to ensure their good dispersion in/on polymer powder particles. Yuan et al. demonstrated the importance of

filler dispersion using the s-CNT/PA12 powders that were prepared by surface-coating the PA12 powder particles with the surfactant-treated CNTs. [191] The surfactant not only served to enhance the dispersion of CNTs onto the PA12 powder particles but also improved the interfacial interaction between treated CNTs and PA12 through covalent bonds **(Figure 21)**. At the loading of only 0.5 wt% s-CNTs, the laser-sintered s-CNT/PA12 specimens were shown to have 31.8%, 84.9% and 37.5% enhancement in their tensile strength, toughness and elongation at break values, respectively, compared to those of the laser-sintered PA12 specimens. [213] In addition to s-CNT/PA12, this surfactant-facilitated surface coating method has been used for preparing s-CNT/TPU [204a] and s-CNT/PA11 [214] composite powders for SLS.

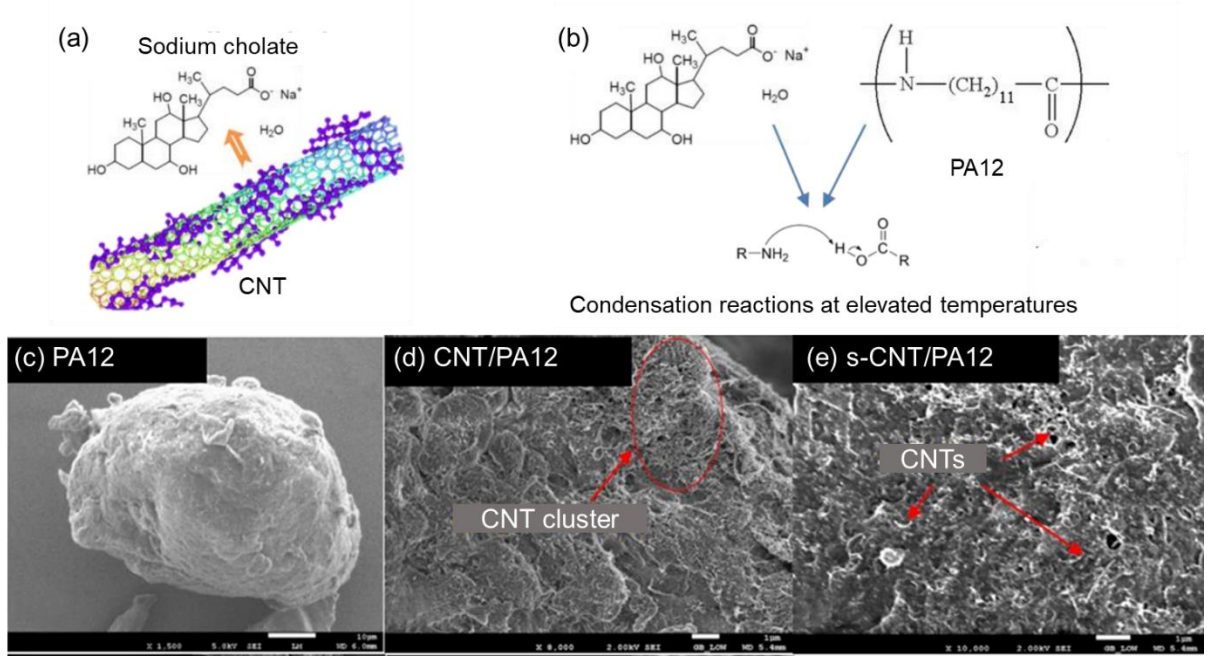

Figure 21. (a) Illustration of the surfactant, sodium cholate, attached onto a CNT. (b) Covalent bond formed between sodium cholate and PA12 at elevated temperature. SEM images of different powder particles: (c) PA12, (d) CNT/PA12 and (e) s-CNT/PA12. Reproduced with permission. [191] Copyright 2016, Elsevier.

While the enhancement of mechanical properties may be one aspect, carbon nanofillers are more often used to impart electrical and thermal conductivity to printed parts. The near

zero-shear-rate manufacturing nature of SLS, coupled with conductive composite powders that are prepared by surface coating, makes SLS an extremely suitable method for fabricating segregated conductive networks. Yuan et al. proposed that segregated fillers that were located on the boundaries of surface-coated powder particles offered an efficient conduction path, thus allowing laser-sintered composites to exhibit enhanced conductivity and ultralow percolation behaviors **(Figure 22a, c)**. [204b] The improvement in electrical conductivity of such laser-sintered composite specimens was exemplified with s-CNT/PA12 and s-CNT/TPU composite specimens, of which the electrical conductivity values increased by seven and eight orders of magnitude compared to their pure polymer specimens, respectively, at a loading of 1 wt% s-CNTs **(Figure 22b)**. With carbon black/PA12 composite powders prepared by surface coating, the conductive percolation threshold of the laser-sintered specimens was at 0.87%, which was significantly lower than the reported 4.3% of compression-molded specimens. [206] By using soft polymer matrices such as TPU, the surface coating of conductive fillers is useful for flexible conductive devices such as piezoresistors. [205]

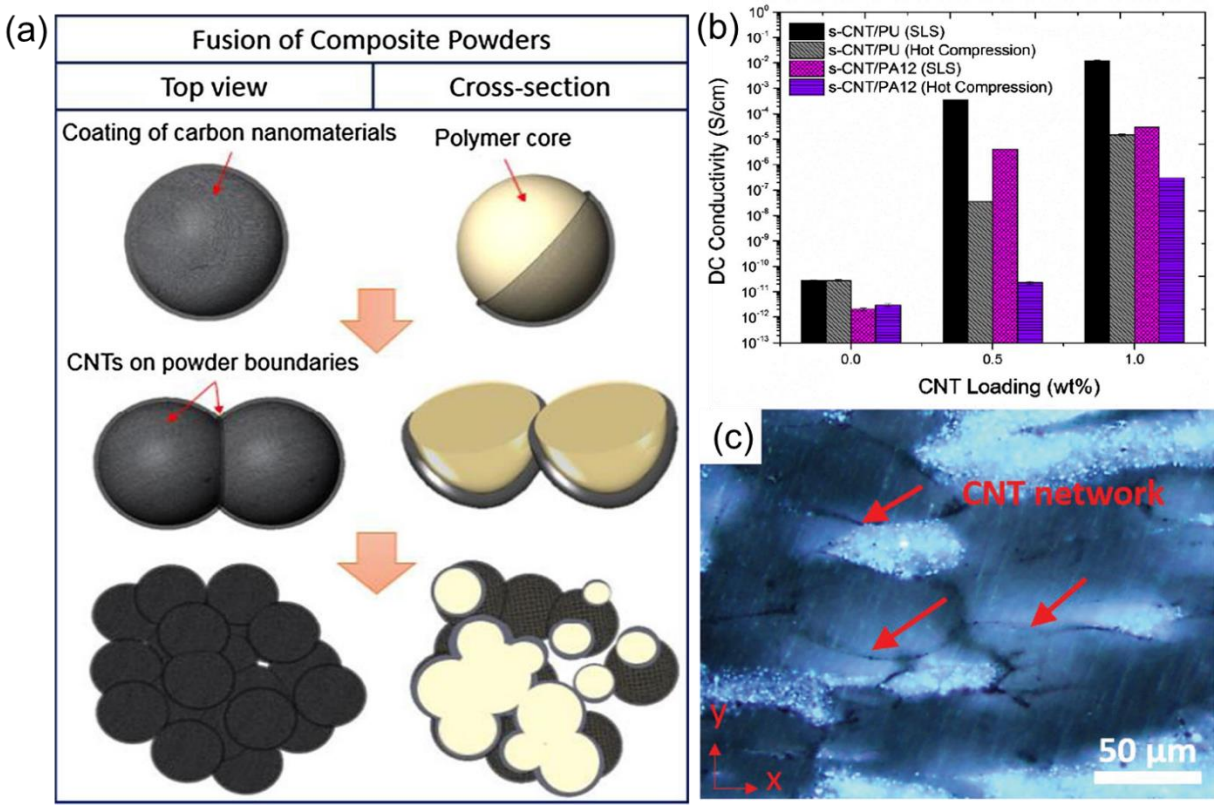

Figure 22. (a) Schematic of the fabrication of a segregated conductive network by laser-sintering composite powders that were prepared by surface coating, and (b) direct-current conductivity values of the laser-sintered and hot-compressed specimens using s-CNT/PA12 and s-CNT/TPU powders that were prepared by surface coating. Reproduced with permission. [204a] Copyright 2018, Elsevier. (c) Microstructure of a laser-sintered specimen with segregated conductive CNT networks. Reproduced with permission. [204b] Copyright 2019, Wiley.

SLS allows the fabrication of structures with controllable microstructure and properties that are critical for determining the cell adhesion, cell growth, nutrient transport, and structural strength of scaffolds. This motivates the development of biocompatible composite powders that can be used to fabricate scaffolds that match complex anatomical structures.

Calcium phosphates are popular for the development of biomaterials due to their osteoconductivity and biomimetic resemblance to the natural bone structure when mixed with other biopolymers. [215] HA is one of the most widely used nanofillers for the use of SLS for biocompatible scaffolds or implants. It is a stable, crystalline calcium phosphate that, when added, can enhance the bioactivity of scaffolds to simulate bone growth. It can also improve

the mechanical strength and cyclic fatigue resistance of scaffolds. [216] HA has been incorporated into PCL, poly(lactide-*co*-glycolide) or aliphatic PC for fabricating scaffolds with well-ordered macropores and interconnected micropores, which favor the seeding and distribution of transplanted cells. [217] Unlike HA that has slow resorption dynamics and mostly integrates itself into newly formed tissue after implantation, TCP is biodegradable and rapidly resorbable. [218] Therefore, TCP is popular for bone reconstruction and repair applications. The development of TCP composite powder for SLS has been exemplified with poly(methyl methacrylate) (PMMA) [219] and PEEK, [220] and can be extended to other polymer matrices.

BAG is another type of bioactive ceramic and can react with physiological fluids to form strong bonds with bones via the formation of bone-like HA layers. Reactions on the surfaces of BAG also lead to the release of ions that can induce favorable cellular responses and promote bone formation. [221] Furthermore, BAG can be added to reduce acidic byproducts generated by the *in vivo* degradation of polymers such as PLA. [222] However, at increasing BAG loadings, the mechanical properties of SLS-fabricated scaffold specimens deteriorate because of the poor interfacial interactions between BAG particles and the PLA matrix. Xu et al. proposed that BAG particles could be modified with cross-linkers that served as bridges between PLA and BAG to improve the interfacial interactions. [223] By using polydopamine as a cross-linker, the mesoporous structure of polydopamine-BAG (p-BAG) was preserved, and the particle dispersion and stress transfer efficiency of the composite was improved **(Figure 23)**. The laser-sintered p-BAG/PLA porous scaffolds exhibited ~30% higher compressive modulus and strength than those of the unmodified BAG/PLA scaffold. Importantly, the cells preferentially adhered to, proliferated, and differentiated on the p-BAG/PLA scaffolds, indicating the good biocompatibility and potential application of p-BAG in tissue engineering applications.

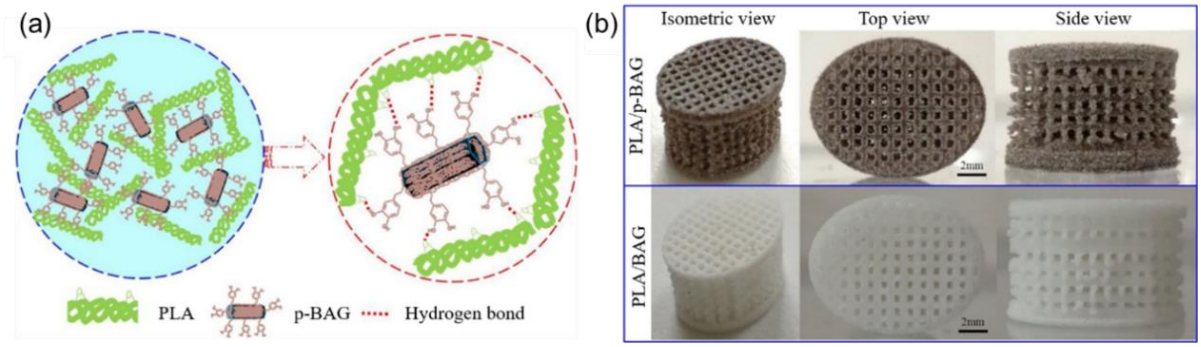

Figure 23. p-BAG/PLA composite scaffolds: (a) the schematic of the interactions between the modified BAG particles and the PLA matrix, and (b) the laser-sintered composite scaffolds measuring 12×9×8 mm^3. Reproduced with permission. [223] Copyright 2018, Elsevier.

The inherent porosity of the powder bed (40–60%) and lack of external pressure in SLS allow the fabrication of porous and highly accessible structures, and the relative density of printed parts can be readily controlled by adjusting the process parameters. [132] This nature of SLS can be exploited to manufacture parts with high accessibility for various flow-related applications, such as analytical chemistry and catalysis. [224] Since active materials for catalysis, adsorbent applications, etc. that are usually in powder form can now be incorporated into a highly accessible solid 3D structure, unfavorable adsorbent packing, uneven eluent flow and excessive channeling associated with the use of powder active materials can be circumvented. Importantly, the reusability of active materials can also be improved.

The high accessibility of laser-sintered parts was confirmed with the metal-organic framework-PA12 (MOF-PA12) composites prepared by Li et al., in which the Brunauer-Emmett-Teller (BET) surface area of the MOF was mostly retained in the printed film after the SLS process **(Figure 24a)**. [224c] The high recyclability of printed MOF-PA12 mixed matrix films was demonstrated with an NH_2-MIL-101(Al)-PA12 matrix film, of which the pollutant removal efficiency was only slightly reduced from ~95% at the first absorption-desorption cycle to ~80% at the fifth cycle **(Figure 24b)**. A similar adsorbent application was demonstrated with printed PA12 columns and meshes that exhibited high selectivity for $[AuCl4]^-$ in the presence of other dissolved metal ions that were at much higher concentrations,

and the PA12 parts remained fully reusable after the removal of the adsorbed ions. [225] The use of SLS for catalysis was demonstrated with a laser-sintered heterogeneous Pd/silica/PP catalyst, which proved to be highly active and reusable for hydrogenation reactions. [224a]

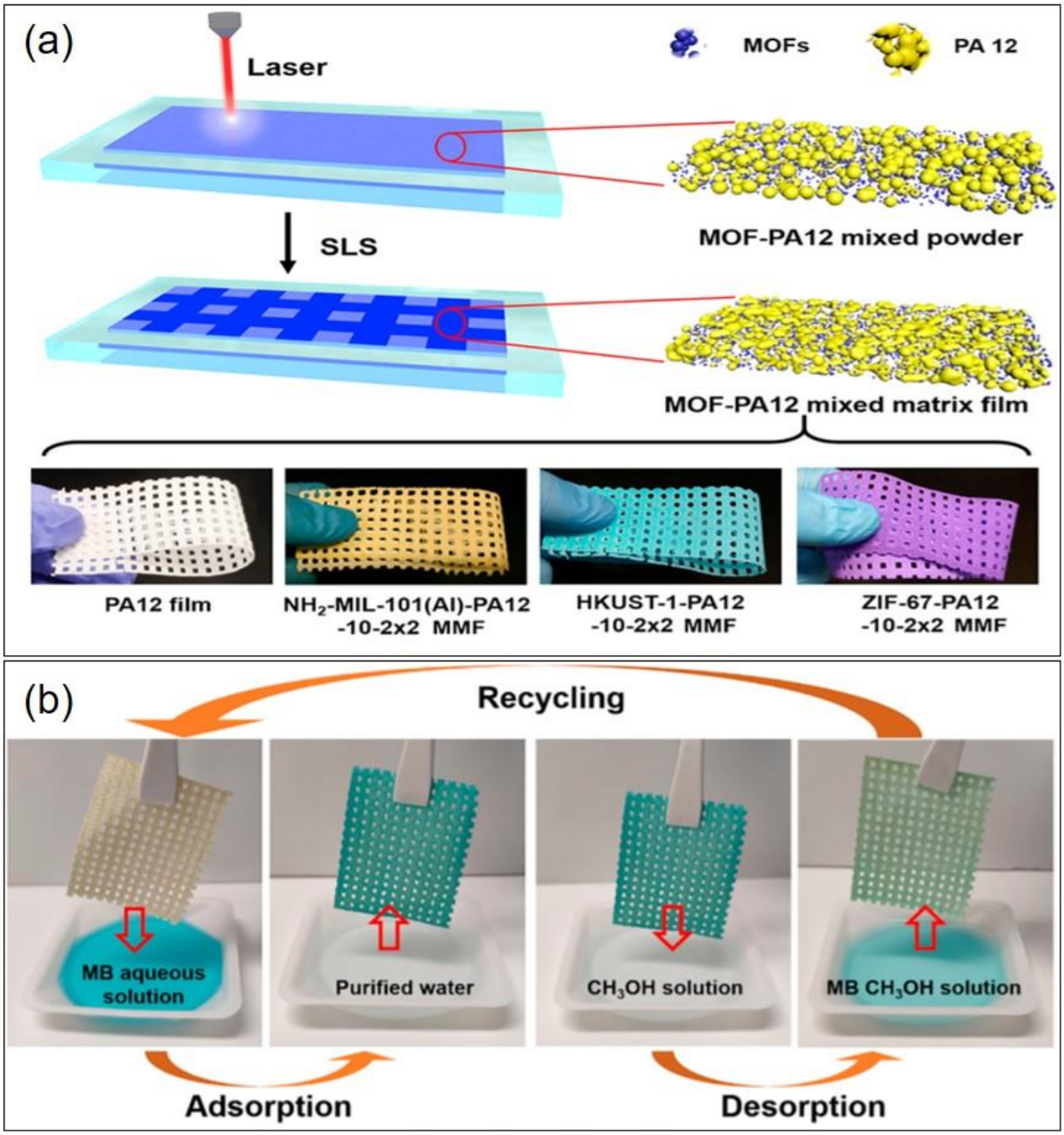

Figure 24. (a) Schematic of the printing of MOF-PA12 mixed matrix films using NH_2-MIL-101(Al)/PA12, HKUST-1/PA12, and ZIF-67/PA12 composite powders. (b) Recycling test of the NH_2-MIL-101(Al)-PA12 mixed matrix film. Reproduced with permission. [224c] Copyright 2019, ACS.

Thermoplastic composite powders have been widely investigated for SLS (summarized in **Table 7**) because the parts fabricated from composite powders can achieve properties that cannot be attained by any of the constituents alone, thus enabling a myriad of applications. Fibers, for example, are the most popular for producing fully functional and load-bearing parts, while other fillers such as glass beads are used as a cost-effective solution for mechanical property enhancement. Nanofillers can significantly enhance the performance of printed parts at low loadings, and are popular for imparting functional properties (e.g., thermal/electrical conductivity, piezoelectricity, bioactivity) to the polymer parts.

Table 7. Polymer composite powders used for SLS and the mechanical properties and the thermal and electrical conductivities of the printed parts.

Filler		Polymer	Modulus (MPa)	Ultimate strength (MPa)	Strain at break (%)	Thermal/ electrical conductivity	Reference
Ceramic	HA	PCL	2.33 [C]	0.6 [C]	-	-	[226]
		HDPE	36–161 [F]	4.5–33 [F]	3.8–8.6 [F]	-	[216]
	Nano-HA	PCL	3.17 [C]	-	-	-	[217a]
		PLGA [a)]	3.28 [C]	32.81 [C]	50	-	[217b]
		PC	25.6 [C]	8.14 [C]	-	-	[217c]
		PEEK	-	23.3	2.7	-	[227]
	BAG	PLA	79 [F]	2.4	6.9	-	[222]
		PLA	3600 [C]	62.9 [C]	-	-	[223]
	Nano-SiO_2	PA12	1980	46.3	20.07	-	[197]
		PA11	720	-	73	-	[228]
	$BaTiO_3$	PA11	2500	47	11	-	[162]
	BN	PA12	755	6.0	-	0.55 W/mK	[195]
	TiO_2	PEEK	-	15.3	5.0	-	[227]
	Al_2O_3	PEEK	-	25.3	8.0	-	[227]
	ZrO_2	PEEK	-	18.1	5.9	-	[227]
	Y_2O_3-stabilized ZrO_2	PA12	-	23	-	-	[198a]
	Montmorillonite	PA12	1870	47.2	17.7	-	[229]
		PLA	680 [F]	-	-	-	[193b]
	Hectorite	PA12	-	26	-	-	[198a]
	GF	PP	1117	19	-	-	[182a]
		PBT	-	60	3	-	[210]
	Wollastonite fiber	PP	709	19	-	-	[182a]
Carbon	CF	PA12	4700 [F]	112 [F]	-	-	[208]
		PA12	5800	80	-	-	[201]
	Nano-carbon black	PA12	1450 [F]	-	-	1×10^{-4} S/cm	[230]
	GNP [b)]	PA12	6200	58	17	-	[231]
		PEEK	-	104	6.5	0.45 S/m	[190b]
	MWCNT	PA12	4000	54	21	0.13 W/mK	[189a]

		PA12	1301	58	33	0.25 W/mK	[213]
		TPU	-	17.5	465	3.6 mS/m	[190a]
Metal	Potassium titanium whisker	PA12	-	68.3	-	-	[232]
	Ti	PA	-	0.04	-	0.588 W/mK	[233]
Wood	Eucalyptus	PA12	180	3.7	-	0.13 W/mK	[211b]
		PES	-	0.014	-	-	[211a]
	Birch powder, wax	Copolyester	-	1.2	-	-	[212c]

[a] Poly(lactic-*co*-glycolic acid); [b] graphene nanoplatelet.
All modulus, ultimate strength and strain at break values were obtained under tensile conditions, except that those denoted by the superscripts F and C were obtained under flexural and compressive conditions, respectively.

5. Thermoplastic filaments

Thermoplastic filaments and their composites can be processed by FDM. In a typical FDM process, the filament is first despooled via a feed pinch roller into the heated liquefier where the lower section of the filament softens or melts, and is then pushed through the nozzle by the solid, upper section of the filament that is entering the heated liquefier. The deposited liquefied filament, known as the printed road, then solidifies on the build platform.

5.1. Material requirements

One of the most important material considerations for FDM arises from the fact that solid filaments used act as a piston under compression during the extrusion process; therefore, they need to have sufficient strength to prevent buckling between the feed pinch roller and the heated liquefier. The critical stress for buckling σ_c (Pa), can be calculated using the formula derived by Euler for long slender columns: [234]

$$\sigma_c = \frac{\pi^2 E d^2}{16 L^2}, \tag{4}$$

where E is the elastic modulus (Pa) of the filament, d the filament diameter (m) (typically 1.5, 1.75 or 3.0 mm), and L the filament length (m) between the roller and the heated liquefier. Owing to the larger diameter of the bore of the liquefier than that of the filament, a correction factor has been suggested for equation 4, increasing the practical critical load to 110% of the

calculated σ_c value. [234a] Although the filaments must have sufficient strength and stiffness to prevent buckling, they also need to be flexible enough to enable their spooling and despooling for printing. [235] Thus, it was suggested that the filaments have a minimum strain at yield of 5%. [236]

As filaments are extruded through the nozzle in the form of a liquefied polymer, those with high viscosity produce large forces on the solid filament. Buckling would likely occur if the ratio of the elastic modulus to the apparent viscosity of a filament was less than 3×10^5 s^{-1}. [237] The high viscosity of polymers is commonly counteracted by increasing the nozzle temperature, and occasionally by utilizing ultrasonic vibration near the nozzle. [238] Higher nozzle temperatures have also proven to be beneficial for enhancing the tensile strength of printed parts because of improved adhesion. [239]

Upon deposition, the liquefied polymer cools to a temperature below the glass transition temperature T_g or melting temperature T_m, and solidifies. As the next line or layer of the polymer is deposited, the interface between the previous and the new printed road is heated to above the T_g value, and softens as a result of heat transfer from the printed road that is at a higher temperature. Intralayer adhesion and interlayer adhesion occur when the new road is deposited beside and on top of a previously printed road, respectively. The fusion of the interface allows intralayer or interlayer adhesion between two roads to occur via a time-dependent mechanism that involves viscous flow and polymer chain diffusion. The fusion is influenced by the rheological properties of the polymer including its viscosity, surface tension, and stress relaxation behavior upon deposition. [237]

The time interval between the deposition of two adjacent roads also plays an important role in adhesion; a longer time interval would lower the temperature at road-road interfaces, which results in poorer viscous flow and slower polymer chain diffusion, leading to poorer adhesion. This time-dependency is evident from the anisotropic mechanical behavior of most

FDM parts, which is a result of the interlayer adhesion being weaker than the intralayer adhesion. [240] The degree of adhesion between printed roads is also important for thermally and electrically conductive parts, since the thermal and electrical conductivity of printed parts are also affected by the presence of air voids and/or a lack of contact between the printed roads within the parts. [240b] If the adhesion between printed roads can be ensured, the thermal and/or electrical conductivity of the filaments can be preserved after printing, in both through-layer and cross-layer directions. [241]

During the FDM process, printed roads undergo shrinkage upon cooling, which is affected by the thermal properties of the filament material including its thermal conductivity, heat capacity, coefficient of thermal expansion and crystallinity (for semi-crystalline filament material). Uneven shrinkage often happens because of thermal gradients between the printed roads, which may lead to warpage and even delamination or cracking of the printed parts.[235] For the same reasons as discussed in Section 4.1, amorphous filaments have a high dimensional accuracy and are thus preferred in FDM; while semi-crystalline filaments can offer better mechanical properties but result in higher shrinkage and warpage. If semi-crystalline filaments are used, those with a low degree of crystallinity, slow crystallization rate and low coefficient of thermal expansion are favored. [242] As low thermal gradients are favored, most FDM systems are equipped with a heated build plate to minimize the temperature differences between the lowest and highest printed layers. Higher-end systems have an enclosed print chamber that allows for more efficient heat redistribution is useful for processing materials that require high extrusion temperatures.

The critical material requirements for FDM are summarized in **Figure 25**. In contrast to the resin- and powder-based AM techniques, a significantly broader range of polymers can be used for FDM. This process theoretically allows the use of any polymer that softens or melts with heat and solidifies upon cooling, which is essentially any thermoplastic.

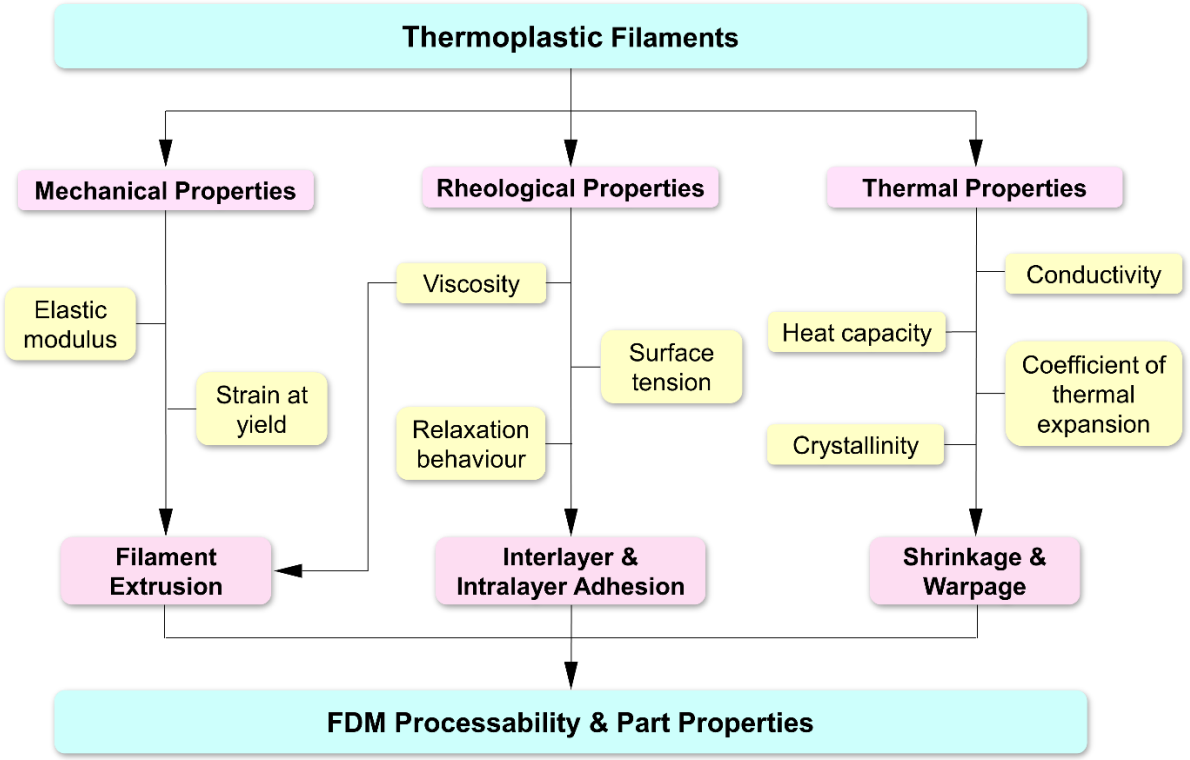

Figure 25. Key properties of a filament and their influences on FDM processability and part properties.

Unfortunately, the type of materials that are used for FDM is still limited because of the restrictions imposed by the use of solid filaments as the intermediate material. This limitation can be overcome with modified FDM systems that allow the use of polymer pellets instead of filaments. Such systems are modified with screw extrusion-based material deposition tools akin to those that are used in injection molding. [243] Since the need to use filament feedstocks is now eliminated, a more diverse range of thermoplastics can be processed. As the attachment of heavy components to the print-head is subject to issues with speed and precision, [244] the modified FDM system can be improved by using a stand-alone screw system that delivers the liquefied polymer through a flexible heated hose to the print-head. [234a] The compatibility of such screw extrusion-based systems with both soft and hard polymer pellets makes them a viable solution for widening the range of materials that can be used for FDM.

5.2. Pure polymer filaments

Polymer filaments used for FDM have mostly been amorphous ABS, acrylonitrile styrene acrylate (ASA) and PLA. In recent years, an increasing number of amorphous (e.g., PC and polyetherimide (PEI)) and semi-crystalline thermoplastics (e.g., PET, PA12 and PEEK) and TPEs have been gaining scientific interest, and some have been adopted commercially. [5b, 237, 245] Recent efforts on material development for FDM involves new polymers, polymer blends and composites. An overview of the FDM materials that are commercially available or have been studied at the laboratory scale is provided in **Figure 26**.

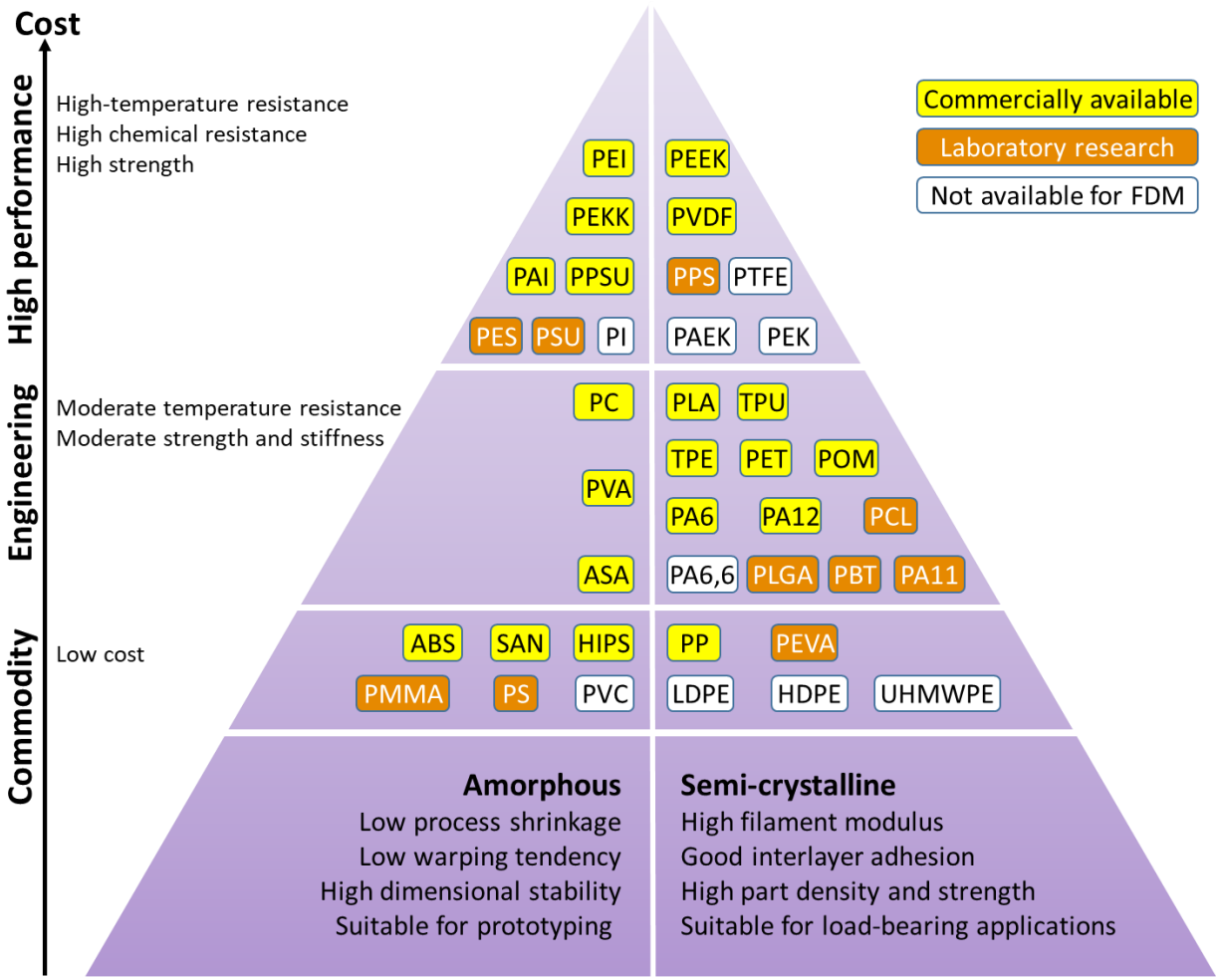

Figure 26. An overview of polymer filaments for FDM that are commercially available or have been reported in scientific literature. The abbreviations listed in this figure that are not used in the main text are as follows: polyethylene vinyl acetate (PEVA) and poly(lactic-*co*-glycolic acid) (PLGA).

Known for its toughness and impact resistance, ABS is one of the most popular polymers for FDM due to its durability, temperature resistance, and filament availability. It is an amorphous terpolymer consisting of polybutadiene and styrene-acrylonitrile copolymer phases, of which the polybutadiene phase imparts toughness, while the styrene-acrylonitrile phase enhances its modulus and tensile strength without affecting its dimensional accuracy. [246] ASA can serve as an alternative to ABS, being similar to it except that acrylate rubber is used instead of polybutadiene. ASA is more weather-resistant than ABS and is thus more suitable for outdoor applications. [247]

PLA is another material commonly used in FDM. [246] It is a biodegradable semi-crystalline thermoplastic derived from renewable resources, and is easier to process than ABS because of its lower coefficient of thermal expansion and lower printing temperature required. Furthermore, printed PLA specimens exhibit higher tensile strength and better finishing than ABS specimens. [248] Therefore, PLA is frequently used with low-cost FDM printers, especially in households, as a more reliable, safer and more environmentally friendly alternative. [240a, 249] Despite the many advantages of PLA, one of its greatest limitations is its poor heat resistance and low heat deflection temperature (HDT) at ~50 °C. This can be alleviated with the development of high-temperature PLA (HTPLA) that has a processability similar to that of PLA. HTPLA parts are heat-treated after printing, upon which they exhibit an increase in crystallinity and thus an improved temperature resistance (HDT > 120 °C) compared to those of PLA and even ABS. [250]

The materials used for support structures are as important as build materials. For systems equipped with only one print nozzle, support structures have to be of the same material as the final part and are removed by a mechanical force that unavoidably creates part defects. On systems with more than one nozzle, the use of a second material for support structure fabrication is possible. Support structures of different material from the final part, for example,

dissolvable materials, are desirable as they can be removed effortlessly, producing final parts with much smoother surfaces. Dissolvable support structures also allow more sophisticated geometry designs that would otherwise be impossible with standard supports. Poly(vinyl alcohol) and high-impact PS are the most common dissolvable support materials used with PLA and ABS, respectively; poly(vinyl alcohol) is water-soluble, while high-impact PS dissolves in *d*-limonene.

A considerable fraction of amorphous polymers are already commercialized due to their lower tendencies toward part shrinkage and warpage arising from their low coefficients of thermal expansion. [242] Comparatively, only a small proportion of semi-crystalline polymers (e.g., PET, PA12 and PP) that promise better mechanical properties and higher service temperatures have been studied or commercialized, which is because of their inclination toward shrinkage and warpage that render the FDM process much more challenging. Nevertheless, semi-crystalline polymers are imperative in advancing FDM from rapid prototyping to a manufacturing process for the direct fabrication of end-use load-bearing components. [251]

High-performance polymers such as PEI and PEEK have gained widespread interest in FDM. Printed PEI and PEEK specimens can achieve tensile strengths of 79–90 MPa and 83–98 MPa, respectively. [252] In comparison, the tensile strength values of ABS, PLA and PC specimens range between 20 MPa and 60 MPa. [248a] The high melting temperatures of PEI and PEEK necessitate nozzle temperatures higher than 360 °C, and with increasing nozzle temperatures, the porosity of printed parts decreases (360–420 °C) and crystallinity increases (380–480 °C), contributing to improved mechanical properties. [252c, 253] Nevertheless, it should be noted that excessive nozzle temperatures can lead to polymer degradation, worsening the mechanical performance of printed parts. [254] The requirement of high temperatures for extruding high-performance polymers renders these polymers more challenging to process due to large temperature differences between the freshly deposited polymer and the previously

printed layers. To reduce large thermal gradients, systems that are equipped with heated build plates and print chambers are desired. Yang et al. showed that as the temperature of the print chamber increased from 25 °C to 200 °C, the crystallinity and thus the mechanical performance of printed PEEK specimens increased. [253] The mechanical properties of printed high-performance polymer specimens can be further improved by thermal post-treatments (e.g., furnace cooling or annealing). [253-254]

TPEs are a special class of materials with unique applications. One of the challenges in using TPE filaments for FDM is their high elasticity and resilience, which renders them susceptible to deformation when gripped by the feed pinch rollers, and buckling under axial stress when fed into the heated liquefier. [234a] Consequently, TPEs that have been commercialized for FDM are limited to those with Shore A hardness greater than 70. To process TPEs with low Shore A hardness, the use of TPE pellets with a modified FDM assembly appears to be the most promising solution. [234a, 244, 255]

Polymer blends are favorable for FDM as they can serve to bridge the gap in performance and processability between amorphous and semi-crystalline polymers. Polymer blends can achieve higher mechanical properties than amorphous polymers, exhibit enhanced surface finish and mechanical isotropy, and even impart functional capabilities such as shape memory or bioactivity. [246, 256] PC/ABS and PC/PEI (Ultem™ 9085) that were originally developed for injection molding applications are currently the most popular blends for FDM. PC/ABS is one of the most widely used thermoplastics in the traditional plastics industry and has recently been processed using FDM; its printed parts demonstrate high strength, toughness, and heat resistance. [257] PC/PEI is a high-performance polymer with high fire retardancy and is certified for use in the automotive, aerospace and medical industries. [258] PC/PEI is currently the standard PEI material used in FDM because of its better viscous flow behavior than that of pure PEI (Ultem™ 1010).

The development of polymer blend filaments for FDM is limited by the miscibility between the constituent polymers and the need for them to have suitable thermal and rheological behaviors. Furthermore, the blend composition and processing parameters must be fine-tuned carefully for successful part fabrication. Presently, blends must be processed into a blend filament before they can be used for FDM. However, if screw-extrusion based FDM systems are used, blends of a wider variety of polymers can be readily used, allowing part fabrication for more diverse applications. The performance of the polymer and polymer blend filaments that have been investigated for FDM are summarized in **Table 8**.

Table 8. Polymer filaments used for FDM and their corresponding part properties.

Polymer	Modulus (MPa)	Ultimate strength (MPa)	Strain at break (%)	Reference
ABS	2400	28	8	Stratasys
PC	1944	57	4.8	Stratasys
PLA	3039	48	2.5	Stratasys
HTPLA	5650	67.4	2	[250a]
PA12	1282	46	30	Stratasys
PA6	2232	67.6	38	Stratasys
TPU	15.3	16.8	552	Stratasys
PEI (Ultem 1010)	3000	80	4	Stratasys
PEEK	4000	90	30	Victrex
PMMA	370 C	-	-	[251a]
Ethylene-vinyl acetate	-	8.83	522	[244]
PC/PEI (Ultem 9085)	2510	69	5.4	Stratasys
ABS/PC	1900	41	6	Stratasys
ABS/SAN	1750	40	6	[246]
ABS/TPE	1580	24	3.4	[256a]
ABS/SEBS a)	-	18.0–26.2	3.6–47.6	[256b]
ABS/UHMWPE/SEBS	-	14.7–23.1	5.7–8.4	[256b]
ABS/PMMA	580	44.1	13.5	[256c]
ABS/PMMA/MBS b)	573	43.9	17.4	[256c]
PCL/PHBV c)	-	15.93 C	-	[256d]

a) styrene-ethylene-butylene-styrene; b) methacrylate-butadiene-styrene; c) poly(3-hydroxybutyrate-co-3-hydroxyvalerate).
All modulus, ultimate strength and strain at break values were obtained under tensile conditions, except that those denoted by the superscript C were obtained under compression.

5.3. Polymer composite filaments

Thermoplastic filaments have been incorporated with a variety of fillers to produce composite filaments with improved mechanical, thermal, and functional (e.g., electrical conductivity and bioactivity) properties. There exist two major challenges for fabricating composite parts via FDM. The first one is composite filament fabrication; it is difficult to achieve homogeneous filler dispersion, prevent void formation, and ensure continuous extrusion of composite filaments simultaneously. [5b, 259] The second arises from the fact that the properties of composite filaments, such as modulus, viscosity, thermal conductivity and coefficient of thermal expansion, have to be appropriate for the FDM process.

The filler material, size (e.g., nano-, micro- or milli-sized), and loading affect the printability of a composite filament. Importantly, while the filler loading has to be sufficiently high to ensure adequate property enhancements, it has to be low enough to avoid nozzle clogging and filament embrittlement. An advantage unique to FDM is that its extrusion nature promotes fiber orientation; therefore, fillers are broadly classified into particle and fiber types.

5.3.1. *Particle fillers*

Particle fillers can conveniently be mixed with polymers and extruded into printable composite filaments for the FDM process, and they bring about isotropic property enhancements since no alignment is involved.

Mineral and glass particle fillers that are commonly used in conventional polymer composites can be used for FDM composite filaments as cost-reducing and/or mechanical property enhancement solutions. [260] The use of other fillers, for example, ceramics, that enhance stiffness, [256a, 261] wear resistance, [262] and dielectricity [263] have also been demonstrated. At high loadings (~40 wt%), ceramic fillers can impart dielectric properties to printed parts, suggesting the viability of using FDM to manufacture electromagnetic devices. [264] Metal fillers are useful for imparting electrical conductivity. [265] Depending on the type of

fillers and their loadings, the electrical conductivity of metal-reinforced polymer composite filaments could be up to 23 times that of their constituent polymer. [266] Another active area of research is the development of biocompatible composite filaments that are mostly based on PLA and PCL. Both of them have established safety records in human applications, but do not promote bone formation on their own; therefore, BAG and synthetic calcium phosphates such as HA and TCP can be incorporated to enhance the bioactivity of polymer composite filaments. [5b, 17, 267]

Nanofillers are popular for their low loadings required and a low tendency toward nozzle clogging when well dispersed. [240b, 268] Furthermore, the shrinkage and warpage of printed parts can be reduced as nanofillers reduce the coefficient of thermal expansion of the polymer. [269] Carbon nanofillers such as CNFs, carbon black, CNTs and graphene are popular for functional applications requiring mechanical strength and thermal and/or electrical conductivity. [270] The high tensile modulus and strength of carbon nanofillers, for example, MWCNTs, can additionally serve to enhance the printability of flexible filaments by increasing their resistance against buckling. [241] This enables the use of conductive flexible filaments (e.g., MWCNT/TPU) as excellent piezoresistive feedstocks for the fabrication of flexible strain sensors, with potential applications in wearable electronics and soft robotics.

Nanofillers are prone to agglomeration because of their high surface-area-to-volume ratio, and thus it is often difficult to achieve homogeneous nanofiller dispersion during continuous composite filament fabrication. The nanofiller aggregation must be minimized as aggregates can clog the nozzle, which then further limits the quantities of nanofillers that can be loaded. [268] To mitigate this issue, the compatibility between nanofillers and their polymer matrix has to be ensured, which is typically achieved with their surface modifications, addition of compatibilizing agents, or modifications to the polymer matrix. The aggregation of carbon nanofillers is commonly reduced by their surface modifications. For instance, reduced GO

(rGO), which has polar functional groups incorporated on its surface, exhibits reduced filler aggregation and better interfacial interaction with the polymer matrix than graphene. [271]

5.3.2. *Fiber fillers*

Unlike particle fillers that provide isotropic property enhancements to their composite parts, fiber fillers can produce more significant mechanical property enhancements along the print direction upon their alignment, and this effect is most prominent for FDM due to the shear force involved during filament extrusion **(Figure 27a-c)**. [272] Conductive fibers also perform better than particles in the through-plane direction as a result of fiber alignment. [273] The alignment effect is observed even for conductive fillers with layered structures such as rGO and graphene nanoplatelets, where lamellar orientation along the printing direction can be achieved. [271, 274]

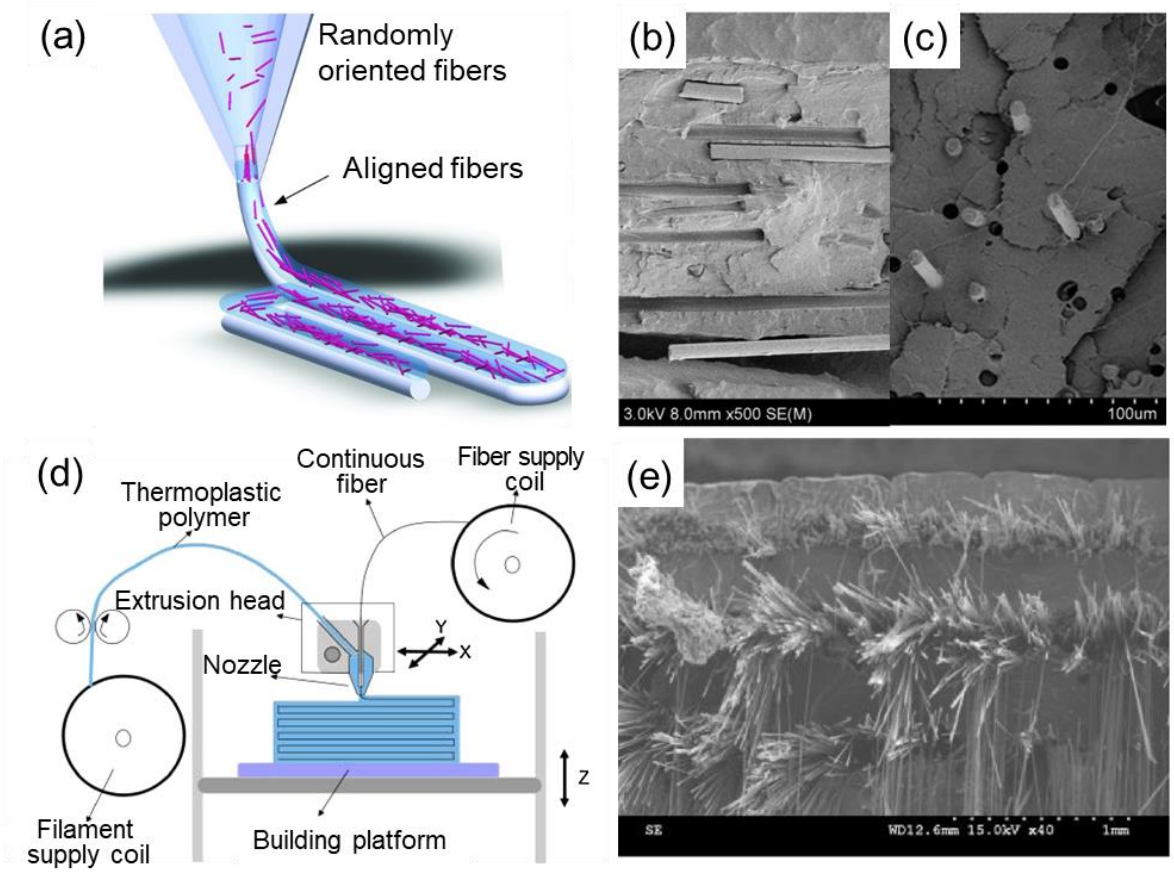

Figure 27. (a) Illustration of the alignment of short fibers as they pass through the nozzle. Reproduced with permission. [272a] Copyright 2019, Wiley. SEM images of the fracture surfaces of the CF/PLA tensile specimens fabricated in different directions: (b) longitudinal and (c) transverse. Reproduced with permission. [272b] Copyright 2020, Wiley. (d) Schematic of the FDM of a continuous fiber-reinforced polymer composite; (e) SEM image of the fracture surface of a printed continuous CF-reinforced PLA part. Reproduced with permission. [275] Copyright 2016, Elsevier.

Both discontinuous and continuous fibers can be used for FDM. Discontinuous fibers are easier to process due to their short lengths ranging between nanometers and millimeters. [272a] The different types of discontinuous fibers include Kevlar®, GFs, and CFs among others. The fiber length and loading influence the fabrication of composite filaments and their processability for FDM. Longer fibers and higher fiber loadings generally contribute to higher tensile modulus and strength of printed parts along the print direction, [269b] but they also embrittle the polymer matrix to a larger extent and are more likely to cause nozzle clogging. As a result, it is more challenging to fabricate continuous polymer composite filaments with

homogeneous filler dispersion using long fibers at high loadings. To ensure processability, the loadings of discontinuous fiber are usually limited to ~40 wt%.

CFs are one of the most widely researched discontinuous fibers due to their excellent mechanical properties and versatility. They have superior fatigue properties, corrosion resistance, stiffness, and heat tolerance, and are used for applications that require high tensile modulus and thermal conductivity. By using the loading of only 2 wt% CFs (212 μm in length), a 22% increase in the tensile strength of the printed continuous CF/ABS specimens, compared to that of the ABS specimens, was achieved, without significant impact on the printability of the composite filaments. [240b] At higher loadings of longer CFs (330 μm in length), the tensile modulus and strength of the printed continuous CF/ABS specimens increased by 700% and 115%, respectively. [276] In addition to ABS, CFs have been used with other polymers such as PLA and PET for enhanced stiffness. [277]

As compared to discontinuous fibers, continuous fibers can be used to produce thermoplastic composites that have remarkably high tensile modulus and strength as mechanical loads can be distributed across their entire length. Continuous fiber-reinforced polymer composite parts are printed either by directly using a continuous fiber-reinforced polymer composite filament, or by feeding polymer matrix filaments and continuous fibers separately and co-extruding them through the FDM nozzle **(Figure 27d)**. [272a, 275] Owing to the continuous nature of continuous fiber-reinforced polymer composite filaments, they typically have to be cut before the next print layer can be deposited, especially for printing parts with complex geometries. However, since the cutting of filaments is disadvantageous to final part properties, an optimized toolpath and part design that would minimize filament cutting is desired.

To date, continuous fiber-reinforced polymer composites based on carbon, Kevlar® and glass have been developed. Continuous CF-reinforced polymer composite filaments are most

popular because of their conductivity and exceptionally high stiffness and strength. With the loading of only 10 wt% continuous CFs, the flexural modulus and strength of the continuous CF/ABS specimens were enhanced to 8 GPa and 125 MPa, respectively. [278] When a higher loading of continuous CF was used with PLA, those values increased to 30 GPa and 335 MPa, respectively, and the fracture surface of the printed specimen showed that the CF bundles were well aligned in the PLA matrix **(Figure 27e)**. [275] When the interfacial interaction between the continuous CFs and polymer matrix was improved by the surface modification of CFs, the tensile strength, flexural strength and storage modulus of the resulting continuous CF/PLA composite specimens were improved by 13.8%, 164% and 351%, respectively, compared with those of the composite specimens with unmodified CFs. [279] To achieve higher impact strength, continuous GFs can be used. [280] Continuous GFs are most commonly used with nylon, [280-281] although other polymers including PLA, TPU and POM have also been demonstrated. [282] The use of both continuous fibers and particulate fillers can potentially produce synergistic effects in mechanical property enhancement. The addition of Kevlar® to PA6 led to significant improvements in tensile modulus (1400%) and strength (530%), and the enhancements were further increased to 680% and 1600%, respectively, when 0.1 wt% amine-modified graphene nanoplatelets were added as a third component. [283]

Various properties of FDM parts, including the mechanical strength, electrical conductivity, dielectricity, and thermal conductivity, can be enhanced by the addition of fillers **(Table 9)**. These fillers are classified into the particle and fiber types, and fiber fillers are further categorized into discontinuous and continuous fibers. Carbon and ceramic fillers are the most popular for FDM, with carbon fillers widely utilized for mechanically strong and thermally or electrically conductive functional parts, and ceramic fillers for bioactive implants and piezoelectric or dielectric devices. Continuous fiber-reinforced thermoplastic composites

boast exceptionally high tensile modulus and strength, and their fabrication has by far been only achieved with FDM.

Table 9. Polymer composite filaments used for FDM and the mechanical properties and the thermal and electrical conductivities of the printed parts.

Filler		Polymer	Modulus (MPa)	Ultimate strength (MPa)	Strain at break (%)	Thermal/ electrical conductivity	Reference
Particle	MWCNT	PLA	134.4	78.4	94.4	0.4 S/cm	[270b]
		ABS	2000 [F]	61 [F]	7.5	-	[260]
		TPU	51	12	120	0.01 S/cm	[241]
	Graphene	PLA	-	13.78	2	11.24 S/m	[240b]
	rGO	PLA	16.80	64.0	8.19	4.876 S/cm	[271]
	GNP [a)]	PA12	2251.7	40.9	12.3	1.1 W/mK	[274]
	TiO_2	ABS	1708	32.2	3.2	-	[256a]
	ZrB_2	ABS	-	32.56	5.7	-	[261]
	Montmorillonite	ABS	3600	39.48	1.5	-	[269c]
		ABS	1950 [F]	64.2 [F]	8.5	-	[260]
	Sepiolite	PA11	1150	46	20	-	[284]
	Nano-SiO_2	ABS	1800 [F]	60 [F]	8	-	[260]
	$CaCO_3$	ABS	2000 [F]	62 [F]	12	-	[260]
		PCL	80.16 [C]	15.43 [C]	-	-	[267d]
		PCL	83 [C]	-	-	-	[267a]
	TCP	PLA	3122	25	0.9	-	[267b]
		PCL	37 [C]	-	-	-	[267a]
	BAG	PCL	158 [C]	-	-	-	[285]
	Al	ABS	-	29.73	6.5	-	[261]
	W	PC	-	40	3.1	-	[286]
	Cu	PE	1200 [F]	19.4 [F]	5.9 [F]	1.63×10^{-5} S/m	[266]
Fiber	CF	ABS	8910	70.69	-	0.397 W/mK	[269a]
		ABS	2500	42	4	-	[269b]
		ABS	1100	36.8	8.69	-	[287]
		ABS	7150	50.9	2	-	[277]
		ABS	14000	65	-	-	[276]
		PLA	9280	68.4	1.8	-	[277]
		PLA	-	27.23	6	3.82×10^{-5} S/m	[240b]
		PET	8470	68.3	4.2	-	[277]
	Continuous CF	ABS	4185 7720 [F]	147 127 [F]	-	-	[278]
		PLA	19500	185.2	0.95	-	[288]
		PLA	30000 [F]	335 [F]	-	-	[275]
		PLA	-	91	-	-	[279]
		Nylon	35700	464.4	1.3–2	-	[289]
		Nylon	13000 38100 [F]	600 430 [F]	-	-	[281b]
		Nylon	7730 13020 [F]	216 250 [F]	4.22	-	[281a]
	Continuous GF	Nylon	7200 14700 [F]	450 149 [F]	-	-	[281b]
		Nylon	3750	206	8.42	-	[281a]
		PLA	19400	234	-	-	[282]
		TPU	18200	227	-	-	[282]
		POM	21500	267	-	-	[282]
	Continuous Kevlar® fiber	Nylon	4370 6650[F]	164 125[F]	4.98		

	Nylon	27000	610	2.7		
Jute fiber	PLA	5110	57.1	1.81	-	[288]
	ABS	1543	25.9	4.5	-	[256a]

[a)] graphene nanoplatelet.
All modulus, ultimate strength and strain at break values were obtained under tensile conditions, except that those denoted by the superscripts [F] and [C] were obtained under flexural and compressive conditions, respectively.

6. Viscous polymer inks

Viscous polymer inks that can be processed by DIW include reactive resins (e.g., photocurable and thermally curable resins), and polymer solutions.

Highly viscous photocurable resins are one of the most popular polymer inks used for DIW. [85a, 290] To process such inks, an external irradiation source, typically UV light, has to be incorporated into DIW systems to photo-cure them upon deposition; the DIW of photosensitive inks is commonly termed UV-assisted DIW. Photo-curable hydrogels that solidify through chemical gelation, for example, gelatin methacrylate (GelMA), are typical materials for DIW. Besides photosensitive resins, thermally curable resins (e.g., epoxy resin) that solidify upon exposure to heat have also been used. [291]

Polymer solution inks are formed by dissolving polymers into a solvent. The viscosity of such inks can be tuned for DIW by varying the molecular weight of the polymers and their volume or mass fractions in the inks. A wide variety of polymer solution inks can be used for DIW, and they include those that are based on hydrogels, for example, alginate and collagen, that solidify by ionic- and pH-driven physical gelation, respectively. [292] Polyelectrolyte solutions that undergo solvent-induced solidification are another type of polymer solution ink. [293]

6.1. Material requirements

To design suitable viscous polymer inks for the DIW process, the criteria associated with the extrusion and solidification processes should be considered. Firstly, viscous inks must exhibit proper rheological properties, including apparent viscosity, yield stress under shear or

compression, and storage modulus G' and loss modulus G''. Suitable ink viscosity for DIW ranges over several orders of magnitude (10^2–10^6 mPa·s at a shear rate of ~0.1 s^{-1}), [294] and thus DIW has been extremely useful for enabling the printing of inks with high viscosity that cannot be processed by other AM techniques. For instance, thermoplastic poly(tetrafluoroethylene) and photosensitive resins based on polyamic acids that have viscosity values (10^6–10^7 mPa·s) too high for typical FDM and VP techniques, respectively, were successfully printed by DIW. [295]

Secondly, viscous inks for DIW should exhibit appropriate thixotropic behavior, i.e., time-dependent shear thinning. Shear thinning is desired for ink extrusion from the nozzle without the need to employ excessively high internal pressure. Meanwhile, the extruded inks should undergo rapid dynamic recovery (~1 s) of their yield stress or modulus to ensure prompt shape retention after extrusion. [296] The recovered mechanical strength of the inks should be high enough to ensure sufficient structural support, especially for overhanging structures. The ratio of loss modulus to storage modulus should ideally be lower than 0.8 to ensure the fabrication of self-supporting architectures. [297] The thixotropic behavior of the inks can be tailored through the interactions between their molecules or particles, which can be temporarily disrupted by a mechanical stimulus (i.e., shear force during the ink deposition process) and then reinstated upon deposition. [297-298]

6.2. Hydrogels

Hydrogels are a class of materials that are widely used for DIW. The DIW process operates under ambient conditions, which allows the incorporation of biologically active ingredients such as growth factors and cells that are favorable for biomedical applications. The printing of biomaterials via DIW is more commonly termed bioprinting.

Hydrogels can be based on natural or synthetic polymers. Nature-derived hydrogels are mainly based on polysaccharides (e.g., alginate and chitosan) and proteins (e.g., collagen, and gelatin), which have the advantage of good biocompatibility. Synthetic hydrogels that are based on PEG, poly(vinyl alcohol), polyacrylamides, etc. typically have higher strength than nature-derived hydrogels. While synthetic hydrogels are often formed by chemical gelation, most nature-derived hydrogels can be formed by both physical and chemical gelation. For instance, alginate, the most widely used natural biopolymer for bioprinting, can form hydrogels by the ionic cross-linking of their anionic polymer backbones in the presence of divalent cations (e.g., Ca^{2+}), or by covalent cross-linking with poly (ethylene glycol)-diamines. [292c, 299] Gelatin, another type of natural polymer, undergoes a phase change that is induced by a temperature change; it is a solution at physiological temperature (~37 °C), but forms a gel network via the association of triple helixes upon cooling (< 29 °C). To improve the printability of gelatin-based hydrogels and their utilization under physiological conditions, GelMA that can undergo photopolymerization to form a stable, covalently cross-linked 3D structure is preferred. [300]

As many DIW-printed hydrogel structures face the problem of low mechanical strength, an alternative approach to ensure the fabrication of self-supporting structures is to dispense inks into a support bath. Gel-in-gel printing, a typical bioprinting process that uses a gel as a support material, is also useful when printed structures are too weak **(Figure 28a, b)**. [301] This printing method has been extremely beneficial for fabricating hydrogel structures in which the printed hydrogel is embedded within a secondary hydrogel that serves as a temporary, removable, and biocompatible support. Lee et al. demonstrated the use of this method for the bioprinting of collagen into components of the human heart, from capillaries to the full organ, that accurately reproduced patient-specific anatomical structure. [292b] Another work by Noor et al. exemplified the use of gel-in-gel printing to fabricate functional vascularized and

perfusable cardiac patches that completely matched the patient's anatomy, as well as a small-scale cellularized human heart with major blood vessels **(Figure 28c-f)**. [302]

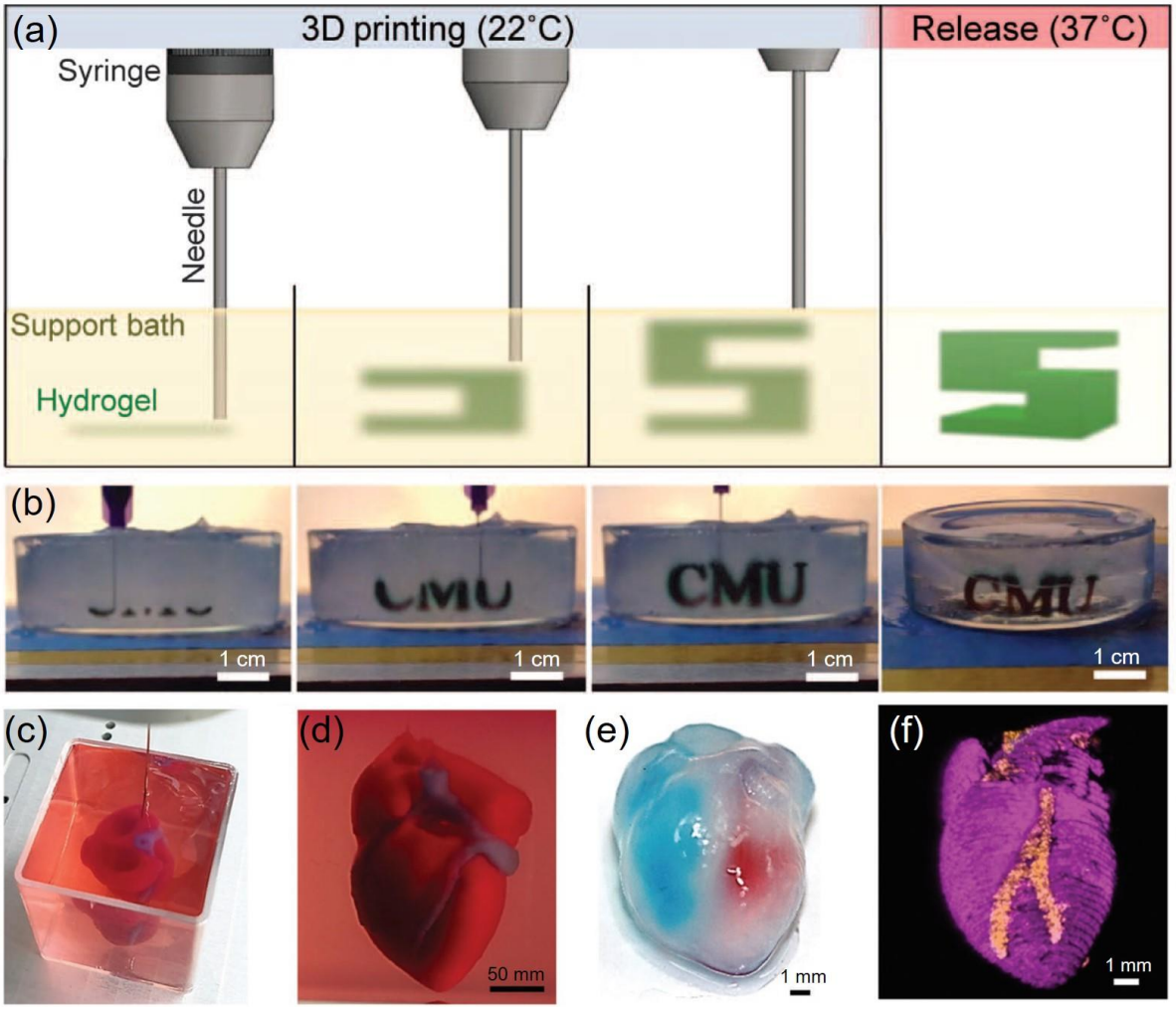

Figure 28. Gel-in-gel printing: (a) a schematic showing the hydrogel being extruded into the (self-healing) support bath, and (b) a freeform helix structure printed in a gelatin support bath. Reproduced with permission. [301] Copyright 2015, AAAS. A small-scale cellularized human heart printed by gel-in-gel printing: (c-d) after printing in a support bath, (e) after extraction (left and right ventricles were injected with red and blue dyes, respectively), and (f) confocal image showing the cardiomyocytes and endothelial cells in pink and orange, respectively. Reproduced with permission. [302] Copyright 2019, Wiley.

Besides biomedical applications, hydrogels are also popular for fabricating stimuli-responsive structures with shape memory and self-assembling capabilities. [303] Hydrogel structures that are temperature-, [304] moisture-, [305] and multi-stimuli-responsive (e.g., to pH

and temperature changes) [306] have been printed by DIW. Gladmaned et al. demonstrated that by making use of the fiber-alignment capability of DIW, it was possible to design complex architectures that showed localized and anisotropic shape changing behavior. [305a] The anisotropy of the printed parts could be controlled by the alignment of the fibers along the prescribed printing pathways **(Figure 29a)**. A hydrogel composite ink composed of stiff cellulose fibrils embedded in a soft acrylamide hydrogel matrix was used **(Figure 29b)**, and the shape change of the printed parts was realized by simply immersing them into water **(Figure 29c)**. By applying theoretical calculations, the alignment patterns for prescribed target shapes could be designed, thus enabling the fabrication of complex bio-inspired 3D architectures.

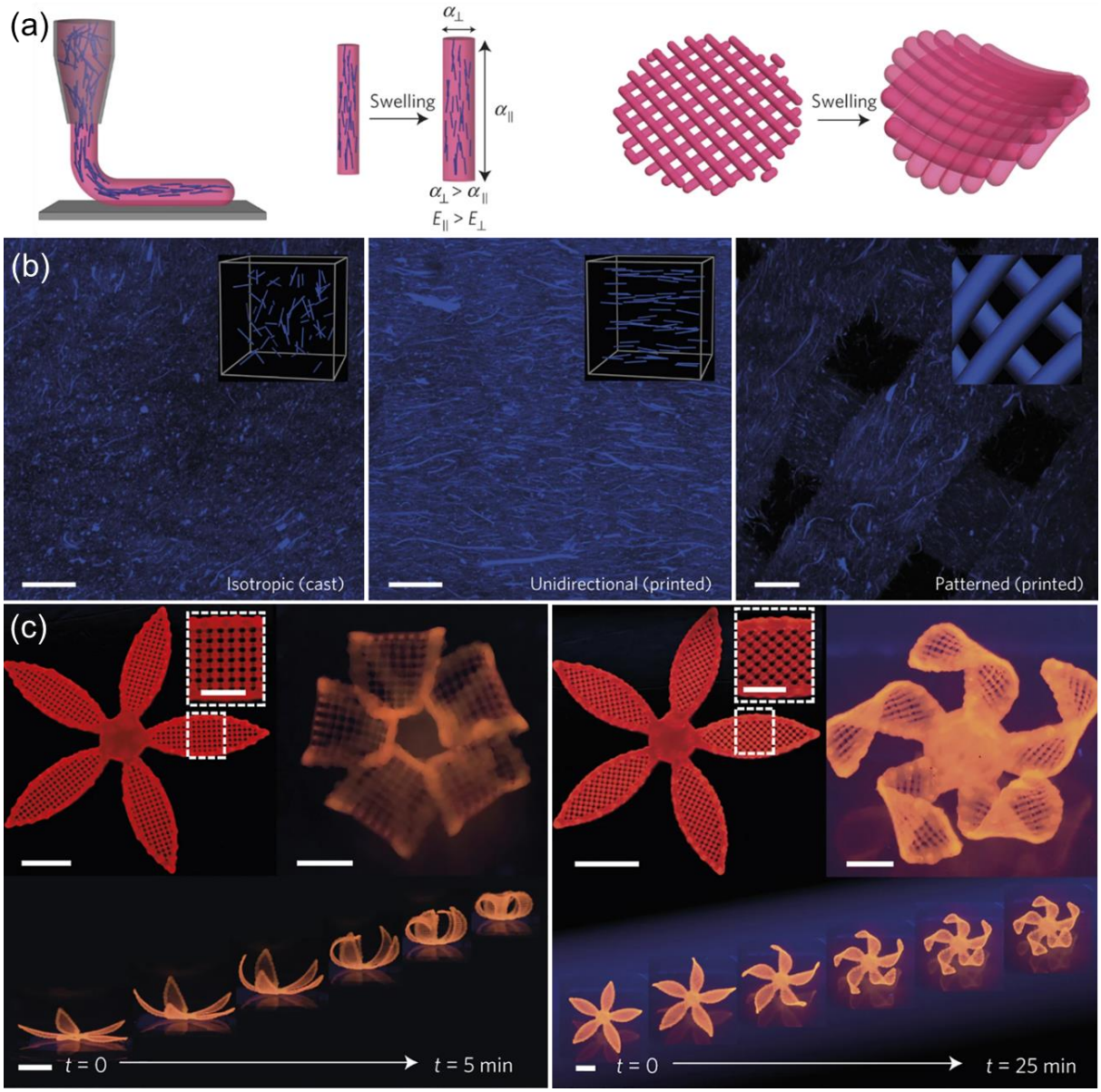

Figure 29. (a) Schematic of the shear-induced alignment of the cellulose-fibrils and its effects on the anisotropic swelling of the printed hydrogel structures. (b) Imaging of the cellulose fibrils (blue) that were randomly and aligned in the casted and printed parts, respectively. Scale bars represent 200 μm. (c) Printed flower bilayers and their shape change upon swelling. Scale bars represent 5 mm, inset scale bars represent 2.5 mm. Reproduced with permission. [305a] Copyright 2016, Springer Nature.

6.3. Other inks

Photosensitive resin inks used for DIW often require UV light for photopolymerization. For dual-cure reactive resin inks, UV light is used to accelerate the curing rate, and a post process, such as thermal curing, is employed to improve the performance of printed parts. All-

aromatic polyimides, such as bismaleimide, have very high processing temperatures (> 400 °C) and low solubility in a solvent, which renders them difficult to be processed by other AM processes. Rau et al. enabled the processing of such polyimides using UV-assisted DIW by developing a high-viscosity resin (770 Pa·s) based on polyamic acids and dimethylaminoethyl acrylate (DMAEMA). [295a, 307] The DMAEMA molecules that were bonded to the polyamic acids by electrostatic forces of attraction were cross-linked upon exposure to UV light, forming a solid structure. Subsequently, the parts were thermally treated, which imidized the polyamic acids into polyimide. The obtained polyimide parts exhibited a storage modulus value above 1 GPa, which was maintained up to 400 °C.

Epoxy resins are a type of reactive material that initially exhibits low viscosity and normally requires a long time for thermal curing. To enable the printability of epoxy resins for DIW, Compton et al. incorporated nano-clay platelets that served as rheology modifiers to the concentrated epoxy-based inks. [291a] The developed ink exhibited significant shear thinning behavior that allowed its extrusion through a micronozzle under ambient conditions, and after exiting the nozzle, it possessed sufficiently high strength to maintain its printed filamentary shape. Finally, the printed structures were thermally cured at elevated temperatures (100–220 °C) for several hours to form the final parts.

Polyelectrolyte inks that are composed of polyanions (e.g., poly(acrylic acid)) and polycations (e.g., poly(ethylenimine)) have also been used for DIW. [293b, 293c, 308] The printing of polyelectrolyte inks typically involves their being dispensed into a solvent reservoir, where solidification occurs in situ upon the contact of the inks with the solvent that promotes polyelectrolyte exchange reactions. The solidification mechanism of polyelectrolyte inks depends on the composition of the coagulation reservoir; solidification can be driven by the electrostatic forces of attraction in a water-rich reservoir, or the solvent-quality effects in an alcohol-rich reservoir. To ensure that the rheology of a polyelectrolyte ink is desirable for DIW,

polyanions and polycations need to have different molecular weights and must be mixed at a nonstoichiometric ratio, where the polyion of higher molecular weight is in excess. Owing to the low viscosity of polyelectrolyte inks (ca. 5–150 Pa·s), microcapillary (0.5–5 μm) nozzles can be used, allowing DIW at the microscale, which would be useful for fabricating templates for photonic structures and biomimetic mineralization. [293a]

The versatility of DIW enables its diverse applications ranging from electronics to biomedical engineering and 4D printing, which are trending areas in today's industry. Printing at the voxel level was previously only achievable with inkjet-based printing, but with multi-material multi-nozzle 3D printing that is capable of patterning a broad range of structural, functional and biological inks developed for DIW, this versatile approach developed will have an immense impact on the fabrication of 3D structures at the voxel level. [19]

7. Conclusions and future perspectives

AM technology that is considered an essential for Industry 4.0 offers tremendous opportunities for product development, efficient production, low-volume production of bespoke products on demand, and production flexibility. The progress of AM has been phenomenal as better-performing materials and larger, more efficient, and more capable systems are continuously introduced into the market. Research on the development of resins, polymer powders, filaments, and inks is rapidly increasing in industries and academia, and many polymer materials new to the AM technology are gaining attention and awaiting the market's acceptance.

The largest share of the total polymer material market for AM is currently taken up by photosensitive resins. Even though the majority of resin formulations are proprietary and are sold by few companies, research activities on developing novel resins are very active, and the development of functional resins with enhanced bioactivity, dielectricity, conductivity,

magnetism, etc. have been extensively explored for the fabrication of biocompatible implants, shape-changing and smart structures. Polymer powders, the second-most used polymer material for AM, are currently largely based on PAs. Nevertheless, high-performance, commodity and TPE polymer powders have also gained significant attention and several of them are now available on the market for functional applications. Meanwhile, polymer filaments are predominantly based on amorphous thermoplastics, but with improved process controls and material modifications, the use of high-performance, flexible, biocompatible, and continuous fiber-reinforced polymer composite filaments for engineering applications is now possible. Viscous inks have been gaining increasing attention because of their versatility and potential use for multi-material part fabrication, which is particularly favorable for printing soft materials and cells for biomedical applications. A wide variety of ink materials have been developed for applications such as biomedical devices, energy storage devices and flexible electronics.

Even with many efforts in developing polymer materials for AM, they still pale in comparison to those of conventional manufacturing processes due to the stringent requirements for AM materials. These materials should i) satisfy the intrinsic material requirements specific to each AM process, ii) be formed into proper feedstocks, and iii) exhibit appropriate service properties. To encourage more research on the development of polymer materials for AM, the perspectives are outlined as follows.

Bottom-up approaches to the design and synthesis of molecular structures can be utilized to develop new polymers with intrinsic properties that are specifically tailored for the AM processes. To ensure that the polymer fusion, solidification and reaction kinetics are aligned with the time-scale of the AM processes, the molecular structure of polymers can be rationally designed at the molecular level to adapt the polymers to each AM process, instead of using readily available polymer formulations that are designed for conventional manufacturing

processes. The optical (e.g., absorptance), thermal (e.g., melting and crystallization behaviors), and rheological (e.g., viscosity and relaxation dynamics) properties of the polymer materials could be tailored for each AM process and application by tuning their molecular chain structure, molecular weight distribution, functional group, degree of functionality, etc.

Feedstock production is crucial to AM as the processability of feedstocks influences the repeatability of the AM processes and the quality of parts produced. Consequently, it is worthwhile to explore novel methods for the manufacture or formulation of feedstocks for the AM processes. The restrictions imposed by the need for appropriate feedstocks are the most evident for the PBF and FDM processes because polymer powders and filaments that PBF and FDM use, respectively, are significantly different from traditionally used polymer pellets. For instance, to produce polymer powder particles with improved physical characteristics (e.g., spherical shape and narrow particle size distribution) for PBF, innovative physicochemical methods (e.g., direct polymerization, dissolution-precipitation and melt emulsification) rather than mechanical grinding are required. Feedstock production methods are also particularly important for composite resins, powders and inks, as the dispersion, stability, and compatibility of fillers in the matrix of a polymer composite are of paramount significance in ensuring the processability of composite feedstocks and the attainment of desired composite part properties. Advanced physical and chemical surface-modification methods (e.g., hyperdispersant treatment and chemical grafting), and compounding or dispersion techniques (e.g., in situ encapsulation/polymerization) can be employed for the preparation of specialized polymer composite feedstocks for AM.

The next level of polymer material development for AM is to achieve improved functionalities including thermal conductivity, electrical conductivity, dielectricity, and biocompatibility. With the popularization of shape-changing and smart materials, localized functionalization and multi-functionalization capabilities are especially desired. Such

functionalization can be achieved with composites and/or spatially discrete multiple materials. The utilization of external force fields (e.g., magnetic and electrical fields) during the layer fabrication processes can serve to control the distribution of functional components (e.g., fillers) in the final parts for localized functionalization. Multi-material AM processes that typically have multiple nozzles or print-heads (e.g., PolyJet and multi-material multi-nozzle 3D printing) can multi-functionalize and enhance the performance of AM parts by varying the material type and compositions within each layer. With an increasing focus towards functional and multi-material printing, issues related to polymer-filler and polymer-polymer interfacial interactions are important for consideration. For multi-material printing, an additional complication arises from the need to design and determine the appropriate material compositions and structures to realize desired functionality.

Processes and materials are tightly related, and an in-depth understanding of the process fundamentals is important for a successful material development. Numerical modelling can be used to aid the multi-scale investigations on the materials at different stages of the AM processes, such as the light-matter interactions, viscous flow behaviors and solidification mechanisms of polymers or polymer composites during printing, and the physical and mechanical properties of the final printed parts. In the VP, MJ and PBF processes where different light sources (e.g., laser, UV, IR and visible light) are involved, energy absorption models for the interactions between the light sources and the polymer powders or liquid resins can be established by using numerical modelling.

The time-dependent density functional theory can be applied to evaluate the absorption and emission spectra of photoinitiators, which is beneficial for the development of novel photosensitive resins. Computational fluid dynamics serves as a mathematical method for solving problems that involve thermal and fluid flow phenomena at the mesoscopic scale, which is particularly useful for the PBF and the ME techniques; fluid flow simulation can be

utilized to gain an in-depth understanding of the viscous flow of non-Newtonian polymer solutions, dispersions, and melts during the different AM processes. The finite element method can be used to simulate the thermo-mechanical behavior of polymer materials, at the macroscale, during and after printing. It is capable of process simulations that can be used to predict the actual state of the materials that are being processed, such as the temperature and stress distribution of a sintered region, by taking into consideration the time- and temperature-dependent material properties. The predictions can additionally serve to provide guidance for process parameter optimization and for improving processing efficiency. The finite element method can also be applied to investigate the mechanical and functional performance of AM-fabricated parts.

To achieve a greater understanding and better control of the AM processes, in situ measurements, offline measurements under conditions analogous to a specific AM process, and in situ process monitoring can be employed to acquire accurate material- and process-related data. The time-, temperature-, and pressure-dependent material properties and the process conditions (e.g., heating rate, cooling rate and shear rate) can be obtained by employing in situ and offline measurement techniques. The measurements can be used as reliable inputs for establishing robust numerical models. In situ process monitoring methods can be utilized to collect real-time data during build processes, which can subsequently be used as high-quality outputs to validate theoretical models. The real-time data can also be fed into closed loop control algorithms for assessing and managing AM machine operations, which helps to enhance the quality assurance of AM-fabricated parts. Depending on the type of measurement method (e.g., laser flash DS and in-situ X-ray scattering/diffraction/microtomography) and monitoring system (e.g., visual camera, pyrometer and IR camera) employed, information regarding the polymer viscosity, surface topography of printed parts, temperature and pressure of the build chamber, etc. can be acquired. These data can provide unprecedented insights and

be used for a better understanding of the process fundamentals, which can then be utilized to develop polymer materials with properties that are more suitable for the AM process.

Artificial intelligence, in particular machine learning (ML), provides a new paradigm to revolutionize and accelerate the development of polymer materials for AM owing to its advantage of automated analytical model-building by learning from data. ML has proven successful in predicting the relationships between molecular structures and material properties, and can be an effective solution for screening a large inventory of materials that are potentially suitable for a specific AM process. Taking the design of novel photoinitiators for VP as an example, ML methods such as Bayesian modelling and support vector machines can be employed to relate the molecular structure information (e.g., atom types, bonds and molecular weight) to the target properties (e.g., photon absorption spectrum and absorption coefficient). The large dataset for model training can be obtained from simulations (e.g., density functional theory calculations) and/or experimental results. The built model can then provide insights into the key molecular characteristics that are linked to the target properties of a resin, which would enable a rapid computational screening of databases to identify candidate molecules that are likely to possess the desired properties. ML can similarly be used to screen suitable thermoplastics, inks, and their composites, etc. for other polymer AM processes. The use of ML can also be extended to material wastage minimization, process control and optimization, part design, etc. all of which would benefit the advancements in AM.

The recent progress on polymer materials for AM is expected to spur further research interests and developments in this field. Given the rapid pace of technological advancements, it is only a matter of time before AM becomes a feasible technology that complements traditional manufacturing techniques.

Acknowledgements

This research work was supported by the Economic Development Board, Singapore and Robert Bosch (SEA) Pte. Ltd. through the Industrial Postgraduate Programme with Nanyang Technological University, Singapore, the National Research Foundation Medium Sized Center, Singapore through the Marine and Offshore Programme, and the Nanyang Environment and Water Research Institute (Core Fund), Nanyang Technological University, Singapore.

Received: ((will be filled in by the editorial staff))
Revised: ((will be filled in by the editorial staff))
Published online: ((will be filled in by the editorial staff))

References

[1] a) N. Guo, M. C. Leu, *Frontiers of Mechanical Engineering* **2013**, 8, 215; b) I. Gibson, D. Rosen, B. Stucker, *Additive manufacturing technologies: 3D printing, rapid prototyping, and direct digital manufacturing*, Springer, **2014**.

[2] a) M. Gebler, A. J. S. Uiterkamp, C. Visser, *Energy Policy* **2014**, 74, 158; b) I. Ribeiro, F. Matos, C. Jacinto, H. Salman, G. Cardeal, H. Carvalho, R. Godina, P. Peças, *Sustainability* **2020**, 12, 929.

[3] Global markets for 3D printing, *BCC Research*, **2018**.

[4] R. Goodridge, C. Tuck, R. Hague, *Progress in Materials Science* **2012**, 57, 229.

[5] a) F. P. Melchels, J. Feijen, D. W. Grijpma, *Biomaterials* **2010**, 31, 6121; b) X. Wang, M. Jiang, Z. Zhou, J. Gou, D. Hui, *Composites Part B: Engineering* **2016**, 110, 442; c) A. Joe Lopes, E. MacDonald, R. B. Wicker, *Rapid Prototyping Journal* **2012**, 18, 129.

[6] J. R. Tumbleston, D. Shirvanyants, N. Ermoshkin, R. Janusziewicz, A. R. Johnson, D. Kelly, K. Chen, R. Pinschmidt, J. P. Rolland, A. Ermoshkin, *Science* **2015**, aaa2397.

[7] D. A. Walker, J. L. Hedrick, C. A. Mirkin, *Science* **2019**, 366, 360.

[8] B. E. Kelly, I. Bhattacharya, H. Heidari, M. Shusteff, C. M. Spadaccini, H. K. Taylor, *Science* **2019**, 363, 1075.

[9] S. K. Saha, D. Wang, V. H. Nguyen, Y. Chang, J. S. Oakdale, S.-C. Chen, *Science* **2019**, 366, 105.

[10] S. Maruo, S. Kawata, *Journal of microelectromechanical systems* **1998**, 7, 411.

[11] L. Li, J. T. Fourkas, *Materials Today* **2007**, 10, 30.

[12] a) J. Lee, H.-C. Kim, J.-W. Choi, I. H. Lee, *International Journal of Precision Engineering and Manufacturing-Green Technology* **2017**, 4, 373; b) I. Gibson, D. W. Rosen, B. Stucker, *Additive manufacturing technologies*, Springer, **2010**.

[13] I. Liashenko, J. Rosell-Llompart, A. Cabot, *Nature Communications* **2020**, 11, 1.

[14] a) M. Schmid, A. Amado, K. Wegener, *Journal of Materials Research* **2014**, 29, 1824; b) J.-P. Kruth, G. Levy, F. Klocke, T. Childs, *CIRP Annals-Manufacturing Technology* **2007**, 56, 730; c) A. T. Sutton, C. S. Kriewall, M. C. Leu, J. W. Newkirk, presented at Proceedings of the 27th Annual International Solid Freeform Fabrication Symposium – An Additive Manufacturing Conference **2016**; d) J.-P. Kruth, X. Wang, T. Laoui, L. Froyen, *Assembly Automation* **2003**, 23, 357.

[15] Hewlett-Packard, HP Multi Jet Fusion technology technical white paper, **2018**.

[16] Z. Xu, Y. Wang, D. Wu, K. P. Ananth, J. Bai, *Journal of Manufacturing Processes* **2019**, 47, 419.

[17] S. Singh, S. Ramakrishna, R. Singh, *Journal of Manufacturing Processes* **2017**, 25, 185.

[18] R. L. Truby, J. A. Lewis, *Nature* **2016**, 540, 371.

[19] M. A. Skylar-Scott, J. Mueller, C. W. Visser, J. A. Lewis, *Nature* **2019**, 575, 330.

[20] M. Ziaee, N. B. Crane, *Additive Manufacturing* **2019**.

[21] R. Janusziewicz, J. R. Tumbleston, A. L. Quintanilla, S. J. Mecham, J. M. DeSimone, *Proceedings of the National Academy of Sciences* **2016**, 113, 11703.

[22] J. V. Crivello, J. Lee, *Journal of Polymer Science Part A: Polymer Chemistry* **1989**, 27, 3951.

[23] J. Crivello, *Annual review of materials science* **1983**, 13, 173.

[24] a) Y. Lu, F. Hasegawa, Y. Kawazu, K. Totani, T. Yamashita, W. Toshiyuki, *Sen'i Gakkaishi* **2004**, 60, 165; b) C. N. LaFratta, T. Baldacchini, *Micromachines* **2017**, 8, 101.

[25] a) S. C. Ligon, R. Liska, J. r. Stampfl, M. Gurr, R. Mülhaupt, *Chemical reviews* **2017**, 117, 10212; b) Z. Li, N. Pucher, K. Cicha, J. Torgersen, S. C. Ligon, A. Ajami, W. Husinsky, A. Rosspeintner, E. Vauthey, S. Naumov, *Macromolecules* **2013**, 46, 352.

[26] C. Mendes-Felipe, J. Oliveira, I. Etxebarria, J. L. Vilas-Vilela, S. Lanceros-Mendez, *Advanced Materials Technologies* **2019**, 4, 1800618.

[27] C. Decker, T. Nguyen Thi Viet, H. Pham Thi, *Polymer International* **2001**, 50, 986.

[28] a) C. Esposito Corcione, R. Striani, F. Montagna, D. Cannoletta, *Polymers for Advanced Technologies* **2015**, 26, 92; b) C. E. Corcione, *Journal of Polymer Engineering* **2014**, 34, 85.

[29] R. Yu, X. Yang, Y. Zhang, X. Zhao, X. Wu, T. Zhao, Y. Zhao, W. Huang, *ACS Applied Materials & Interfaces* **2017**, 9, 1820.

[30] L. Li, L. J. Lee, *Polymer Engineering & Science* **2001**, 41, 53.

[31] R. J. Mondschein, A. Kanitkar, C. B. Williams, S. S. Verbridge, T. E. Long, *Biomaterials* **2017**, 140, 170.

[32] J. Z. Manapat, Q. Chen, P. Ye, R. C. Advincula, *Macromolecular Materials and Engineering* **2017**, 302, 1600553.

[33] L. Elomaa, S. Teixeira, R. Hakala, H. Korhonen, D. W. Grijpma, J. V. Seppälä, *Acta Biomaterialia* **2011**, 7, 3850.

[34] F. P. W. Melchels, J. Feijen, D. W. Grijpma, *Biomaterials* **2009**, 30, 3801.

[35] D. Bourell, J. P. Kruth, M. Leu, G. Levy, D. Rosen, A. M. Beese, A. Clare, *CIRP Annals - Manufacturing Technology* **2017**, 66, 659.

[36] B. Derby, *Annual Review of Materials Research* **2010**, 40, 395.

[37] A. M. Elliott, O. S. Ivanova, C. B. Williams, T. A. Campbell, *Advanced Engineering Materials* **2013**, 15, 903.

[38] A. Hancock, L. Lin, *Pigment & resin technology* **2004**, 33, 280.

[39] F. P. W. Melchels, K. Bertoldi, R. Gabbrielli, A. H. Velders, J. Feijen, D. W. Grijpma, *Biomaterials* **2010**, 31, 6909.

[40] A. M. Greiner, B. Richter, M. Bastmeyer, *Macromolecular bioscience* **2012**, 12, 1301.

[41] F. J. O'brien, *Materials today* **2011**, 14, 88.

[42] R. Liska, M. Schuster, R. InfŘhr, C. Turecek, C. Fritscher, B. Seidl, V. Schmidt, L. Kuna, A. Haase, F. Varga, *Journal of Coatings Technology and Research* **2007**, 4, 505.

[43] S. J. Leigh, H. T. Gilbert, I. A. Barker, J. M. Becker, S. M. Richardson, J. A. Hoyland, J. A. Covington, A. P. Dove, *Biomacromolecules* **2012**, 14, 186.

[44] V. Popov, A. Evseev, A. Ivanov, V. Roginski, A. Volozhin, S. Howdle, *Journal of Materials Science: Materials in Medicine* **2004**, 15, 123.

[45] E. Yoshii, *Journal of Biomedical Materials Research: An Official Journal of The Society for Biomaterials and The Japanese Society for Biomaterials* **1997**, 37, 517.

[46] a) M. Schuster, C. Turecek, B. Kaiser, J. Stampfl, R. Liska, F. Varga, *Journal of Macromolecular Science, Part A* **2007**, 44, 547; b) M. Schuster, C. Turecek, A. Mateos,

J. Stampfl, R. Liska, F. Varga, *Monatshefte für Chemie/Chemical Monthly* **2007**, 138, 261.

[47] J. W. Lee, P. X. Lan, B. Kim, G. Lim, D.-W. Cho, *Microelectronic Engineering* **2007**, 84, 1702.

[48] K. Kim, D. Dean, J. Wallace, R. Breithaupt, A. G. Mikos, J. P. Fisher, *Biomaterials* **2011**, 32, 3750.

[49] P. X. Lan, J. W. Lee, Y.-J. Seol, D.-W. Cho, *Journal of Materials Science: Materials in Medicine* **2009**, 20, 271.

[50] F. P. W. Melchels, D. W. Grijpma, J. Feijen, *Journal of Controlled Release* **2008**, 132, e71.

[51] T. M. Seck, F. P. W. Melchels, J. Feijen, D. W. Grijpma, *Journal of Controlled Release* **2010**, 148, 34.

[52] Y.-L. Cheng, F. Chen, *Materials Science and Engineering: C* **2017**, 81, 66.

[53] J. Jansen, F. P. W. Melchels, D. W. Grijpma, J. Feijen, *Biomacromolecules* **2009**, 10, 214.

[54] S. Schüller-Ravoo, S. M. Teixeira, J. Feijen, D. W. Grijpma, A. A. Poot, *Macromolecular Bioscience* **2013**, 13, 1711.

[55] S. Schüller-Ravoo, J. Feijen, D. W. Grijpma, *Macromolecular Bioscience* **2011**, 11, 1662.

[56] S. Schüller-Ravoo, E. Zant, J. Feijen, D. W. Grijpma, *Advanced healthcare materials* **2014**, 3, 2004.

[57] J. Liang, D. W. Grijpma, A. A. Poot, *European Polymer Journal* **2020**, 123, 109420.

[58] W. Zhu, S.-H. Pyo, P. Wang, S. You, C. Yu, J. Alido, J. Liu, Y. Leong, S. Chen, *ACS applied materials & interfaces* **2018**, 10, 5331.

[59] E. O. Bachtiar, O. Erol, M. Millrod, R. Tao, D. H. Gracias, L. H. Romer, S. H. Kang, *Journal of the Mechanical Behavior of Biomedical Materials* **2020**, 104, 103649.

[60] L. Elomaa, C.-C. Pan, Y. Shanjani, A. Malkovskiy, J. V. Seppala, Y. Yang, *Journal of Materials Chemistry B* **2015**, 3, 8348.

[61] V. B. Morris, S. Nimbalkar, M. Younesi, P. McClellan, O. Akkus, *Annals of biomedical engineering* **2017**, 45, 286.

[62] B. Dhariwala, E. Hunt, T. Boland, *Tissue engineering* **2004**, 10, 1316.

[63] W. Meyer, S. Engelhardt, E. Novosel, B. Elling, M. Wegener, H. Krüger, *Journal of Functional Biomaterials* **2012**, 3, 257.

[64] B. Huber, S. Engelhardt, W. Meyer, H. Krüger, A. Wenz, V. Schönhaar, G. E. Tovar, P. J. Kluger, K. Borchers, *Journal of functional biomaterials* **2016**, 7, 11.

[65] R. Gauvin, Y.-C. Chen, J. W. Lee, P. Soman, P. Zorlutuna, J. W. Nichol, H. Bae, S. Chen, A. Khademhosseini, *Biomaterials* **2012**, 33, 3824.

[66] S. Wadnap, S. Krishnamoorthy, Z. Zhang, C. Xu, *Journal of Materials Science: Materials in Medicine* **2019**, 30, 36.

[67] M. Schuster, C. Turecek, G. Weigel, R. Saf, J. Stampfl, F. Varga, R. Liska, *Journal of Polymer Science Part A: Polymer Chemistry* **2009**, 47, 7078.

[68] M. Schmidt, M. Merklein, D. Bourell, D. Dimitrov, T. Hausotte, K. Wegener, L. Overmeyer, F. Vollertsen, G. N. Levy, *CIRP Annals - Manufacturing Technology* **2017**, 66, 561.

[69] T. Matsuda, M. Mizutani, *Journal of Biomedical Materials Research* **2002**, 62, 395.

[70] E. M. Wilts, A. Gula, C. Davis, N. Chartrain, C. B. Williams, T. E. Long, *European Polymer Journal* **2020**, 109693.

[71] B. van Bochove, D. W. Grijpma, *Journal of Biomaterials Science, Polymer Edition* **2019**, 30, 77.

[72] D. Dean, J. Wallace, K. Kim, A. Mikos, J. Fisher, presented at 4th International Conference on Advanced Research in Virtual and Physical Prototyping, VRAP 2009 **2010**.

[73] K.-W. Lee, S. Wang, B. C. Fox, E. L. Ritman, M. J. Yaszemski, L. Lu, *Biomacromolecules* **2007**, 8, 1077.

[74] a) R. F. Pereira, P. J. Bártolo, in *Tissue Engineering*, Springer **2014**, p. 149; b) S. He, M. Timmer, M. J. Yaszemski, A. Yasko, P. Engel, A. Mikos, *Polymer* **2001**, 42, 1251.

[75] E. C. Beck, M. Barragan, M. H. Tadros, S. H. Gehrke, M. S. Detamore, *Acta biomaterialia* **2016**, 38, 94.

[76] a) E. F. Morgan, G. U. Unnikrisnan, A. I. Hussein, *Annual review of biomedical engineering* **2018**, 20, 119; b) C. E. Misch, Z. Qu, M. W. Bidez, *Journal of oral and maxillofacial surgery* **1999**, 57, 700.

[77] Q. L. Loh, C. Choong, *Tissue Engineering Part B: Reviews* **2013**, 19, 485.

[78] a) L. Peponi, I. Navarro-Baena, J. Kenny, in *Smart polymers and their applications*, Elsevier **2014**, p. 204; b) J. Leng, X. Lan, Y. Liu, S. Du, *Progress in Materials Science* **2011**, 56, 1077.

[79] D. L. Safranski, K. Gall, *Polymer* **2008**, 49, 4446.

[80] a) H. Wu, P. Chen, C. Yan, C. Cai, Y. Shi, *Materials & Design* **2019**, 171, 107704; b) Y. Y. C. Choong, S. Maleksaeedi, H. Eng, J. Wei, P.-C. Su, *Materials & Design* **2017**, 126, 219; c) T. Zhao, R. Yu, X. Li, B. Cheng, Y. Zhang, X. Yang, X. Zhao, Y. Zhao,

W. Huang, *European Polymer Journal* **2018**, 101, 120; d) C. M. Yakacki, R. Shandas, C. Lanning, B. Rech, A. Eckstein, K. Gall, *Biomaterials* **2007**, 28, 2255; e) Q. Ge, A. H. Sakhaei, H. Lee, C. K. Dunn, N. X. Fang, M. L. Dunn, *Scientific Reports* **2016**, 6, 31110.

[81] D. K. Patel, A. H. Sakhaei, M. Layani, B. Zhang, Q. Ge, S. Magdassi, *Advanced Materials* **2017**, 29.

[82] Z. Zhao, J. Wu, X. Mu, H. Chen, H. J. Qi, D. Fang, *Macromolecular rapid communications* **2017**, 38, 1600625.

[83] a) Y. Y. C. Choong, S. Maleksaeedi, H. Eng, P.-C. Su, J. Wei, *Virtual and Physical Prototyping* **2017**, 12, 77; b) Q. Ge, A. H. Sakhaei, H. Lee, C. K. Dunn, N. X. Fang, M. L. Dunn, *Scientific Reports* **2016**, 6.

[84] a) Y. Dong, S. Wang, Y. Ke, L. Ding, X. Zeng, S. Magdassi, Y. Long, *Advanced Materials Technologies* **2020**; b) B. Huang, R. Hu, Z. Xue, J. Zhao, Q. Li, T. Xia, W. Zhang, C. Lu, *Carbohydrate Polymers* **2020**, 231, 115736.

[85] a) S. E. Bakarich, R. Gorkin III, M. I. H. Panhuis, G. M. Spinks, *Macromolecular rapid communications* **2015**, 36, 1211; b) M. N. I. Shiblee, K. Ahmed, A. Khosla, M. Kawakami, H. Furukawa, *Soft matter* **2018**, 14, 7809.

[86] Y. Mao, Z. Ding, C. Yuan, S. Ai, M. Isakov, J. Wu, T. Wang, M. L. Dunn, H. J. Qi, *Scientific Reports* **2016**, 6, 24761.

[87] Z. X. Khoo, J. E. M. Teoh, Y. Liu, C. K. Chua, S. Yang, J. An, K. F. Leong, W. Y. Yeong, *Virtual and Physical Prototyping* **2015**, 10, 103.

[88] Y. Hong, M. Wu, G. Chen, Z. Dai, Y. Zhang, G. Chen, X. Dong, *ACS Applied Materials & Interfaces* **2016**, 8, 32940.

[89] a) P. Laszczak, L. Jiang, D. L. Bader, D. Moser, S. Zahedi, *Medical Engineering & Physics* **2015**, 37, 132; b) J. Zhao, M. Liu, L. Liang, W. Wang, J. Xie, *Sensors and Actuators A: Physical* **2016**, 238, 379.

[90] a) K. Yu, A. Ritchie, Y. Mao, M. L. Dunn, H. J. Qi, *Procedia IUTAM* **2015**, 12, 193; b) J. Teoh, J. An, C. Chua, M. Lv, V. Krishnasamy, Y. Liu, *Virtual and Physical Prototyping* **2017**, 12, 61.

[91] Q. Ge, H. J. Qi, M. L. Dunn, *Applied Physics Letters* **2013**, 103, 131901.

[92] a) Q. Ge, C. K. Dunn, H. J. Qi, M. L. Dunn, *Smart Materials and Structures* **2014**, 23, 094007; b) J. Wu, C. Yuan, Z. Ding, M. Isakov, Y. Mao, T. Wang, M. L. Dunn, H. J. Qi, *Scientific Reports* **2016**, 6.

[93] Z. Ding, C. Yuan, X. Peng, T. Wang, H. J. Qi, M. L. Dunn, *Science advances* **2017**, 3, e1602890.

[94] a) L. S. Dimas, G. H. Bratzel, I. Eylon, M. J. Buehler, *Advanced Functional Materials* **2013**, 23, 4629; b) O. Al-Ketan, R. K. A. Al-Rub, R. Rowshan, *Advanced Materials Technologies* **2017**, 2, 1600235; c) G. X. Gu, S. Wettermark, M. J. Buehler, *Additive*

Manufacturing **2017**, 17, 47; d) G. X. Gu, M. Takaffoli, A. J. Hsieh, M. J. Buehler, *Extreme Mechanics Letters* **2016**, 9, 317.

[95] Y. Yap, V. Dikshit, S. Lionar, H. Yang, J. Lim, X. Qi, W. Yeong, J. Wei, presented at Proceedings of the 27th Annual International Solid Freeform Fabrication Symposium – An Additive Manufacturing Conference. **2016**.

[96] a) S. J. Leigh, C. Purssell, J. Bowen, D. A. Hutchins, J. A. Covington, D. Billson, *Sensors and Actuators A: Physical* **2011**, 168, 66; b) P. Calvert, R. Crockett, *Chemistry of Materials* **1997**, 9, 650; c) M. Gurr, D. Hofmann, M. Ehm, Y. Thomann, R. Kübler, R. Mülhaupt, *Advanced Functional Materials* **2008**, 18, 2390.

[97] D. Yugang, Z. Yuan, T. Yiping, L. Dichen, *Rapid Prototyping Journal* **2011**, 17, 247.

[98] a) C. J. Hansen, in *3D and 4D Printing of Polymer Nanocomposite Materials*, Elsevier **2020**, p. 25; b) X. Zhang, X. Jiang, C. Sun, *Sensors and Actuators A: Physical* **1999**, 77, 149; c) C. Sun, X. Zhang, *Journal of Applied Physics* **2002**, 92, 4796.

[99] A. Badev, Y. Abouliatim, T. Chartier, L. Lecamp, P. Lebaudy, C. Chaput, C. Delage, *Journal of Photochemistry and Photobiology A: Chemistry* **2011**, 222, 117.

[100] A. Sakly, S. Kenzari, D. Bonina, S. Corbel, V. Fournée, *Materials & Design (1980-2015)* **2014**, 56, 280.

[101] M. Zarek, M. Layani, I. Cooperstein, E. Sachyani, D. Cohn, S. Magdassi, *Advanced Materials* **2015**, 28, 4449.

[102] E. Fantino, A. Chiappone, F. Calignano, M. Fontana, F. Pirri, I. Roppolo, *Materials* **2016**, 9, 589.

[103] R. J. Furbank, J. F. Morris, *Physics of Fluids* **2004**, 16, 1777.

[104] D. Graf, A. Bermejo, L. Martinez, U. Gleissner, C. Megnin, T. Eiselt, M. Mauck, T. Hanemann, presented at MikroSystemTechnik Kongress **2017**.

[105] a) J. W. Lee, G. Ahn, D. S. Kim, D.-W. Cho, *Microelectronic Engineering* **2009**, 86, 1465; b) A. Ronca, L. Ambrosio, D. Grijpma, *Acta Biomaterialia* **2013**, 9, 5989; c) M. A. Geven, V. Varjas, L. Kamer, X. Wang, J. Peng, D. Eglin, D. W. Grijpma, *Polymers for Advanced Technologies* **2015**, 26, 1433.

[106] K. E. Dienel, B. van Bochove, J. V. Seppälä, *Biomacromolecules* **2019**, 21, 366.

[107] L. Elomaa, A. Kokkari, T. Närhi, J. V. Seppälä, *Composites Science and Technology* **2013**, 74, 99.

[108] a) X. Chen, H. O. T. Ware, E. Baker, W. Chu, J. Hu, C. Sun, *Procedia CIRP* **2017**, 65, 157; b) Y. Zhang, H. Li, X. Yang, T. Zhang, K. Zhu, W. Si, Z. Liu, H. Sun, *Polymer Composites* **2016**.

[109] a) D. Lin, S. Jin, F. Zhang, C. Wang, Y. Wang, C. Zhou, G. J. Cheng, *Nanotechnology* **2015**, 26, 434003; b) J. H. Sandoval, K. F. Soto, L. E. Murr, R. B. Wicker, *Journal of Materials Science* **2007**, 42, 156; c) H. Eng, S. Maleksaeedi, S. Yu, Y. Y. C. Choong,

F. E. Wiria, R. E. Kheng, J. Wei, P.-C. Su, H. P. Tham, *Rapid Prototyping Journal* **2017**.

[110] Q. Mu, L. Wang, C. K. Dunn, X. Kuang, F. Duan, Z. Zhang, H. J. Qi, T. Wang, *Additive Manufacturing* **2017**, 18, 74.

[111] K. Kim, W. Zhu, X. Qu, C. Aaronson, W. R. McCall, S. Chen, D. J. Sirbuly, *ACS Nano* **2014**, 8, 9799.

[112] J. Greenhall, B. Raeymaekers, *Advanced Materials Technologies* **2017**, 2, 1700122.

[113] J. J. Martin, B. E. Fiore, R. M. Erb, *Nature Communications* **2015**, 6.

[114] Y. Yang, Z. Chen, X. Song, Z. Zhang, J. Zhang, K. K. Shung, Q. Zhou, Y. Chen, *Advanced materials* **2017**, 29, 1605750.

[115] W. Wang, J. Sun, B. Guo, X. Chen, K. P. Ananth, J. Bai, *Journal of the European Ceramic Society* **2020**, 40, 682.

[116] M. Schwentenwein, J. Homa, *International Journal of Applied Ceramic Technology* **2015**, 12, 1.

[117] Z. C. Eckel, C. Zhou, J. H. Martin, A. J. Jacobsen, W. B. Carter, T. A. Schaedler, *Science* **2016**, 351, 58.

[118] a) P. Sokolov, D. Komissarenko, I. Shmeleva, I. Slyusar, G. Dosovitskiy, P. Evdokimov, V. Putlyaev, A. Dosovitskiy, presented at IOP Conference Series: Materials Science and Engineering **2018**; b) Q. Lian, W. Sui, X. Wu, F. Yang, S. Yang, *Rapid Prototyping Journal* **2018**, 24, 114.

[119] E. Zanchetta, M. Cattaldo, G. Franchin, M. Schwentenwein, J. Homa, G. Brusatin, P. Colombo, *Advanced Materials* **2016**, 28, 370.

[120] J. J. A. Barry, A. V. Evseev, M. A. Markov, C. E. Upton, C. A. Scotchford, V. K. Popov, S. M. Howdle, *Acta Biomaterialia* **2008**, 4, 1603.

[121] S. Kumar, M. Hofmann, B. Steinmann, E. J. Foster, C. Weder, *ACS Applied Materials & Interfaces* **2012**, 4, 5399.

[122] H. Liu, J. Mo, *Journal of Reinforced Plastics and Composites* **2010**, 29, 909.

[123] U. Kalsoom, A. Peristyy, P. Nesterenko, B. Paull, *RSC Advances* **2016**, 6, 38140.

[124] X. Song, Z. Chen, L. Lei, K. Shung, Q. Zhou, Y. Chen, *Rapid Prototyping Journal* **2017**.

[125] H. Wu, Y. Cheng, W. Liu, R. He, M. Zhou, S. Wu, X. Song, Y. Chen, *Ceramics International* **2016**, 42, 17290.

[126] L. He, F. Fei, W. Wang, X. Song, *ACS applied materials & interfaces* **2019**, 11, 18849.

[127] G. Vasquez, C. E. Majewski, B. Haworth, N. Hopkinson, *Additive Manufacturing* **2014**, 1, 127.

[128] P. Hejmady, L. C. van Breemen, P. D. Anderson, R. Cardinaels, *Soft matter* **2019**, 15, 1373.

[129] M. Schmid, R. Kleijnen, M. Vetterli, K. Wegener, *Applied Sciences* **2017**, 7, 462.

[130] D. Drummer, D. Rietzel, F. Kühnlein, *Physics Procedia* **2010**, 5, 533.

[131] L. Verbelen, Towards scientifically based screening criteria for polymer laser sintering, KU Leuven, November, **2016**.

[132] J. J. Beaman, J. W. Barlow, D. L. Bourell, R. H. Crawford, H. L. Marcus, K. P. McAlea, *Kluwer Academic Publishers, Norwell, MA* **1997**, 2061, 25.

[133] M. Schmid, *Laser Sintering with Plastics: Technology, Processes, and Materials*, Hanser Publishers, **2018**.

[134] a) Y. Shi, Z. Li, H. Sun, S. Huang, F. Zeng, *Proceedings of the Institution of Mechanical Engineers, Part L: Journal of Materials Design and Applications* **2004**, 218, 247; b) Y. Shi, Y. Zhang, *Applied Physics A* **2008**, 92, 621.

[135] S. Berretta, O. Ghita, K. E. Evans, *European Polymer Journal* **2014**, 59, 218.

[136] S. Ziegelmeier, P. Christou, F. Wöllecke, C. Tuck, R. Goodridge, R. Hague, E. Krampe, E. Wintermantel, *Journal of Materials Processing Technology* **2015**, 215, 239.

[137] A. Amado, M. Schmid, G. Levy, K. Wegener, *Group* **2011**, 7, 12.

[138] M. A. Dechet, A. Goblirsch, S. Romeis, M. Zhao, F. J. Lanyi, J. Kaschta, D. W. Schubert, D. Drummer, W. Peukert, J. Schmidt, *Chemical Engineering Science* **2019**, 197, 11.

[139] a) S. Ziegelmeier, F. Wöllecke, C. J. Tuck, R. D. Goodridge, R. J. Hague, *Journal of Materials Research* **2014**, 29, 1841; b) F. Shen, S. Yuan, Y. Guo, B. Zhao, J. Bai, M. Qwamizadeh, C. K. Chua, J. Wei, K. Zhou, *International Journal of Applied Mechanics* **2016**, 8, 1640006; c) S. Yuan, F. Shen, J. Bai, C. K. Chua, J. Wei, K. Zhou, *Materials & Design* **2017**, 120, 317.

[140] L. J. Tan, W. Zhu, K. Zhou, *Powder Technology* **2020**, 369, 25.

[141] A. Wegner, *Physics Procedia* **2016**, 83, 1003.

[142] a) Y. Shi, J. Chen, Y. Wang, Z. Li, S. Huang, *Proceedings of the Institution of Mechanical Engineers, Part L: Journal of Materials: Design and Applications* **2007**, 221, 37; b) Y. Shi, Y. Wang, J. Chen, S. Huang, *Journal of applied polymer science* **2008**, 108, 535; c) J. Yang, Y. Shi, Q. Shen, C. Yan, *Journal of Materials Processing Technology* **2009**, 209, 1901.

[143] M. A. Dechet, J. S. Gómez Bonilla, L. Lanzl, D. Drummer, A. Bück, J. Schmidt, W. Peukert, *Polymers* **2018**, 10, 1373.

[144] J. Schmidt, M. Sachs, C. Blümel, B. Winzer, F. Toni, K.-E. Wirth, W. Peukert, *Powder technology* **2014**, 261, 78.

[145] J. Schmidt, M. Plata, S. Tröger, W. Peukert, *Powder technology* **2012**, 228, 84.

[146] G. Wang, P. Wang, Z. Zhen, W. Zhang, J. Ji, *Materials & Design* **2015**, 87, 656.

[147] P. Chen, H. Wu, W. Zhu, L. Yang, Z. Li, C. Yan, S. Wen, Y. Shi, *Polymer Testing* **2018**, 69, 366.

[148] S. J. Wang, J. Y. Liu, L. Q. Chu, H. Zou, S. J. Zhang, C. J. Wu, *Journal of Polymer Science Part B: Polymer Physics* **2017**, 55, 320.

[149] M. A. Dechet, I. Baumeister, J. Schmidt, *Materials* **2020**, 13, 1535.

[150] S. Kloos, M. A. Dechet, W. Peukert, J. Schmidt, *Powder Technology* **2018**, 335, 275.

[151] K. Loyen, H. Senff, F.-X. Pauly, U.S. Patent 8,124,686 B2, **2012**.

[152] S. Fanselow, S. E. Emamjomeh, K.-E. Wirth, J. Schmidt, W. Peukert, *Chemical Engineering Science* **2016**, 141, 282.

[153] X. Yang, Y. Wei, S. Xi, Y. Huang, M. Kong, G. Li, *Polymer* **2019**, 172, 58.

[154] a) J. Schmidt, M. Sachs, S. Fanselow, M. Zhao, S. Romeis, D. Drummer, K.-E. Wirth, W. Peukert, *Chemical Engineering Science* **2016**, 156, 1; b) J. Schmidt, M. Sachs, C. Blümel, B. Winzer, F. Toni, K.-E. Wirth, W. Peukert, *Procedia Engineering* **2015**, 102, 550; c) J. Schmidt, M. Sachs, S. Fanselow, K. Wirth, W. Peukert, presented at Proceedings of the 27th Annual International Solid Freeform Fabrication Symposium - An Additive Manufacturing Conference. **2016**.

[155] M. Sachs, J. Schmidt, F. Toni, C. Blümel, B. Winzer, W. Peukert, K.-E. Wirth, *Procedia Engineering* **2015**, 102, 542.

[156] R. G. Kleijnen, M. Schmid, K. Wegener, *Applied Sciences* **2019**, 9, 1308.

[157] H. C. H. Ho, W. L. Cheung, I. Gibson, *Industrial & engineering chemistry research* **2003**, 42, 1850.

[158] E. D. Bain, E. J. Garboczi, J. E. Seppala, T. C. Parker, K. B. Migler, *Integrating Materials and Manufacturing Innovation* **2019**, 8, 335.

[159] F. Sillani, R. G. Kleijnen, M. Vetterli, M. Schmid, K. Wegener, *Additive Manufacturing* **2019**, 27, 32.

[160] Hewlett-Packard, HP 3D printing materials for the HP Jet Fusion 5200 Series 3D printing solution - Mechanical properties. Technical white paper, **2020**.

[161] a) H. J. O'Connor, A. N. Dickson, D. P. Dowling, *Additive Manufacturing* **2018**, 22, 381; b) J. Riedelbauch, D. Rietzel, G. Witt, *Additive Manufacturing* **2019**, 27, 259.

[162] F. Qi, N. Chen, Q. Wang, *Materials & Design* **2017**, 131, 135.

[163] H. Gu, Z. Bashir, L. Yang, *Additive Manufacturing* **2019**, 28, 194.

[164] Z. Bashir, H. Gu, L. Yang, *Polymer Engineering & Science* **2017**, 58, 1888.

[165] H. Gu, F. AlFayez, T. Ahmed, Z. Bashir, *Polymers* **2019**, 11, 2041.

[166] S. Arai, S. Tsunoda, R. Kawamura, K. Kuboyama, T. Ougizawa, *Materials & Design* **2017**, 113, 214.

[167] L. W. McKeen, *Fatigue and tribological properties of plastics and elastomers*, William Andrew, **2016**.

[168] S. Dadbakhsh, L. Verbelen, T. Vandeputte, D. Strobbe, P. Van Puyvelde, J.-P. Kruth, *Physics Procedia* **2016**, 83, 971.

[169] S. Yuan, J. Bai, C. K. Chua, K. Zhou, J. Wei, *Journal of Computing and Information Science in Engineering* **2016**, 16, 041007.

[170] N. Mys, A. Verberckmoes, L. Cardon, *Polymers* **2016**, 8, 383.

[171] a) G. Vaganov, A. Didenko, E. Ivan'kova, E. Popova, V. Yudin, V. Elokhovskii, I. Lasota, *Journal of Materials Research* **2019**, 34, 2895; b) L. Benedetti, B. Brulé, N. Decreamer, K. Evans, O. Ghita, *Materials & Design* **2019**, 181, 107906.

[172] C. Campanelli, R. D. Wildman, C. J. Tuck, presented at Proceedings of the 29th Annual International Solid Freeform Fabrication Symposium – An Additive Manufacturing Conference. **2018**.

[173] M. Yan, X. Tian, G. Peng, D. Li, X. Zhang, *Composites Science and Technology* **2018**, 165, 140.

[174] a) T. Hoskins, K. Dearn, S. Kukureka, *Polymer Testing* **2018**, 70, 511; b) T. Niino, T. Uehara, presented at Proceedings of the 26th Annual International Solid Freeform Fabrication Symposium – An Additive Manufacturing Conference. **2015**.

[175] S. Berretta, Poly Ether Ether Ketone (PEEK) polymers for High Temperature Laser Sintering (HT-LS), University of Exeter, May, **2015**.

[176] A. Das, C. A. Chatham, J. J. Fallon, C. E. Zawaski, E. L. Gilmer, C. B. Williams, M. J. Bortner, *Additive Manufacturing* **2020**, 101218.

[177] M. Beard, O. Ghita, J. Bradbury, S. Flint, K. Evans, *Innovative Developments in Virtual and Physical Prototyping* **2011**, 329.

[178] a) C. A. Chatham, T. E. Long, C. B. Williams, *Additive Manufacturing* **2019**, 28, 506; b) F. Ito, T. Niino, presented at Proceedings of the 27th Annual International Solid Freeform Fabrication Symposium – An Additive Manufacturing Conference. **2016**.

[179] T. Niino, H. Haraguchi, Y. Itagaki, S. Iguchi, M. Hagiwara, presented at Proceedings of the 22nd Annual International Solid Freeform Fabrication Symposium – An Additive Manufacturing Conference. **2011**.

[180] D. Strobbe, O. Verkinderen, L. Verbelen, B. Goderis, J.-P. Kruth, P. Van Puyvelde, *Materials & Design* **2018**, 153, 15.

[181] a) I. Flores Ituarte, O. Wiikinkoski, A. Jansson, *Polymers* **2018**, 10, 1293; b) L. Fang, Y. Wang, Y. Xu, *Advances in Polymer Technology* **2019**, 2019; c) B. Haworth, J. R. Tyrer, Z. Zhou, *Rapid Prototyping Journal* **2018**; d) W. Zhu, C. Yan, Y. Shi, S. Wen, J. Liu, Y. Shi, *Materials & Design* **2015**, 82, 37; e) W. Zhu, C. Yan, Y. Shi, S. Wen, C. Han, C. Cai, J. Liu, Y. Shi, R. I. Campbell, I. Gibson, *Rapid Prototyping Journal* **2016**, 22.

[182] a) R. Kleijnen, J. Sesseg, M. Schmid, K. Wegener, presented at AIP Conference Proceedings **2017**; b) M. M. Lexow, D. Drummer, *Journal of Powder Technology* **2016**, 2016.

[183] a) J. Bai, B. Zhang, J. Song, G. Bi, P. Wang, J. Wei, *Polymer Testing* **2016**, 52, 89; b) G. V. Salmoria, C. H. Ahrens, P. Klauss, R. A. Paggi, R. G. Oliveira, A. Lago, *Materials Research* **2007**, 10, 211.

[184] a) R. D. Goodridge, R. J. Hague, C. J. Tuck, *Journal of Materials Processing Technology* **2010**, 210, 72; b) C. Song, A. Huang, Y. Yang, Z. Xiao, J.-k. Yu, *Rapid Prototyping Journal* **2017**, 23, 1069; c) Y. Khalil, N. Hopkinson, A. Kowalski, J. P. A. Fairclough, *Materials* **2019**, 12, 3496; d) N. H. Y. Khalil, A. Kowalski, J. P. A. Fairclough, presented at Proceedings of the 27th Annual International Solid Freeform Fabrication Symposium – An Additive Manufacturing Conference. **2016**.

[185] a) G. V. Salmoria, J. L. Leite, R. A. Paggi, *Polymer Testing* **2009**, 28, 746; b) G. Salmoria, J. Leite, L. Vieira, A. Pires, C. Roesler, *Polymer Testing* **2012**, 31, 411; c) G. Salmoria, J. Leite, R. Paggi, A. Lago, A. Pires, *Polymer Testing* **2008**, 27, 654.

[186] S. Greiner, K. Wudy, L. Lanzl, D. Drummer, *Polymer Testing* **2017**, 64, 136.

[187] a) D. Drummer, K. Wudy, F. Kühnlein, M. Drexler, *Physics Procedia* **2012**, 39, 509; b) S. Yusheng, L. Zhichong, S. Haixiao, H. Shuhuai, Z. Fandi, *Proceedings of the Institution of Mechanical Engineers, Part L: Journal of Materials: Design and Applications* **2004**, 218, 299.

[188] C. Dongyu, J. Jie, S. Mo, World Patent WO/2009/034361 A3 **2009**.

[189] a) J. Bai, R. D. Goodridge, R. J. M. Hague, M. Song, *Polymer Engineering & Science* **2013**, 53, 1937; b) J. Bai, R. D. Goodridge, R. J. Hague, M. Song, M. Okamoto, *Polymer Testing* **2014**, 36, 95; c) J. Bai, R. D. Goodridge, S. Yuan, K. Zhou, C. K. Chua, J. Wei, *Molecules* **2015**, 20, 19041.

[190] a) Z. Li, Z. Wang, X. Gan, D. Fu, G. Fei, H. Xia, *Macromolecular Materials and Engineering* **2017**, 302; b) B. Chen, S. Berretta, K. Evans, K. Smith, O. Ghita, *Applied Surface Science* **2018**, 428, 1018.

[191] S. Yuan, J. Bai, C. K. Chua, J. Wei, K. Zhou, *Composites Part A: Applied Science and Manufacturing* **2016**, 90, 699.

[192] A. Ronca, G. Rollo, P. Cerruti, G. Fei, X. Gan, G. G. Buonocore, M. Lavorgna, H. Xia, C. Silvestre, L. Ambrosio, *Applied Sciences* **2019**, 9, 864.

[193] a) A. Almansoori, K. J. Abrams, A. D. G. Al-Rubaye, C. Majewski, C. Rodenburg, *Additive Manufacturing* **2019**, 25, 297; b) J. Bai, R. D. Goodridge, R. J. Hague, M. Okamoto, *Polymer Composites* **2017**, 38, 2570.

[194] R. Goodridge, M. Shofner, R. Hague, M. McClelland, M. Schlea, R. Johnson, C. Tuck, *Polymer Testing* **2011**, 30, 94.

[195] L. Yang, L. Wang, Y. Chen, *Journal of Applied Polymer Science* **2020**, 137, 48766.

[196] W. Zhu, C. Yan, Y. Shi, S. Wen, J. Liu, Q. Wei, Y. Shi, *Scientific reports* **2016**, 6, 33780.

[197] C. Yan, Y. Shi, J. Yang, J. Liu, *Journal of Reinforced Plastics and Composites* **2009**, 28, 2889.

[198] a) M. Wahab, K. Dalgarno, R. Cochrane, S. Hassan, presented at Proceedings of the World Congress on Engineering WCE **2009**; b) B. Duan, M. Wang, W. Y. Zhou, W. L. Cheung, Z. Y. Li, W. W. Lu, *Acta biomaterialia* **2010**, 6, 4495.

[199] H. Zheng, J. Zhang, S. Lu, G. Wang, Z. Xu, *Materials Letters* **2006**, 60, 1219.

[200] a) L. Lanzl, K. Wudy, S. Greiner, D. Drummer, *Polymer Composites* **2018**; b) S. Balzereit, F. Proes, V. Altstädt, C. Emmelmann, *Additive Manufacturing* **2018**, 23, 347.

[201] W. Jing, C. Hui, W. Qiong, L. Hongbo, L. Zhanjun, *Materials & Design* **2017**, 116, 253.

[202] L. Lanzl, K. Wudy, D. Drummer, *Polymer Testing* **2020**, 106313.

[203] S. R. Athreya, K. Kalaitzidou, S. Das, *Composites science and technology* **2011**, 71, 506.

[204] a) S. Yuan, Y. Zheng, C. Kai Chua, Q. Yan, K. Zhou, *Composites Part A: Applied Science and Manufacturing* **2018**, 105, 203; b) S. Yuan, C. K. Chua, K. Zhou, *Advanced Materials Technologies* **2019**, 4, 1800419.

[205] X. Gan, J. Wang, Z. Wang, Z. Zheng, M. Lavorgna, A. Ronca, G. Fei, H. Xia, *Materials & Design* **2019**, 178, 107874.

[206] R. Hong, Z. Zhao, J. Leng, J. Wu, J. Zhang, *Composites Part B: Engineering* **2019**, 176, 107214.

[207] B. Chen, R. Davies, Y. Liu, N. Yi, D. Qiang, Y. Zhu, O. Ghita, *Additive Manufacturing* **2020**, 101363.

[208] C. Yan, L. Hao, L. Xu, Y. Shi, *Composites Science and Technology* **2011**, 71, 1834.

[209] B. Duan, M. Wang, W. Zhou, W. Cheung, *Applied Surface Science* **2008**, 255, 529.

[210] S. Arai, S. Tsunoda, A. Yamaguchi, T. Ougizawa, *Additive Manufacturing* **2018**, 21, 683.

[211] a) K. Y. Jiang, Y. L. Guo, W. L. Zeng, Z. S. Xin, *Advanced Materials Research* **2010**, 113, 1722; b) K. Jiang, Y. Guo, D. L. Bourell, presented at Proceedings of the 25th Annual International Solid Freeform Fabrication Symposium – An Additive Manufacturing Conference. **2014**; c) Y. Guo, K. Jiang, D. L. Bourell, *Polymer Testing* **2014**, 37, 210.

[212] a) K. Jiang, Y. Guo, D. L. Bourell, presented at Proceedings of the 24th Annual International Solid Freeform Fabrication Symposium – An Additive Manufacturing Conference. **2013**; b) K. Y. Jiang, Y. Guo, W. Zeng, Z. Xin, X. Liu, *Advanced Materials Research* **2010**, 136, 131; c) W. Zeng, Y. Guo, K. Jiang, Z. Yu, Y. Liu, Y. Shen, J. Deng, P. Wang, *Journal of Thermoplastic Composite Materials* **2012**, 26, 125.

[213] S. Yuan, J. Bai, C. K. Chua, J. Wei, K. Zhou, *Polymers* **2016**, 8, 370.

[214] J. Bai, S. Yuan, F. Shen, B. Zhang, C. K. Chua, K. Zhou, J. Wei, *Virtual and Physical Prototyping* **2017**, 12, 235.

[215] R. Narayan, *Rapid Prototyping of Biomaterials: Techniques in Additive Manufacturing*, Woodhead Publishing, **2019**.

[216] G. V. Salmoria, E. A. Fancello, C. R. M. Roesler, F. Dabbas, *The International Journal of Advanced Manufacturing Technology* **2013**, 65, 1529.

[217] a) Y. Xia, P. Zhou, X. Cheng, Y. Xie, C. Liang, C. Li, S. Xu, *International Journal of Nanomedicine* **2013**, 8, 4197; b) C. Shuai, B. Yang, S. Peng, Z. Li, *The International Journal of Advanced Manufacturing Technology* **2013**, 69, 51; c) S. XiaoHui, L. Wei, S. PingHui, S. QingYong, W. QingSong, S. YuSheng, L. Kai, L. WenGuang, *The International Journal of Advanced Manufacturing Technology* **2015**, 81, 15.

[218] S. K. Sinha, in *3D and 4D Printing of Polymer Nanocomposite Materials*, Elsevier **2020**, p. 119.

[219] a) R. Velu, B. P. Kamarajan, M. Ananthasubramanian, T. Ngo, S. Singamneni, *Journal of Materials Research* **2018**, 1; b) R. Velu, S. Singamneni, *Journal of Materials Research* **2014**, 29, 1883.

[220] D. Pohle, S. Ponader, T. Rechtenwald, M. Schmidt, K. A. Schlegel, H. Münstedt, F. W. Neukam, E. Nkenke, C. von Wilmowsky, presented at Macromolecular Symposia **2007**.

[221] M. Navarro, T. Serra, in *Biomineralization and Biomaterials*, Elsevier **2016**, p. 315.

[222] G. V. Salmoria, R. V. Pereira, M. C. Fredel, A. P. Casadei, *Polymer Bulletin* **2018**, 75, 1299.

[223] Y. Xu, P. Wu, P. Feng, W. Guo, W. Yang, C. Shuai, *Colloids and Surfaces B: Biointerfaces* **2018**.

[224] a) E. Lahtinen, L. Turunen, M. M. Hänninen, K. Kolari, H. M. Tuononen, M. Haukka, *ACS Omega* **2019**, 4, 12012; b) S. Kulomäki, E. Lahtinen, S. Perämäki, A. Väisänen, *Analytica Chimica Acta* **2019**; c) R. Li, S. Yuan, W. Zhang, H. Zheng, W. Zhu, B. Li, M. Zhou, A. W.-K. Law, K. Zhou, *ACS Applied Materials & Interfaces* **2019**; d) K.

Wudy, M. Hinze, F. Ranft, D. Drummer, W. Schwieger, *Journal of Materials Processing Technology* **2017**, 246, 136; e) E. Lahtinen, M. M. Hänninen, K. Kinnunen, H. M. Tuononen, A. Väisänen, K. Rissanen, M. Haukka, *Advanced Sustainable Systems* **2018**, 2, 1800048.

[225] E. Lahtinen, L. Kivijärvi, R. Tatikonda, A. Väisänen, K. Rissanen, M. Haukka, *ACS Omega* **2017**, 2, 7299.

[226] S. Eosoly, D. Brabazon, S. Lohfeld, L. Looney, *Acta Biomaterialia* **2010**, 6, 2511.

[227] I. Shishkovsky, V. Sherbakov, I. Ibatullin, V. Volchkov, L. Volova, *Composite Structures* **2018**.

[228] H. Chung, S. Das, *Materials Science and Engineering: A* **2008**, 487, 251.

[229] C. Yan, Y. Shi, J. Yang, J. Liu, *Rapid Prototyping Journal* **2011**, 17, 28.

[230] S. R. Athreya, K. Kalaitzidou, S. Das, *Materials Science and Engineering: A* **2010**, 527, 2637.

[231] H. C. Kim, H. T. Hahn, Y. S. Yang, *Journal of Composite Materials* **2013**, 47, 501.

[232] J. Yang, Y. Shi, C. Yan, *Journal of Applied Polymer Science* **2010**, 117, 2196.

[233] A. Jayakumar, S. Singamneni, M. Ramos, A. M. Al-Jumaily, S. S. Pethaiah, *Materials* **2017**, 10, 796.

[234] a) M. A. H. Khondoker, D. Sameoto, *Progress in Additive Manufacturing* **2019**, 4, 197; b) N. Venkataraman, S. Rangarajan, M. Matthewson, B. Harper, A. Safari, S. Danforth, G. Wu, N. Langrana, S. Guceri, A. Yardimci, *Rapid Prototyping Journal* **2000**.

[235] B. N. Turner, S. A. Gold, *Rapid Prototyping Journal* **2015**, 21, 250.

[236] M. Spoerk, C. Savandaiah, F. Arbeiter, J. Sapkota, C. Holzer, *Polymer Composites* **2019**, 40, 638.

[237] B. N. Turner, R. Strong, S. A. Gold, *Rapid Prototyping Journal* **2014**, 20, 192.

[238] I. Gunduz, M. McClain, P. Cattani, G.-C. Chiu, J. Rhoads, S. Son, *Additive Manufacturing* **2018**, 22, 98.

[239] N. Aliheidari, J. Christ, R. Tripuraneni, S. Nadimpalli, A. Ameli, *Materials & Design* **2018**, 156, 351.

[240] a) D. Popescu, A. Zapciu, C. Amza, F. Baciu, R. Marinescu, *Polymer Testing* **2018**, 69, 157; b) J. Girdis, M. McCaffrey, G. Proust, presented at Proceedings of the 27th Annual International Solid Freeform Fabrication Symposium – An Additive Manufacturing Conference. **2016**; c) M. Namiki, M. Ueda, A. Todoroki, Y. Hirano, R. Matsuzaki, *Proceedings of the Society of the Advancement of Material and Process Engineering* **2014**.

[241] J. F. Christ, N. Aliheidari, A. Ameli, P. Pötschke, *Materials & Design* **2017**, 131, 394.

[242] M. Spoerk, C. Holzer, J. Gonzalez-Gutierrez, *Journal of Applied Polymer Science* **2019**.

[243] a) A. Bellini, L. Shor, S. I. Guceri, *Rapid Prototyping Journal* **2005**, 11, 214; b) J.-W. Tseng, C.-Y. Liu, Y.-K. Yen, J. Belkner, T. Bremicker, B. H. Liu, T.-J. Sun, A.-B. Wang, *Materials & Design* **2018**, 140, 209.

[244] N. Kumar, P. K. Jain, P. Tandon, P. M. Pandey, *Journal of Manufacturing Processes* **2018**, 35, 317.

[245] a) J.-Y. Lee, J. An, C. K. Chua, *Applied Materials Today* **2017**, 7, 120; b) A. D. Valino, J. R. C. Dizon, A. H. Espera Jr, Q. Chen, J. Messman, R. C. Advincula, *Progress in Polymer Science* **2019**, 101162; c) Y. H. Cha, K. H. Lee, H. J. Ryu, I. W. Joo, A. Seo, D.-H. Kim, S. J. Kim, *Applied Bionics and Biomechanics* **2017**, 2017.

[246] J. Zhu, Y. Hu, Y. Tang, B. Wang, *Journal of Applied Polymer Science* **2017**, 134.

[247] S. Guessasma, S. Belhabib, H. Nouri, *Macromolecular Materials and Engineering* **2019**, 304, 1800793.

[248] a) Y. Song, Y. Li, W. Song, K. Yee, K. Y. Lee, V. L. Tagarielli, *Materials & Design* **2017**, 123, 154; b) J. Milde, R. Hrušecký, R. Zaujec, L. Morovič, A. Görög, *Annals of DAAAM & Proceedings* **2017**, 28, 812.

[249] S. Wojtyła, P. Klama, T. Baran, *Journal of occupational and environmental hygiene* **2017**, 14, D80.

[250] a) B. Akhoundi, M. Nabipour, F. Hajami, D. Shakoori, *Polymer Engineering & Science* **2020**; b) I. A. Carrete, D. Bermudez, C. Aguirre, F. A. Alvarez-Primo, S. Anil-Kumar, P. Chinolla, M. Gamboa, S. A. Gonzalez, H. E. Heredia, A. M. Hernandez, *Journal of Failure Analysis and Prevention* **2019**, 19, 418.

[251] a) D. Bourell, B. Stucker, D. Espalin, K. Arcaute, D. Rodriguez, F. Medina, M. Posner, R. Wicker, *Rapid Prototyping Journal* **2010**, 16, 164; b) H.-J. Yen, C.-S. Tseng, S.-h. Hsu, C.-L. Tsai, *Biomedical Microdevices* **2009**, 11, 615; c) C.-T. Kao, C.-C. Lin, Y.-W. Chen, C.-H. Yeh, H.-Y. Fang, M.-Y. Shie, *Materials Science and Engineering: C* **2015**, 56, 165.

[252] a) M. Arif, S. Kumar, K. Varadarajan, W. Cantwell, *Materials & Design* **2018**; b) M. Rinaldi, T. Ghidini, F. Cecchini, A. Brandao, F. Nanni, *Composites Part B: Engineering* **2018**, 145, 162; c) S. Ding, B. Zou, P. Wang, H. Ding, *Polymer Testing* **2019**, 78, 105948; d) G. Taylor, X. Wang, L. Mason, M. C. Leu, K. Chandrashekhara, T. Schniepp, R. Jones, *Rapid Prototyping Journal* **2018**.

[253] C. Yang, X. Tian, D. Li, Y. Cao, F. Zhao, C. Shi, *Journal of Materials Processing Technology* **2017**, 248, 1.

[254] Y. Zhao, K. Zhao, Y. Li, F. Chen, *Journal of Manufacturing Processes* **2020**, 56, 28.

[255] M. Saari, M. Galla, B. Cox, P. Krueger, A. Cohen, E. Richer, presented at Proceedings of the 26th Annual International Solid Freeform Fabrication Symposium – An Additive Manufacturing Conference **2015**.

[256] a) A. R. Torrado Perez, D. A. Roberson, R. B. Wicker, *Journal of Failure Analysis and Prevention* **2014**, 14, 343; b) C. R. Rocha, A. R. T. Perez, D. A. Roberson, C. M. Shemelya, E. MacDonald, R. B. Wicker, *Journal of Materials Research* **2014**, 29, 1859; c) S. Chen, J. Lu, J. Feng, *Industrial & Engineering Chemistry Research* **2018**; d) W. Kosorn, M. Sakulsumbat, P. Uppanan, P. Kaewkong, S. Chantaweroad, J. Jitsaard, K. Sitthiseripratip, W. Janvikul, *Journal of Biomedical Materials Research Part B: Applied Biomaterials* **2016**, 105, 1141; e) Q. Ou-Yang, B. Guo, J. Xu, *ACS Omega* **2018**, 3, 14309; f) S. Chen, Q. Zhang, J. Feng, *Journal of Materials Chemistry C* **2017**, 5, 8361; g) Y.-G. Zhou, B. Su, L.-s. Turng, *Rapid Prototyping Journal* **2017**, 23, 869; h) M. Harris, J. Potgieter, S. Ray, R. Archer, K. M. Arif, *Materials* **2019**, 12, 4167.

[257] O. A. Mohamed, S. H. Masood, J. L. Bhowmik, *Materials letters* **2017**, 193, 58.

[258] a) G. Cicala, G. Ognibene, S. Portuesi, I. Blanco, M. Rapisarda, E. Pergolizzi, G. Recca, *Materials* **2018**, 11, 285; b) A. Gebisa, H. Lemu, *Materials* **2018**, 11, 500.

[259] J. Wu, N. Chen, F. Bai, Q. Wang, *Polymer Composites* **2018**, 39, E508.

[260] S. Meng, H. He, Y. Jia, P. Yu, B. Huang, J. Chen, *Journal of Applied Polymer Science* **2017**, 134.

[261] E. Çantı, M. Aydin, *Rapid Prototyping Journal* **2018**, 24, 171.

[262] K. Boparai, R. Singh, H. Singh, *Virtual and Physical Prototyping* **2015**, 10, 59.

[263] a) X. Jiao, H. He, W. Qian, G. Li, G. Shen, X. Li, C. Ding, D. White, S. Scearce, Y. Yang, *IEEE Transactions on Electromagnetic Compatibility* **2015**, 57, 868; b) P. S. Grant, F. Castles, Q. Lei, Y. Wang, J. Janurudin, D. Isakov, S. Speller, C. Dancer, C. Grovenor, *Phillosophical Transactions of the Royal Society A* **2015**, 373, 20140353; c) D. V. Isakov, Q. Lei, F. Castles, C. J. Stevens, C. R. M. Grovenor, P. S. Grant, *Materials & Design* **2016**, 93, 423.

[264] F. Castles, D. Isakov, A. Lui, Q. Lei, C. E. J. Dancer, Y. Wang, J. M. Janurudin, S. C. Speller, C. R. M. Grovenor, P. S. Grant, *Scientific Reports* **2016**, 6, 22714.

[265] a) M. Nikzad, S. Masood, I. Sbarski, *Materials & Design* **2011**, 32, 3448; b) N. Sa'ude, S. Masood, M. Nikzad, M. Ibrahim, M. Ibrahim, *International Journal of Engineering Research and Applications* **2013**, 3, 1257.

[266] M. Nabipour, B. Akhoundi, A. Bagheri Saed, *Journal of Applied Polymer Science* **2019**, 48717.

[267] a) E. Nyberg, A. Rindone, A. Dorafshar, W. L. Grayson, *Tissue Engineering Part A* **2017**, 23, 503; b) D. Drummer, S. Cifuentes-Cuéllar, D. Rietzel, *Rapid Prototyping Journal* **2012**, 18, 500; c) F. Senatov, K. Niaza, A. Stepashkin, S. Kaloshkin, *Composites Part B: Engineering* **2016**, 97, 193; d) N. Xu, X. Ye, D. Wei, J. Zhong, Y. Chen, G. Xu, D. He, *ACS Applied Materials & Interfaces* **2014**, 6, 14952.

[268] X. Wei, D. Li, W. Jiang, Z. Gu, X. Wang, Z. Zhang, Z. Sun, *Scientific Reports* **2015**, 5.

[269] a) L. J. Love, V. Kunc, O. Rios, C. E. Duty, A. M. Elliott, B. K. Post, R. J. Smith, C. A. Blue, *Journal of Materials Research* **2014**, 29, 1893; b) F. Ning, W. Cong, J. Qiu, J.

Wei, S. Wang, *Composites Part B: Engineering* **2015**, 80, 369; c) Z. Weng, J. Wang, T. Senthil, L. Wu, *Materials & Design* **2016**, 102, 276.

[270] a) S. J. Leigh, R. J. Bradley, C. P. Purssell, D. R. Billson, D. A. Hutchins, *PloS one* **2012**, 7, e49365; b) J. Luo, H. Wang, D. Zuo, A. Ji, Y. Liu, *Micromachines* **2018**, 9, 635; c) T. Sathies, P. Senthil, M. Anoop, *Rapid Prototyping Journal* **2020**; d) S. Berretta, R. Davies, Y. Shyng, Y. Wang, O. Ghita, *Polymer Testing* **2017**, 63, 251.

[271] D. Zhang, B. Chi, B. Li, Z. Gao, Y. Du, J. Guo, J. Wei, *Synthetic Metals* **2016**, 217, 79.

[272] a) G. D. Goh, Y. L. Yap, S. Agarwala, W. Y. Yeong, *Advanced Materials Technologies* **2019**, 4, 1800271; b) Q. Ding, X. Li, D. Zhang, G. Zhao, Z. Sun, *Journal of Applied Polymer Science* **2020**, 137, 48786.

[273] T. Mulholland, A. Falke, N. Rudolph, presented at Proceedings of the 27th Annual International Solid Freeform Fabrication Symposium – An Additive Manufacturing Conference. **2016**.

[274] D. Zhu, Y. Ren, G. Liao, S. Jiang, F. Liu, J. Guo, G. Xu, *Journal of Applied Polymer Science* **2017**, 134, 45332.

[275] X. Tian, T. Liu, C. Yang, Q. Wang, D. Li, *Composites Part A: Applied Science and Manufacturing* **2016**, 88, 198.

[276] H. L. Tekinalp, V. Kunc, G. M. Velez-Garcia, C. E. Duty, L. J. Love, A. K. Naskar, C. A. Blue, S. Ozcan, *Composites Science and Technology* **2014**, 105, 144.

[277] D. Jiang, D. Smith, presented at Proceedings of the 27th Annual International Solid Freeform Fabrication Symposium – An Additive Manufacturing Conference. **2016**.

[278] C. Yang, X. Tian, T. Liu, Y. Cao, D. Li, *Rapid Prototyping Journal* **2017**, 23, 209.

[279] N. Li, Y. Li, S. Liu, *Journal of Materials Processing Technology* **2016**, 238, 218.

[280] M. Caminero, J. Chacón, I. García-Moreno, G. Rodríguez, *Composites Part B: Engineering* **2018**, 148, 93.

[281] a) A. N. Dickson, J. N. Barry, K. A. McDonnell, D. P. Dowling, *Additive Manufacturing* **2017**, 16, 146; b) G. D. Goh, V. Dikshit, A. P. Nagalingam, G. L. Goh, S. Agarwala, S. L. Sing, J. Wei, W. Y. Yeong, *Materials & Design* **2018**, 137, 79.

[282] B. Akhoundi, A. H. Behravesh, A. Bagheri Saed, *Proceedings of the Institution of Mechanical Engineers, Part B: Journal of Engineering Manufacture* **2020**, 234, 243.

[283] Z. Liu, Y. Wang, J. Shi, *Journal of Micro and Nano-Manufacturing* **2019**, 7.

[284] M. Herrero, F. Peng, K. C. Núñez Carrero, J. C. Merino, B. D. Vogt, *ACS Sustainable Chem. Eng.* **2018**.

[285] J. Korpela, A. Kokkari, H. Korhonen, M. Malin, T. Närhi, J. Seppälä, *Journal of Biomedical Materials Research Part B: Applied Biomaterials* **2013**, 101, 610.

[286] C. M. Shemelya, A. Rivera, A. T. Perez, C. Rocha, M. Liang, X. Yu, C. Kief, D. Alexander, J. Stegeman, H. Xin, *Journal of Electronic Materials* **2015**, 44, 2598.

[287] F. Ning, W. Cong, Y. Hu, H. Wang, *Journal of Composite Materials* **2017**, 51, 451.

[288] R. Matsuzaki, M. Ueda, M. Namiki, T.-K. Jeong, H. Asahara, K. Horiguchi, T. Nakamura, A. Todoroki, Y. Hirano, *Scientific Reports* **2016**, 6, 23058.

[289] F. Van Der Klift, Y. Koga, A. Todoroki, M. Ueda, Y. Hirano, R. Matsuzaki, *Open Journal of Composite Materials* **2016**, 6, 18.

[290] a) J. M. McCracken, A. Badea, M. E. Kandel, A. S. Gladman, D. J. Wetzel, G. Popescu, J. A. Lewis, R. G. Nuzzo, *Advanced healthcare materials* **2016**, 5, 1025; b) P. Jiang, C. Yan, Y. Guo, X. Zhang, M. Cai, X. Jia, X. Wang, F. Zhou, *Biomaterials science* **2019**, 7, 1805; c) C. B. Highley, C. B. Rodell, J. A. Burdick, *Advanced Materials* **2015**, 27, 5075; d) M. Zhang, A. Vora, W. Han, R. J. Wojtecki, H. Maune, A. B. Le, L. E. Thompson, G. M. McClelland, F. Ribet, A. C. Engler, *Macromolecules* **2015**, 48, 6482.

[291] a) B. G. Compton, J. A. Lewis, *Advanced materials* **2014**, 26, 5930; b) Q. Chen, J. Zhao, J. Ren, L. Rong, P. F. Cao, R. C. Advincula, *Advanced Functional Materials* **2019**, 29, 1900469; c) L.-y. Zhou, Q. Gao, J.-z. Fu, Q.-y. Chen, J.-p. Zhu, Y. Sun, Y. He, *ACS applied materials & interfaces* **2019**, 11, 23573.

[292] a) K. Markstedt, A. Mantas, I. Tournier, H. c. Martínez Ávila, D. Hagg, P. Gatenholm, *Biomacromolecules* **2015**, 16, 1489; b) A. Lee, A. Hudson, D. Shiwarski, J. Tashman, T. Hinton, S. Yerneni, J. Bliley, P. Campbell, A. Feinberg, *Science* **2019**, 365, 482; c) L. Valot, J. Martinez, A. Mehdi, G. Subra, *Chemical Society Reviews* **2019**, 48, 4049.

[293] a) J. A. Lewis, *Advanced Functional Materials* **2006**, 16, 2193; b) G. M. Gratson, J. A. Lewis, *Langmuir* **2005**, 21, 457; c) G. M. Gratson, M. Xu, J. A. Lewis, *nature* **2004**, 428, 386.

[294] M. Wei, F. Zhang, W. Wang, P. Alexandridis, C. Zhou, G. Wu, *Journal of Power Sources* **2017**, 354, 134.

[295] a) D. A. Rau, J. Herzberger, T. E. Long, C. B. Williams, *ACS applied materials & interfaces* **2018**, 10, 34828; b) Z. Jiang, O. Erol, D. Chatterjee, W. Xu, N. Hibino, L. H. Romer, S. H. Kang, D. H. Gracias, *ACS applied materials & interfaces* **2019**, 11, 28289.

[296] J. A. Lewis, J. E. Smay, J. Stuecker, J. Cesarano, *Journal of the American Ceramic Society* **2006**, 89, 3599.

[297] L. Li, Q. Lin, M. Tang, A. J. Duncan, C. Ke, *Chemistry–A European Journal* **2019**.

[298] K. B. Manning, N. Wyatt, L. Hughes, A. Cook, N. H. Giron, E. Martinez, C. G. Campbell, M. C. Celina, *Macromolecular Materials and Engineering* **2019**, 304, 1800511.

[299] I. Donderwinkel, J. C. Van Hest, N. R. Cameron, *Polymer Chemistry* **2017**, 8, 4451.

[300] H. Li, C. Tan, L. Li, *Materials & Design* **2018**, 159, 20.

[301] T. J. Hinton, Q. Jallerat, R. N. Palchesko, J. H. Park, M. S. Grodzicki, H.-J. Shue, M. H. Ramadan, A. R. Hudson, A. W. Feinberg, *Science advances* **2015**, 1, e1500758.

[302] N. Noor, A. Shapira, R. Edri, I. Gal, L. Wertheim, T. Dvir, *Advanced Science* **2019**, 6, 1900344.

[303] a) X. Wan, H. Wei, F. Zhang, Y. Liu, J. Leng, *Journal of Applied Polymer Science* **2019**, 48177; b) X. Kuang, K. Chen, C. K. Dunn, J. Wu, V. C. Li, H. J. Qi, *ACS applied materials & interfaces* **2018**, 10, 7381; c) K. Chen, X. Kuang, V. Li, G. Kang, H. J. Qi, *Soft matter* **2018**, 14, 1879; d) H. Wei, Q. Zhang, Y. Yao, L. Liu, Y. Liu, J. Leng, *ACS applied materials & interfaces* **2016**, 9, 876.

[304] T. Uchida, H. Onoe, *Micromachines* **2019**, 10, 433.

[305] a) A. S. Gladman, E. A. Matsumoto, R. G. Nuzzo, L. Mahadevan, J. A. Lewis, *Nature materials* **2016**; b) J. Liu, W. Liu, A. Pantula, Z. Wang, D. H. Gracias, T. D. Nguyen, *Extreme Mechanics Letters* **2019**, 30, 100514.

[306] D. Kim, A. Jo, K. B. C. Imani, D. Kim, J.-W. Chung, J. Yoon, *Langmuir* **2018**, 34, 4351.

[307] a) Y. Guo, J. Xu, C. Yan, Y. Chen, X. Zhang, X. Jia, Y. Liu, X. Wang, F. Zhou, *Advanced Engineering Materials* **2019**, 21, 1801314; b) T. Wu, P. Jiang, X. Zhang, Y. Guo, Z. Ji, X. Jia, X. Wang, F. Zhou, W. Liu, *Materials & Design* **2019**, 180, 107947.

[308] Y. Sun, C. Peng, X. Wang, R. Wang, J. Yang, D. Zhang, *Powder technology* **2017**, 320, 223.

Author biography

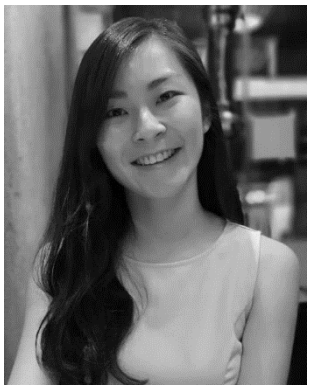

Lisa Tan is a Ph.D. student under the supervision of Prof. Kun Zhou at the School of Mechanical & Aerospace Engineering, Nanyang Technological University (NTU), Singapore. She received her B.S. degree (first class honours) in Chemistry and Biological Chemistry from NTU in 2016. Her research interest lies in additive manufacturing of polymer materials.

Wei Zhu is a Research Fellow under the supervision of Prof. Kun Zhou at the Singapore Center for 3D Printing , School of Mechanical & Aerospace Engineering, NTU, Singapore. He received his Ph.D. in Mechanical and Electronic Engineering from Huazhong University of Science and Technology, China in 2018. His research interest lies in additive manufacturing of polymeric and ceramic composites.

Kun Zhou is an Associate Professor at the School of Mechanical & Aerospace Engineering, NTU, Singapore. His research interests focus on additive manufacturing, mechanics of materials, and modelling and design of sustainable materials. He has edited one book and published over 300 papers in refereed international journals. He serves as a founding Editor of Journal of Micromechanics and Molecular Physics, an Associate Editor of Mechanics Research Communications, and an Editorial Board Member of Virtual and Physical Prototyping and a few other international journals.

Table of contents

Additive manufacturing (AM) has emerged as a disruptive technology that fabricates products with complex geometries to enable great design freedom. This article provides a comprehensive review on the recent progress on polymer materials for various AM techniques. Polymer materials developed for AM and their requirements and applications are discussed. The major challenges and future research directions in this field are identified.

Keywords: 3D printing, additive manufacturing, vat photopolymerization, material jetting, powder bed fusion, material extrusion

*Lisa Jiaying Tan, Wei Zhu, Kun Zhou**

Recent progress on polymers for additive manufacturing

ToC figure